Giant magnetoresistive sensors and magnetic labels for chip-scale detection of immunosorbent assays

by

Rachel Lora Millen

A dissertation submitted to the graduate faculty

in partial fulfillment of the requirements for the degree of

DOCTOR OF PHILOSOPHY

Major: Analytical Chemistry (Materials Chemistry)

Program of Study Committee:
Marc D. Porter, Major Professor
Scott Chumbley
R. S. Houk
Victor Shang-Yi Lin
E. S. Yeung

Iowa State University

Ames, Iowa

2005

Graduate College
Iowa State University

This is to certify that the doctoral dissertation of

Rachel Lora Millen

has met the dissertation requirements of Iowa State University

Major Professor

For the Major Program

TABLE OF CONTENTS

ACKNOWLEDGEMENTS vi

GENERAL INTRODUCTION 1

Dissertation Organization 1

Literature Review 2

References 15

CHAPTER 1: GIANT MAGNETORESISTIVE SENSORS AND SUPERPARAMAGNETIC NANOPARTICLES: A CHIP-SCALE DETECTION STRATEGY FOR IMMUNOSORBENT ASSAYS

Abstract 18

Introduction 19

Experimental Section 22

Results and Discussion 27

Conclusions 33

Acknowledgements 34

References 34

CHAPTER 2: GIANT MAGNETORESISTIVE SENSORS FOR CHIP-SCALE DETECTION OF BIORECOGNITION EVENTS USING SURFACE MODIFICATION AND MAGNETIC LABELS

Abstract 49

Introduction 50

Experimental Section 51

Results and Discussion 57

Conclusions 64

Acknowledgements 65

References 66

CHAPTER 3: CHIP-SCALE DETECTION OF ANTIBODY-ANTIGEN RECOGNITION EVENTS OF RABBIT IgG USING GIANT MAGNETORESISTIVE SENSORS, MAGNETIC LABELS, AND AN INTEGRATED MAGNETIC REFERENCE

Abstract 80

Introduction 81

Experimental Section 83

Results and Discussion 89

Conclusions 96

Acknowledgements 96

References 97

CHAPTER 4: GIANT MAGNETORESISTIVE SENSORS FOR SIMULTANEOUS CHIP-SCALE DETECTION OF MULTIPLE IgG PROTEINS

Abstract 109

Introduction 110

Experimental Section 112

Results and Discussion 118

Conclusions 122

Acknowledgements 122

References 123

GENERAL CONCLUSIONS 135

Research Overview 135

Prospectus 135

References 138

ACKNOWLEDGEMENTS

This thesis was the result of the work and support of many people. First I would like to thank my major professor, Marc Porter, for providing his guidance and insights during my years here, as well as the freedom to pursue really interesting things. Thank you for teaching me that work, and especially research should be exciting and fun!

I would also like to thank past and present members of the Porter Group. In particular, I thank Mike Granger, with his complete goofiness and creativity, for starting me on the GMR path, and Toshi Kawaguchi, Nikola Pekas, and especially John Nordling for assisting with the GMR trials and tribulations along the way. Thanks also to John for the many lunch trips and conversations – research and otherwise. I would like to thank Heather Bullen for teaching me that a positive attitude can make even disappointing results something to learn from, the worst day not so bad, and a good day better. I also thank my office mates on the "South Side", Karen Kwarta and Jeremy Driskell, for the many informal group meetings as well as for their research ideas, friendship, and support, even through dolphin drenching. I would also like to thank Becky Staedtler for knowing things – all kinds of things, Jill Uhlenkamp for her friendship and support, and Grant Edwards for his help and friendship.

I would like to thank Jack Barrow, for beginning as my study partner, and turning into my video game buddy, closest friend, and finally adopted fourth brother. Thanks to you and Christa for letting me see the miracle of Jacob.

Thanks also to my parents, Clinton and Olinda Fuerst, for supporting me through all my years of school. Thank you for always being there to listen and for the patience I learned from you. Thanks also to my brothers, sisters, and in-laws for making sure that I grew up

with a fully developed sense of humor that turned out to be incredibly useful in research, and in life. Thanks also to my nieces and nephews, and to the Millens just for being a regular supportive family.

Finally, I would like to thank my husband and best friend in the world, Alex, for his love and support. You have always believed that I could do this, even when I did not. Thank you for listening to my work stories, whether good or bad, and for giving me needed hugs, laughs, and even a kitty, at the appropriate times. I could not have done this without you. Thank you, sweetheart.

Ames Laboratory is operated for the U.S. Department of Energy by Iowa State University under contract number W-7405-eng-82. The United States Government has assigned the DOE Report number IS-T 2751 to this thesis.

GENERAL INTRODUCTION

Dissertation Organization

The combination of giant magnetoresistive sensors, magnetic labeling strategies, and biomolecule detection is just beginning to be explored. New readout methods and assay formats are necessary for biomolecules detection to flourish. The work presented in this dissertation describes steps toward the creation of a novel detection method for bioassays utilizing giant magnetoresistive sensors as the readout method.

The introduction section contains a brief review of some of the current methods of bioassay readout. The theoretical underpinnings of the giant magnetoresistive effect are also discussed. Finally, the more prominent types of giant magnetoresistive sensors are described, as well as their complicated fabrication. Four data chapters follow the introduction; each chapter is presented as a separate manuscript, either already published or soon to be submitted.

Chapter 1 presents research efforts toward the production of a bioassay on the surface of a gold-modified GMR sensor. The testing of this methodology involved the capture of goat α-mouse-coated magnetic nanoparticles on the mouse IgG-modified gold surface.

The second, third and fourth chapters describe the utilization of a self-referenced sample stick for scanning across the GMR sensor. The sample stick consisted of alternating magnetic reference and bioactive gold addresses. Chapter 2 is concerned with the characterization of both the scanning readout method and the binding and detection of streptavidin-coated magnetic particles to a biotinylated surface. Chapter 3 advances the sample stick readout with the use of the system for detection of a sandwich immunoassay

with rabbit IgG proteins. Finally, simultaneous detection of three IgG proteins is demonstrated in Chapter 4. The dissertation is concluded with a brief summary of the research presented and a discussion of the possible future applications and direction of this work.

Literature Review

The first biosensor was reported in 1962 by Clark and Lyons.[1, 2] Since then, there has been an explosive growth in the interest in the clinical and field application of biosensors. However, the types of biosensor have been numerous and varied, with each having its own set of strengths and drawbacks.

Radioactive isotopes were used as labels for sensitive immunoassays for a number of years.[3] Other sensor and label types have been explored due to the danger and difficulty in the handling, storage, and disposal of radioactive reagents and waste.[4] Enzymes labels are one of the most prevalent alternatives to radioactive immunoassay labels, due to their ease of handling and potential for signal amplification by enzymatic catalysis.[2] Enzyme-linked immunosorbent assay (ELISA) takes advantage of the enzyme label, and is often used for the determination of biological molecules.[5, 6] While sensitive and well understood, the potential for multiplexing ELISA is limited due to the lack of unique labels.[5]

Cell culturing is commonly used for bacterial tests and for genetic analysis of cells,[7] but the process can take days and may have limited portability.[8]

Polymerase chain reaction (PCR) is a frequent alternative method in pathogen determination, particularly when culturing is not an option. PCR is the amplification and detection of small amounts of DNA; however, this procedure requires trained operators.

Through PCR, contamination can result in numerous copies of DNA from contaminants, which can lead to incorrect readings. PCR also requires a purification step for most samples.[9]

Fluorescently labeled antibodies and DNA are commonly used for bioassays, and although the assays are very sensitive, there are some limitations with respect to the fluorophores. Fluorophores typically have broad absorption/emission profiles, which may limit the simultaneous detection of multiple analytes, and are prone to photobleaching, which may effect the ability to signal average and reduce detection levels.[10, 11] Quantum dots have the narrow line widths and longevity desired for fluorescent labels, but more work is needed in this emerging technology for reproducible, robust, and flexible bioconjugation.[10]

Label-free bioassays are another avenue of recent research exploration. The three main types of label-free biodetection are optical biosensors that utilize surface plasmon resonance, acoustic biosensors such as the quartz crystal microbalance, and micro-calorimetry.[12] Label-free detection methods allow a large amount of flexibility in assay design; however, the integration of the sensor, fluid handling, reaction chemistry, signal processing and data management, especially in a portable platform is still under development.[12] Finally, mass spectrometry is another method for label-free detection of biological molecules.[13-15]

It was the search for a novel sensor with the traits of sensitivity, small size, speed, and a potential for multiplexing,[16] that led to the consideration of the giant magnetoresistor (GMR) for the detection of magnetically-labeled bioanalytes. The GMR, which was discovered in 1988 by Baibich and co-workers has revolutionized the computer industry.[17, 18] The majority of read/write heads in the hard drives of personal computers use GMRs for

compact, high density, and high speed information retrieval. For example, GMRs have the capability of reading a 0.0065-μm^2 bit at 300 Mb/s.[19]

The use of the GMR as a biosensor was first reported in the literature by researchers at NRL in 1998 with the detection of superparamagnetic particles allowed to settle on multilayer GMR sensors,[20] and was continued in 2000[21] and 2001[22] with the detection of DNA hybridization events. Other laboratories provided further DNA detection demonstrations,[23-25] and some used biotin and streptavidin interactions to examine the GMR response to magnetic particles.[26, 27]

In fact, the popularity of the GMR sensor for the detection of biolytes is only increasing.[28-30] Our laboratory and others have been working toward the creation of other magnetic tools for possible integration with GMR detection, such as microfluidic pumps,[31, 32] magnetic sample diverters,[33, 34] and detection of flowing magnetic entities.[35, 36]

Magnetoresistance

Magnetoresistance is the dependence of resistivity on the strength of an applied external magnetic field (H_{app}).[37] All conductors display some level of magnetoresistance, usually with a change in resistivity of less than 1%. However, some structures can be created with a much larger magnetoresistive effect, called giant magnetoresistance. These microfabricated structures are composed of alternating layers of magnetic and non-magnetic conductors (e.g., iron and copper).[18, 37-41]

GMR Theory

The GMR phenomenon is a quantum-mechanical effect caused by the spin-dependent scattering of spin-polarized conduction electrons in the ferromagnetic layers. Ferromagnetic materials often have a disparity in the number of spin-up and spin-down electrons at the

Fermi level (E_F), and therefore display spin-polarized electron transport. The density of states accessible to the spin-up and spin-down charge carriers is usually close to equal in ferromagnetic metals, but there is an offset energy.

Figure 1 shows a schematic of this split in the two densities of states, in which the difference between the energies of the magnetic spin moment is the quantum-mechanical exchange energy.

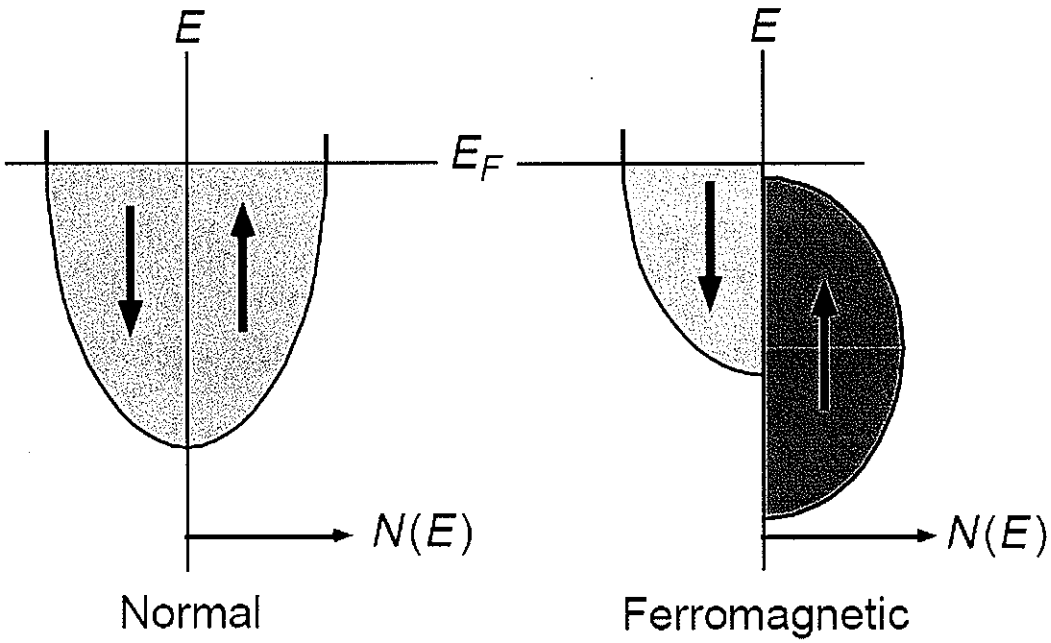

Figure 1. A schematic representing the 100% polarized state of the density of electronic states (N(E)) versus electron energy (E) for a normal and ferromagnetic metal.[18]

This figure is simplified in that the spin-up state is completely below the Fermi energy and therefore 100% polarized. Common ferromagnetic materials (i.e., Fe, Co, Ni, and their alloys) are only partially polarized, with 40-50% of the charge carriers in a particular spin state. The imbalance in spin states is responsible for the ferromagnetism of the metal, and

the difference between the number, nature, and mobility of spin-up and spin-down carriers, since the electrons fill the energy bands unequally.[18, 37]

If 100% spin polarization is assumed for visualization purposes in Figure 1, energy states are only available to spin-down charge carriers, and vice versa if the magnetization of the material is reversed. Therefore, the material can behave as either an electron insulator or conductor for electrons of a specific spin state, depending on the direction of magnetization. Prinz compares this effect to polarized light passing through an analyzer, although the light polarizer depends on a 90° rotation, and the magnetization depends on a 180° magnetic field rotation.[18]

In the case of the alternating ferromagnetic and nonmagnetic layers in GMRs, the magnetic direction of the ferromagnetic layers aligns in an antiparallel fashion throughout the structure due to exchange coupling. This alternating magnetic alignment corresponds to an interchange of the spin character of the states available states to accept an electron. Electron scattering then becomes more probable, the electron mean free path decreases, and therefore resistance increases. When a strong enough external field is applied to saturate the GMR, the ferromagnetic layer alignment becomes mostly parallel, electron scattering becomes less probable, electron mean free path increases, and resistance decreases.

This effect with respect to spin-polarized transport is illustrated schematically in Figure 2. The schematic illustrates the movement of electrons from a ferromagnetic layer, to a nonmagnetic layer, and again to a ferromagnetic layer. As in Figure 1, 100% spin polarization is assumed. In the low resistance state, i.e., with a magnetic field applied to align the ferromagnetic layers, spin-down electrons can move through the layers without a spin-flip being required.

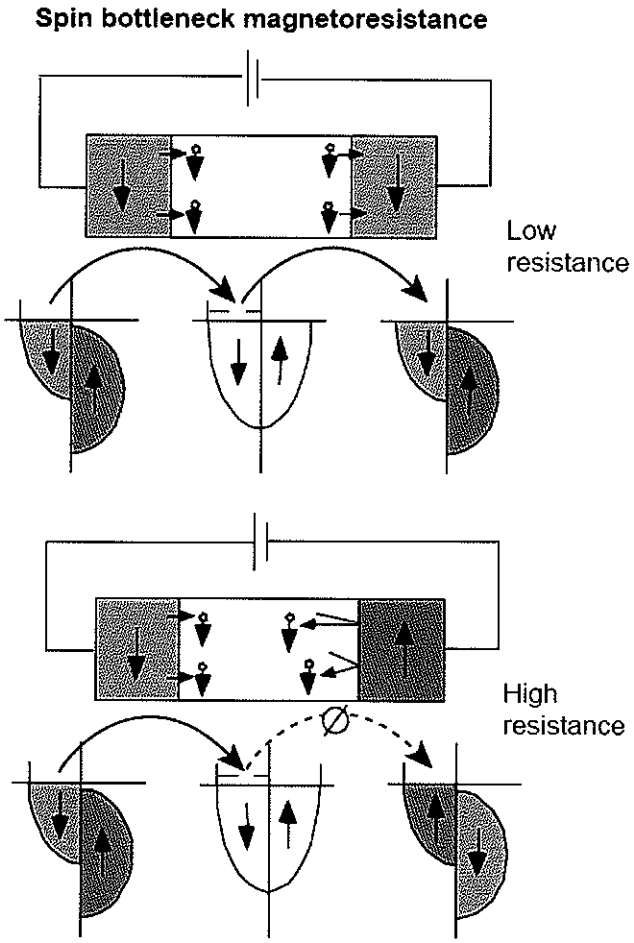

Figure 2. Schematic representation of spin-polarized transport.[18]

However, without the presence of the magnetic field, the layered structure returns to the antiparallel alignment of magnetic layers. In this case, the previous transport path would require the electron to become spin-up to enter the available energy states in the third layer, which increases the probability of electron scattering, and therefore the resistance is increased when compared to the aligned state.[18]

Another way of visualizing electron transport in the parallel and antiparallel conditions of the GMR is the equivalent circuit shown in Figure 3, in which the smaller R_l

represents the resistivity of electron transport to an energy state with the same spin-character, and the larger R_2 is the resistivity from electron transport that would require a change in spin-state.

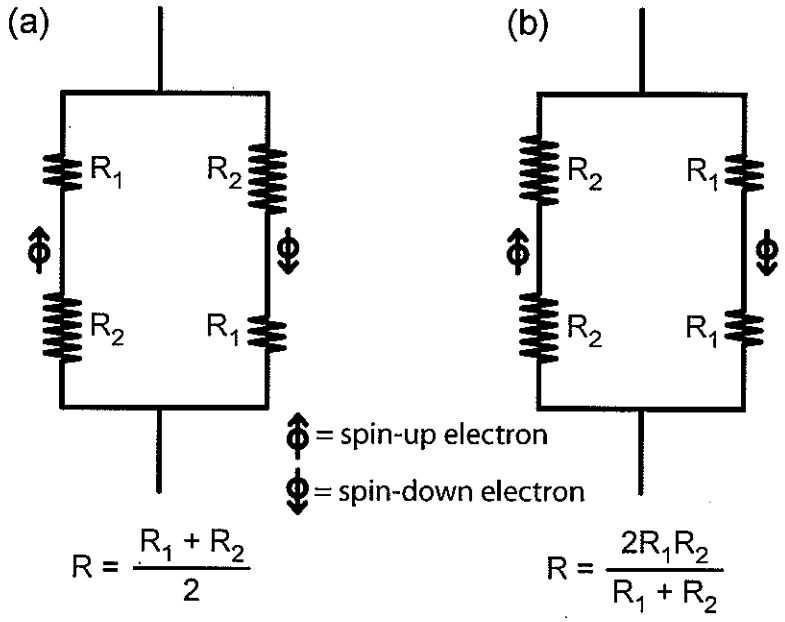

Figure 3. Equivalent resistor representation of giant magnetoresistance in the (a) antiparallel and (b) parallel states layer magnetizations.[37]

In Figure 3, the left path of both equivalent circuits corresponds to spin-up electron transport, and the right path to spin-down electron transport. When no magnetic field is applied, the circuit in Figure 3a applies in that neither the spin-up nor the spin-down electrons can travel through all the ferromagnetic layers freely. However, when an external magnetic field is applied in the direction of the spin-down electrons, in this particular example, half the electrons can travel through the layers with low scattering probability as shown in Figure 3b. Therefore, the resistance of the equivalent circuit is less when the external magnetic field is applied.[37]

The number, arrangement, and composition of the layers determines the type of GMR formed, but the common factor is that the thickness of each layer must be on the order of the mean free path of an electron in the material.[41] There are different structures that utilize the GMR effect, including the spin-valve, the sandwich, and the multilayer GMR.[42] The magnetic tunnel junction is a further variation of the GMR structure, although the tunnel junction technology is still being developed.[43-45]

Spin-Valve GMR Devices

The spin-valve GMR (Figure 4a) is made from four layers of material – two ferromagnetic (FM) layers sandwiched around a nonmagnetic layer and an antiferromagnetic (AF) pinning layer.[42, 46, 47] One of the ferromagnetic layers is free to rotate in response to an applied magnetic field, while the ferromagnetic layer adjacent to the antiferromagnetic layer is pinned in the direction parallel to that of the antiferromagnetic layer. The resistance of the device depends on the angle of magnetization of the free layer with respect to that of the pinned layer. As with all GMR structures, the resistance is lowest when the magnetizations of the layers are parallel, and highest when the layers are antiparallel.

The response of a spin-valve GMR sensor with respect to applied magnetic field is shown in Figure 4b.[35] At low magnetic fields, if the free layer direction rotates in the plane of the film, and the resistance increases and decreases smoothly with changing field. In this case, the highest sensitivity region is at low fields, surrounding 0 Oe. However, caution must be used since a large enough applied magnetic can also change the alignment of the pinned magnetic layer.

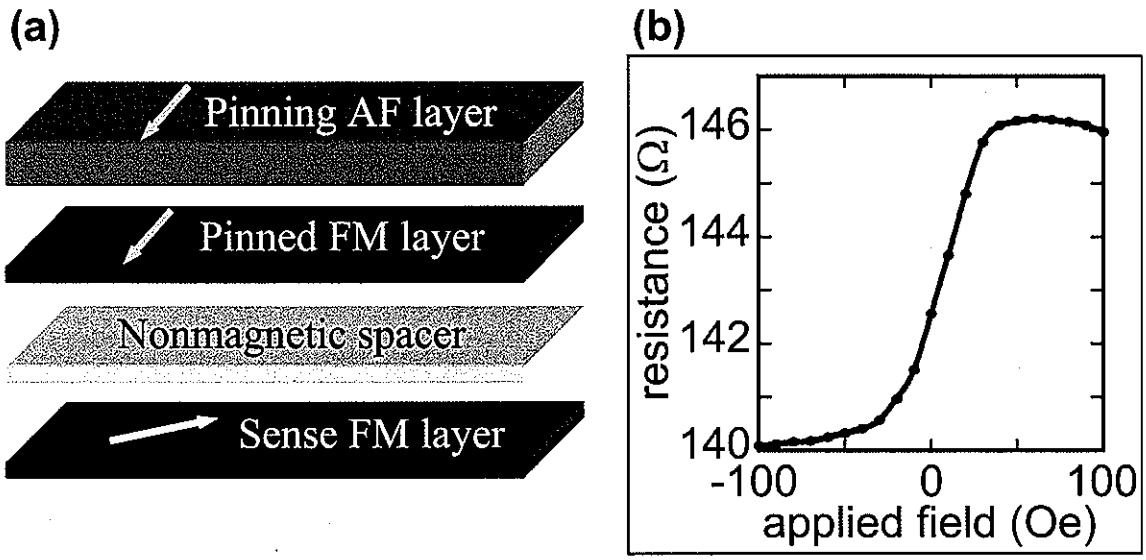

Figure 4. (a) Schematic representation of a spin-valve structure. (b) Change in resistance of a single spin-valve GMR with respect to magnetic field.[35]

Unpinned GMR Sandwich

The sandwich GMR consists of two ferromagnetic layers sandwiched around a nonmagnetic layer, which is similar to a spin-valve design, without the stabilization of the pinning layer. Despite being of a simpler construction than the spin-valve, the resistance change versus applied magnetic field is more complicated, since both ferromagnetic layers are free to rotate in response to an applied magnetic field. These sensors are less frequently used due to the particularly careful construction and design required for the sensors to be useful.[41, 48]

Multilayer GMR Sensors

The GMR used exclusively in the work described in this thesis is the multilayer GMR. The multilayer is made of several repeating units of ferromagnetic and nonmagnetic

layers.[17] The change in scattering in a multilayer GMR is shown schematically in Figure 5, where the length of the arrows represents the distance traveled by an electron before scattering.

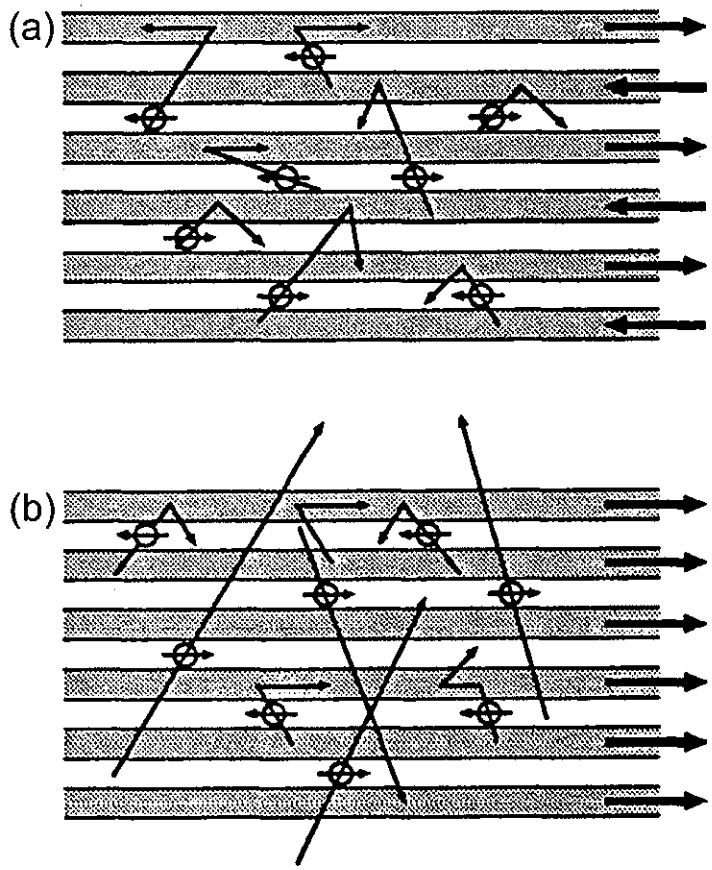

Figure 5. Schematic representation of electron conduction through a multilayer GMR in (a) the antiparallel and (b) the parallel condition of layer magnetization.[37, 49]

Figure 5a shows the antiparallel magnetization alignment resulting in a higher scattering probability, and therefore, a higher resistance state. Figure 5b shows the parallel magnetization alignment, due to an external field, resulting in a lower scattering probability, and therefore a state of lower resistance.[37] It is interesting to note that the net current flow

through the structures described so far is in the plane of the GMR films. In such a case, most electrons do not have enough energy to cross to another magnetic layer, whether or not their spin-states are aligned. Therefore, the GMR effect is due only to a small fraction of conduction electrons. Much higher levels of the GMR effect have been observed when passing the current perpendicular to the magnetic films, although the perpendicular resistance of the thin film is so small that attachment of electrical contacts to such a thin film requires extreme measures so these devices are still in development.[42]

The response of a GMR sensor to a scanned H_{app} is shown in Figure 6, which is a plot of GMR resistance as H_{app} was swept from at +560 to -560 Oe, and back again.

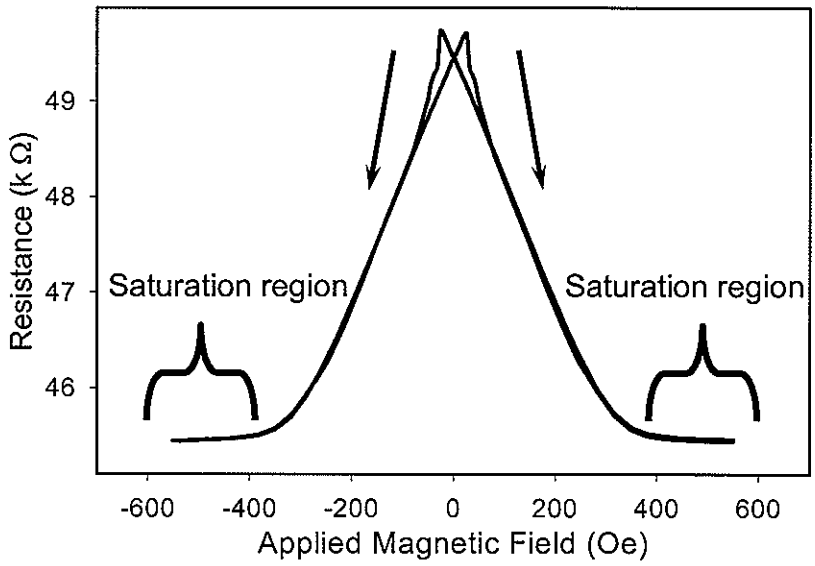

Figure 6. Change in resistance of a single multilayer GMR with respect to magnetic field.[50]

There are three different regions of response on the plot: 1) field saturation, 2) linear response, 3) hysteretic region. Field saturation occurs when the field is strong enough (approximately ±400 Oe) so that the change in resistance with H_{app} is relatively small, due to the spin alignment of all the magnetic layers. At lower strength fields, the resistance change

of the GMR become linear with the external field, as the spin alignments change proportionately with H_{app}. However, at fields near zero the GMR response becomes somewhat erratic as the signal hysteresis becomes a factor from the delay in the realignment of the spins as H_{app} changes direction.[51] Although the response at 0 Oe displays hysteresis, as H_{app} is scanned beyond 0 Oe, the sensor again enters a linear response region.

GMR Fabrication

The GMR devices, although complicated, were created using standard microfabrication techniques.[52] Two formulas of GMR construction were used in the work described herein, although both have the characteristic alternating magnetic and nonmagnetic layers. Figure 7 displays both structures schematically (not to scale).

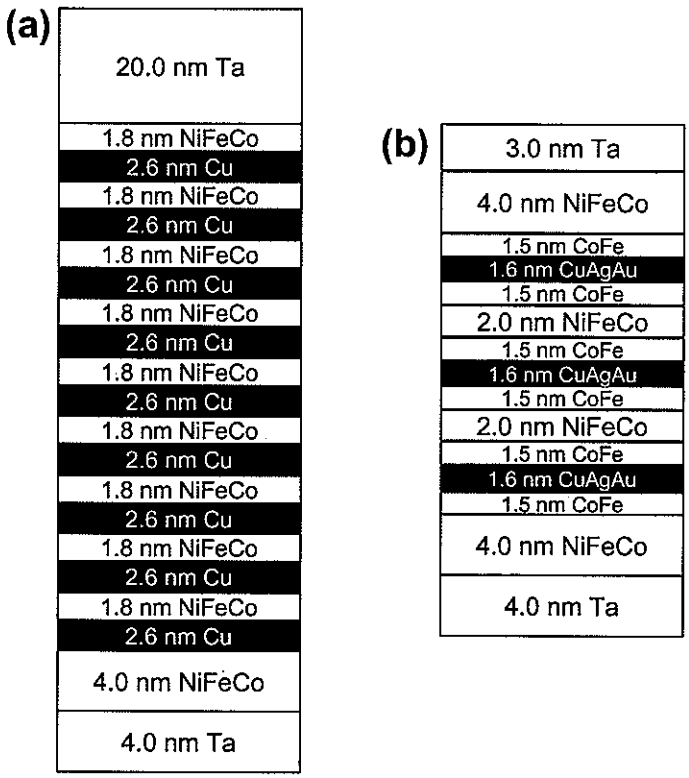

Figure 7. Composition of multilayer GMR structure used in Chapter 1 (a) and Chapters 2-4 (b) of this work.[50, 53]

A device created from nine repeating units of the magnetic alloy $Ni_{65}Fe_{15}Co_{20}$, where the subscripts represent atomic percentage, and Cu with a total thickness of 57 nm is shown in Figure 7a.[50] Figure 7b is a structure that is thinner overall (33 nm) consisting of repeated layers of ferromagnetic layers of $Ni_{65}Fe_{15}Co_{20}$, $Co_{95}Fe_5$, and nonmagnetic $Cu_{69}Ag_{27}Au_4$ layer.[53]

The creation of the GMR sensor does not just involve the fabrication of the multilayered material, but the means of connecting the chip to the outside world must also be built. The design and construction of the entire GMR chip is a complicated process. A cross-sectional view of the many layers involved is presented in Figure 8.

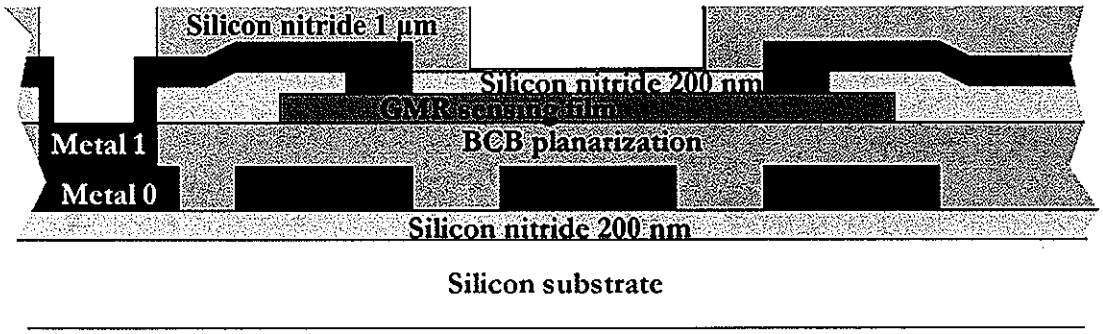

Figure 8. Cross-section schematic of the GMR microchip.[54]

The device is built on a nitride-modified silicon wafer. Two separate steps of aluminum deposition (Metal 1 and Metal 0) are necessary for the wiring of the GMR chip. The polymer bisbenzocyclobutene (BCB) is used to level surface after the creation of the aluminum wires. Layers of silicon nitride are used to protect both the GMR and the remaining chip surface from further processing steps. The layout, shape, and size of the GMR sensors themselves will be discussed in subsequent chapters.

Dissertation Overview

GMRs are small, sensitive, high-speed sensors, commonly manufactured for computer hard drives. Each of the following chapters is presented as an individual manuscript that describes the research effort to incorporate GMRs as a bioanalytical tool. Chapter 1 utilizes a gold-coated GMR for the detection of magnetic nanoparticles selectively bound to the surface through protein-protein interactions. The streptavidin-biotin interaction is the method of choice for capturing magnetic labels in the second, third, and fourth chapters – first to a biotinylated surface, then to the biotinylated target antibody of a sandwich immunoassay, and finally for purposes of multianalyte detection. The last three chapters utilize a self-referenced sample stick that enables the scanning of bioactive addresses over the GMR for readout. The dissertation is concluded with a summary of the research work presented along with a discussion of future applications and directions of this work.

References

(1) Clark Jr., L. C.; Lyons, C. *Ann N Y Acad. Sci.* **1962**, *102*, 29-45.
(2) D'Orazio, P. *Clin. Chim. Acta* **2003**, *334*, 41-69.
(3) Gosling, J. P. In *Immunoassay: Laboratory Analysis and Clinical Applications*; Gosling, J. P., Basso, L. V., Eds.; Butterworth-Heinemann: Boston, 1994, pp 1-30.
(4) White, S. R.; Chiu, N. H. L.; Christopoulos, T. K. *Methods* **2000**, *22*, 24-32.
(5) Christopoulos, T. K.; Diamandis, E. P. *Immunoassay*; Academic Press: New York, 1996.
(6) Meng, Y.; High, K.; Antonello, J.; Washabaugh Michael, W.; Zhao, Q. *Anal. Biochem.* **2005**, *345*, 227-36.
(7) Goto, M.; Sato, K.; Murakami, A.; Tokeshi, M.; Kitamori, T. *Anal. Chem.* **2005**, *77*, 2125-31.
(8) Lagally, E. T.; Mathies, R. A. *J. Phys. D: Appl. Phys.* **2004**, *37*, 245-61.
(9) Roper, M. G.; Easley, C. J.; Landers, J. P. *Anal. Chem.* **2005**, *77*, 3887-94.
(10) Medintz, I. L.; Uyeda, H. T.; Goldman, E. R.; Mattoussi, H. *Nat. Mater.* **2005**, *4*, 435-46.
(11) Demchenko, A. P. *Anal. Biochem.* **2005**, *343*, 1-22.
(12) Cooper, M. A. *Anal. Bioanal. Chem.* **2003**, *377*, 834-42.

(13) Cargile, B. J.; Bundy, J. L.; Grunden, A. M.; Stephenson, J. L. *Anal. Chem.* **2004**, *76*, 86-97.
(14) Nedelkov, D.; Nelson, R. W. *Appl. Environ. Microbiol.* **2003**, *69*, 5212-15.
(15) Schweigert, F. J.; Wirth, K.; Raila, J. *Proteome Science* **2004**, *2*, No pp. given.
(16) Vilkner, T.; Janasek, D.; Manz, A. *Anal. Chem.* **2004**, *76*, 3373-86.
(17) Baibich, M.; Broto, J. M.; Fert, A.; Van Dau, N.; Petroff, F. *Phys. Rev. Lett.* **1988**, *61*, 2472-75.
(18) Prinz, G. A. *Science* **1998**, *282*, 1660-63.
(19) Zhang, Z.; Feng, Y. C.; Clinton, T.; Badran, G.; Yeh, N.-H.; Tarnopolsky, G.; Girt, E.; Munteanu, M.; Harkness, S.; Richter, H.; Nolan, T.; Ranjan, R.; Hwang, S.; Rauch, G.; Ghaly, M.; Larson, D.; Singleton, E.; Vas'ko, V.; Ho, J.; Stageberg, F.; Kong, V.; Duxstad, K.; Slade, S. *IEEE Trans. Magn.* **2002**, *38*, 1861-66.
(20) Baselt, D. R.; Lee, G. U.; Natesan, M.; Metzger, S. W.; Sheehan, P. E.; Colton, R. J. *Biosens. Bioelectron.* **1998**, *13*, 731-39.
(21) Edelstein, R. L.; Tamanaha, C. R.; Sheehan, P. E.; Miller, M. M.; Baselt, D. R.; Whitman, L. J.; Colton, R. J. *Biosens. Bioelectron.* **2000**, *14*, 805-13.
(22) Miller, M. M.; Sheehan, P. E.; Edelstein, R. L.; Tamanaha, C. R.; Zhong, L.; Bounnak, S.; Whitman, L. J.; Colton, R. J. *J. Magn. Magn. Mater.* **2001**, *225*, 138-44.
(23) Graham, D. L.; Ferreira, H. A.; Feliciano, N.; Freitas, P. P.; Clarke, L. A.; Amaral, M. D. *Sens. Actuators, B* **2005**, *107*, 936-44.
(24) Schotter, J.; Kamp, P. B.; Becker, A.; Pühler, A.; Brinkmann, D.; Schepper, W. B., H.; Reiss, G. *IEEE Trans. Magn.* **2002**, *38*, 3365.
(25) Schotter, J.; Kamp, P. B.; Becker, A.; Pühler, A.; Reiss, G.; Brückl, H. *Biosens. Bioelectron.* **2004**, *19*, 1149-56.
(26) Ferreira, H. A.; Graham, D. L.; Freitas, P. P.; Cabral, J. M. S. *J. Appl. Phys.* **2003**, *93*, 7281-86.
(27) Graham, D. L.; Ferreira, H. A.; Freitas, P. P.; Cabral, J. M. S. *Biosens. Bioelectron.* **2003**, *18*, 483-88.
(28) Megens, M.; Prins, M. *J. Magn. Magn. Mater.* **2005**, *293*, 702-08.
(29) Graham, D. L.; Ferreira, H. A.; Freitas, P. P. *Trends in Biotechnology* **2004**, *22*, 455-62.
(30) Wood, D. K.; Ni, K. K.; Schmidt, D. R.; Cleland, A. N. *Sens. Actuators, A* **2005**, *120*, 1-6.
(31) Melikhov, Y.; Lee, S. J.; Jiles, D. C.; Schmidt, D. H.; Porter, M. D.; Shinar, R. *J. Appl. Phys.* **2003**, *93*, 8438-40.
(32) He, W.; Lee, S. J.; Jiles, D. C.; Schmidt, D. H.; Porter, M. D.; Shinar, R. *J. Appl. Phys.* **2003**, *93*, 7459-61.
(33) Tondra, M.; Granger, M.; Fuerst, R.; Porter, M.; Nordman, C.; Taylor, J.; Akou, S. *IEEE Trans. Magn.* **2001**, *37*, 2621-23.
(34) Pekas, N.; Granger, M. C.; Tondra, M.; Popple, A.; Porter, M. D. *J. Magn. Magn. Mater.* **2005**, *293*, 584-88.
(35) Pekas, N.; Porter, M. D.; Tondra, M.; Popple, A.; Jander, A. *Appl. Phys. Lett.* **2004**, *85*, 4783-85.
(36) Ferreira, H. A.; Graham, D. L.; Parracho, P.; Soares, V.; Freitas, P. P. *IEEE Trans. Magn.* **2004**, *40*, 2652-54.

(37) White, R. L. *IEEE Trans. Magn.* **1992**, *28*, 2482-86.
(38) Mapps, D. J. *Sens. Actuators, A* **1997**, *59*, 9-19.
(39) Barthelemy, A.; Cros, V.; Duvail, J. L.; Fert, A.; Morel, R.; Parent, F.; Petroff, F.; Steren, L. B. *Nanostr. Mat.* **1995**, *6*, 217-26.
(40) Johnson, M. *J. Phys. Chem. B* **2005**, *109*, 14278-91.
(41) Daughton, J. M.; Bade, P. A.; Jenson, M. L.; Rahmati, M. M. M. *IEEE Trans. Magn.* **1992**, *28*, 2488-93.
(42) Hauser, H.; Tondra, M. In *Magnetic Sensors and Magnetometers,* 1st ed.; Ripka, P., Ed.; Artech House: Boston, 2001, pp 129-71.
(43) Grancharov, S. G.; Zeng, H.; Sun, S.; Wang, S. X.; O'Brien, S.; Murray, C. B.; Kirtley, J. R.; Held, G. A. *J. Phys. Chem. B* **2005**, *109*, 13030-35.
(44) Parkin, S. S. P.; Kaiser, C.; Panchula, A.; Rice, P. M.; Hughes, B.; Samant, M.; Yang, S.-H. *Nat. Mater.* **2004**, *3*, 862-66.
(45) Djayaprawira, D. D.; Tsunekawa, K.; Nagai, M.; Maehara, H.; Yamagata, S.; Watanabe, N.; Yuasa, S.; Suzuki, Y.; Ando, K. *Appl. Phys. Lett.* **2005**, *86*, 092502/1-02/3.
(46) Qian, Z.; Daughton, J. M.; Wang, D.; Tondra, M. *IEEE Trans. Magn.* **2003**, *39*, 3322-24.
(47) Tsang, C.; Fontana, R. E.; Lin, T.; Heim, D. E.; Speriosu, V. S.; Gurney, B. A.; Williams, M. L. *Magnetics, IEEE Transactions on* **1994**, *30*, 3801-06.
(48) Daughton, J. M. *Magnetics, IEEE Transactions on* **1994**, *30*, 364-68.
(49) Inomata, K. *J. Electroceram.* **1998**, *2*, 283-93.
(50) Millen, R. L.; Kawaguchi, T.; Granger, M. C.; Porter, M. D.; Tondra, M. *Anal. Chem.* **2005**, *77*, 6581-87.
(51) Clemens, W.; van den Berg, H. A. M.; Rupp, G.; Schelter, W.; Vieth, M.; Wecker, J. *J. Appl. Phys.* **1997**, *81*, 4310-12.
(52) Tondra, M.; Anderson, J. M. Magnetizable bead detector. U.S. Patent 6,743,639, June 1, 2004.
(53) Rife, J. C.; Miller, M. M.; Sheehan, P. E.; Tamanaha, C. R.; Tondra, M.; Whitman, L. J. *Sens. Actuators, A* **2003**, *107*, 209-18.
(54) Tondra, M.; Popple, A.; Jander, A.; Millen, R. L.; Pekas, N.; Porter, M. D. *J. Magn. Magn. Mater.* **2005**, *293*, 725-30.

CHAPTER 1: GIANT MAGNETORESISTIVE SENSORS AND SUPERPARAMAGNETIC NANOPARTICLES: A CHIP-SCALE DETECTION STRATEGY FOR IMMUNOSORBENT ASSAYS

A paper published in *Analytical Chemistry*[1]

Rachel L. Millen, Toshikazu Kawaguchi, Michael C. Granger, and Marc D. Porter

Departments of Chemistry and Chemical Engineering, Ames Laboratory-USDOE, and

Institute for Combinatorial Discovery, Iowa State University, Ames, IA 50011

Mark Tondra

NVE Corporation, Eden Prairie, MN 55433

Abstract

Thin structures of alternating magnetic and non-magnetic layers with a total thickness of a few hundred nanometers exhibit a phenomenon known as giant magnetoresistance. The resistance of microfabricated giant magnetoresistors (GMRs) is dependent on the strength of an external magnetic field. This paper examines magnetic labeling methodologies and surface derivatization approaches based on protein-protein binding that are aimed at forming a general set of protocols to move GMR concepts into the bioanalytical arena. As such, GMRs have been used to observe and quantify the immunological interaction between surface-bound mouse IgG and α–mouse IgG coated on superparamagnetic particles. Results show the response of a GMR network connected together as a set of two sense GMRs and two reference GMRs in a Wheatstone bridge as a means to compensate for temperature effects. The response can be readily correlated to the amount of the magnetically labeled

---

α-mouse IgG that is captured by an immobilized layer of mouse IgG, the presence of which is confirmed with X-ray photoelectron spectroscopy and atomic force microscopy. These results, along with a detailed description of the experimental testing platform, are described in terms of sensitivity, detection limits, and potential for multiplexing.

Introduction

Baibich and co-workers discovered the giant magnetoresistance effect in 1988.[1] This development has had an immeasurable impact on magnetic data storage technology.[2] Nearly all read/write heads used in personal computers today employ giant magnetoresistors (GMRs) for compact, high density, and high speed information retrieval. These tools are also extremely sensitive, with the capability of reading a 0.0065-μm^2 bit at 300 Mb/s.[3]

Sensitivity, small size, and speed are also key attributes of portable bioanalytical sensors, suggesting that GMR technology may serve as one of the tools in this arena.[4] To this end, GMRs have been utilized with various magnetic labeling strategies for the detection of DNA hybridization[5-7] and streptavidin-biotin binding.[8, 9] As part of our interests in this area,[10, 11] we have been exploring the use of magnetic concepts in miniaturized fluid actuation devices (i.e., pumps),[12, 13] sample and label diverters,[14, 15] and flow detection.[16] This paper describes the first results from a series of investigations aimed at incorporating GMRs and superparamagnetic labels into a platform for immunosorbent assays. The long range goal is to develop a basis for the creation of chip-scale analytical sensing devices by coupling the highly miniaturized format of GMRs, which have a footprint of only a few hundred micrometers or less, with microfluidic systems.

Magnetoresistance is the dependence of material resistivity on an applied magnetic field (H_{app}). All conductors exhibit some level of magnetoresistance, typically with a change in resistivity below 1%. GMRs are microfabricated structures that are a few hundred micrometers in length and width. They are composed of alternating layers of magnetic and non-magnetic conductors in which the combined thickness of the multilayered slab is comparable to the mean free path of an electron in the material.[17] It is this unique composition that leads to the quantum mechanical GMR effect, which arises from the spin-dependent scattering of conduction electrons in ferromagnetic materials. As fabricated, the magnetic moments between adjacent magnetic layers are anti-parallel due to anti-ferromagnetic exchange coupling, and the spin-dependent electron scattering in the multilayer structure is at a maximum.[18] This situation corresponds to the high resistance state of the device. If, however, an external magnetic field is applied in the plane of the multilayer slab, exchange coupling can be overcome and the spins in the magnetic layers brought into alignment with the external field. This alignment lowers the spin-dependent electron scattering, and therefore, the resistance of the GMR.[2, 17, 19, 20] Importantly, the degree of parallel/anti-parallel alignment of the ferromagnetic layers is extremely sensitive to the strength of H_{app}. As a consequence, GMRs can show up to an 80% change in resistivity at room temperature and at modest magnetic fields (e.g., 10-2000 Oe). An even higher dependence (>200%) is observed in structures known as magnetic tunnel junctions, though this technology is in its developmental stages.[21-23]

The response of a GMR to a change in H_{app}, which was obtained by starting the sweep at +560 Oe, is shown in Figure 1. It is composed of three different regions. At the two high field limits, the change in resistance is relatively small, which reflects saturation of

spin alignment. As the field becomes smaller, the response enters a linearly dependent region. This region arises from a proportionate change in spin alignment with the applied magnetic field. Near an applied field of zero however, the response displays hysteresis due to the lag in the realignment of the magnetic spins. The external field must therefore pass through zero and begin to increase in the opposite field direction in order to switch the alignment of the magnetic moments and again start the process of spin saturation.

Our approach for exploring the attributes of GMRs in a miniaturized immunosorbent assay is illustrated in Scheme 1 (not drawn to scale in order to present each of the key functional components). It requires the creation of: 1) a capture antibody surface directly above the GMR sensing area; and 2) a labeling step in which a magnetic nanoparticle (MNP) is coupled to the target antigen. The presence of the MNP-labeled antigen is then determined by the change in resistance before and after exposing the capture antibody surface to the labeled sample. This paper reports on the design and fabrication of a GMR-based platform and the testing of experimental hardware that is applied to an immunosorbent assay by using a capture antibody surface composed of mouse IgG and MNPs modified with a layer of goat α-mouse IgG. The experiments examined the GMR response as a function of the concentration of the antibody-labeled MNP solution. The responses are correlated with the presence of selectively captured MNPs as determined by atomic force microscopy (AFM) and X-ray photoelectron spectroscopy (XPS). Assessments of GMR detection capabilities and potential applications are also discussed.

Experimental Section

Design, Layout, and Fabrication of GMR Chips

Figures 2 and 3 detail the device layout, wiring, and the fluidic network (not used in this study) of our chip-scale GMR sensor platform and test system. Figure 2 is a photomicrograph of the platform before creation of the capture antibody surface. Each sensor consists of four GMRs, detailed schematically (not to scale) in Figure 3a, that are laid out in a serpentine pattern and electrically wired to function as the four resistors in a Wheatstone bridge. Two of the GMRs act as the sense resistors R_{S1} and R_{S2} and are set in proximity to form an interdigitated 215 × 315 μm "sense pad". Each sense-GMR consists of a 2-μm wide strip that has a total length of over 11,000 μm and a spacing between neighboring strips of 2 μm. The two remaining GMRs function as reference resistors R_{R1} and R_{R2} and are employed to reduce complications associated with the sensitivity of GMRs to temperature and stray magnetic fields.[24, 25] The 2-μm wide strips of each of the reference GMRs are also separated by 2 μm in the narrow region of the serpentine pattern, but are separated by 6 μm in the wider area of the pattern. The edges of the sense and reference GMRs are separated by 30 μm.

The reference GMRs are coated with a 7-μm layer of polymer derived from bisbenzocyclobutene (BCB). The BCB layer performs two functions. First, it buries the two reference GMRs at a depth sufficient to screen against the detection of stray MNPs on the reference GMRs.[10] Second, it is a mechanically stable polymer that can be used to photolithographically define the shape and height of the micrometer-sized fluid channels and the fluid inlet/outlet reservoirs that will be used in future applications. A 200-nm passivation

layer of Si_3N_4 protects the entire device (with the exception of the aluminum electrical contact areas) during subsequent processing steps, device applications, or both.

The GMR chips (NVE Corp.) and support structures were prepared by standard microfabrication processing.[26] The GMRs were composed of alternating layers of Ta, the alloy NiFeCo (65/15/20, respective atomic percentages), and Cu. Starting from the bottom layer, the GMRs consisted of Ta (40) / NiFeCo (40) / [(Cu (25.5) / NiFeCo (18)] x 9 / Ta (200), where the thicknesses of each layer is given parenthetically in angstroms and a portion of the intervening Cu/NiFeCo stack is repeated nine times.

GMR Instrumentation

The magnetic probe station is shown in the photograph and block diagram in Figure 4. The GMR chip is the small, rectangular object surrounded by the electromagnet which is insulated by electrical tape. A Keithley 220 current source supplied a source current, I_{src}, and a Keithley 2400 multimeter was used to monitor the voltage drop across the bridge (E_1-E_2). A bipolar operational power supply (Kepco BOP 20-20M) energized the yoke-shaped electromagnet, which was manufactured in house by wrapping 560 turns of copper wire around an iron core. The 28 Oe/s scan rate of the magnetic field corresponded to a current scan rate of 1 A/s. The field strength at the GMR surface as a function of the applied current was determined by a Hall probe gaussmeter (F. W. Bell, Model 5070).

The GMR chip was connected to the macroscopic environment through a probe card (Sigma Probe). The probe card had tungsten wires precisely positioned to come into contact with the aluminum pads on the chip surface when the card was lowered with the probe station mechanics. The probe card was wired to a breakout box, which was connected to the digital voltmeter and current source. A Gateway E-4200 PC, a GPIB interface board

(National Instruments), and a Labview program, written in-house, were employed to control and monitor the current source, multimeter, and power supply.

All response characterizations used a four-point probe, which sourced a 5.0 mA current (I_{src}) and measured the change in resistance or voltage across the bridge (E_1-E_2) as the applied magnetic field was scanned. Each measurement cycle consisted of scanning the magnetic field from -475 to +475 Oe at a rate of 28 Oe/s.

Surface Modification

The surfaces of the sense pads were modified with a 30-nm gold film via a multistep process. The first step applied a 1.2-μm film of photoresist (Microposit S1811), which was subsequently photopatterned to expose the underlying sense pad (Figure 2). An electron beam evaporator (Thermionics) was used to coat thin titanium (5 nm) and gold (30 nm) films onto the substrates at a chamber temperature of 100 °C and pressure of 8×10^{-8} Torr. The titanium adhesion layer was deposited at a rate of 0.13 nm/s, while that for the gold toplayer was 0.0033 nm/s. This process forms a titanium adhesion layer and gold toplayer that span completely across both the GMR sense pad, i.e., the GMR strips and the gaps between the strips. The gold coating on the photoresist was removed by immersion in 1-methyl-2-pyrrolidinone for 30 min at 80 °C. The samples were then rinsed with ethanol, and dried with nitrogen. To remove residual photoresist from the electrical contact pads, the chips were sonicated in acetone for 5 min, followed by immersion in acetone for 1 h. Finally, the devices were dried with a stream of high-purity nitrogen, and then cleaned in an air plasma at 20 W and 500 mTorr for 15 min.

Covalent Immobilization of Mouse IgG

The capture antibody surface was prepared by covalently linking mouse IgG (Pierce) to the gold toplayer via the disulfide-based coupling agent, dithiobis (succinimidyl undecanoate) (DSU).[27-29] The immobilization process entailed the immersion of the gold-coated GMR chips into a dilute (0.2 mM) ethanolic solution of DSU for ~24 h. After immersion, the chips are rinsed extensively with ethanol and thoroughly dried under a high-purity nitrogen stream. Next, 15 μL of mouse IgG in 0.05 M borate buffer (adjusted to pH 9.0 with NaOH) was pipetted onto the DSU-derived adlayer, incubated for 24 h in a humidity chamber, and then rinsed with borate buffer. The incubation process yields a single layer of a fairly dense packed protein[28] by the formation of an amide linkage between the primary amines on the lysine residues of the protein with the succinimidyl end-group of the DSU-derived monolayer.[27]

All buffer solutions contained 0.02% wt % sodium azide (NaN_3), which functioned as a preservative, and 1% Tween 80, which served as a surfactant to minimize nonspecific adsorption. To further combat non-specific adsorption, the protein-modified samples were immersed for ~1 h in a 0.5% (w/w) solution of the blocking agent bovine serum albumin (BSA) in borate buffer (pH 9.0). The samples were again rinsed extensively with borate buffer and immediately used.

Magnetic Particle Immobilization and Characterization

Following the immobilization of mouse IgG, the samples were incubated with MNPs (~60 nm) conjugated with a coating of goat α-mouse IgG (Immunicon Corp.). The superparamagnetic particles, as characterized by AFM, were 55-65 nm in diameter and were suspended in an unbuffered solution of 0.3% BSA and 0.05% ProClin 300, which acted as a

preservative. Vendor specifications indicated that the MNPs were fully coated with a layer of goat α-mouse IgG. All dilutions to the stock MNP solution were made with 0.3% BSA and 0.02% NaN_3 in high-purity water. A 15-μL volume of the MNPs was then incubated with the capture antibody modified samples for 24 h, followed by extensive rinsing with high-purity water and drying with a nitrogen stream.

Atomic Force Microscopy

TappingMode topographic images were collected by using a Multimode NanoScope IIIa AFM (Digital Instruments) equipped with a 150-μm tube scanner and 124-μm silicon cantilevers with resonance frequencies between 270 and 350 kHz (Nanosensors). All images were obtained at a scan rate of 1.0 Hz, with the set point voltage adjusted to 80% of the free oscillation amplitude. For comparison with the observed GMR responses, the number of MNPs on the surface was quantified by using the NanoScope IIIa software for size-threshold particle counting after application of the resident image flattening algorithm. The results are reported as the average of 10-μm scans taken at five to seven separate locations on each sample. The size threshold for particle counting was set at 30 nm.

X-ray Photoelectron Spectroscopy

A Physical Electronics Industries 5500 Surface System was used for XPS characterization of particle loading. This system is equipped with a hemispherical analyzer, toroidal monochromator, and multichannel detector. A pass energy of 29.35 eV was used with a resolution of ~0.3 eV. Monochromatic Al Kα radiation (1486.6 eV) at 250 W was used for excitation. Photoelectrons were collected at 45° from the surface normal with acquisition times ranging from 0.15 s to 17.12 min. The Au($4f_{7/2}$) emission band served as an internal reference for binding energies. The base pressure of the XPS chamber was less

than 9×10^{-10} Torr during all analyses, and the sampling area was ~2 mm^2. All XPS data were collected using 1 × 1 cm silicon substrates (Montco Silicon) coated with a thin (200 nm) Si_3N_4 passivation layer to emulate the GMR surface (i.e., GMR-analog surfaces). The subsequent Au/Ti layer and other coatings were deposited on these substrates by the procedures described earlier.

Reagents

The sodium borate buffer packets and rabbit IgG were purchased from Pierce and used as received. All dilutions used distilled water that was further purified by passage through a Millipore Milli-Q system. Acetone (ACS grade), 1-methyl-2-pyrrolidinone (purified grade), Contrad®, and methanol (HPLC grade) were purchased from Fisher, NaN_3 (99% purity) was from ACROS Organics, ethanol (USP grade) from AAPER Alcohol & Chemical Co., BSA (essentially IgG free) from Sigma, and Tween 80 from Aldrich.

Results and Discussion

Verification of Selective Nanoparticle Binding by AFM and XPS

To validate the GMR response, the dependence of captured particle-labeled antigens with respect to MNP solution concentration was first monitored by AFM and XPS. The AFM experiments characterized this dependence by enumerating the surface concentrations of captured MNPs, whereas the XPS investigation probed correlations based on the intensities of features in the Fe(2p) binding energy region.

An AFM image (10 × 10 μm) of a Au/Ti-coated GMR sense pad after capture antibody binding but before exposure to a solution of antigen-coupled MNPs is shown in Figure 5a. The footprint of the underlying GMR is revealed by the faint, slightly elevated

stripes that are ~2-μm wide in the image. The elevation (~700 nm) is a result of the process employed in forming the serpentine pattern of the multilayer stack of magnetic and nonmagnetic conductors. The root-mean-square roughness in the areas between and on the GMR strips is ~8 and 11 nm, respectively. For particle counting purposes, images were acquired with the scan direction aligned in parallel with the strips so that the image-flattening algorithm resident in the AFM software could more effectively compensate for the topographic offsets in the two different regions of the image. The reported surface concentrations for the MNPs were determined over the entire image.

Evidence for MNP binding is shown in the AFM images presented in Figures 5b and c. These images were obtained after exposure of separate GMR sense pads to 15-μL volumes of different concentrations (7 and 13 pM) of antibody-conjugated MNP solutions. In both cases, a large number of particles are distributed across the surface. Many of the particles appear to be individually isolated and have an average size of ~60 nm as determined from height-based changes in topography (data not shown). Several small aggregates of particles are also apparent. As expected, the number of particles observed in the two images tracks with the difference in the relative concentration of labeled MNPs; i.e., there are more particles evident in the image shown in Figure 5c than in Figure 5b. These and several other images were used to construct a plot of the surface concentration of MNPs (particles/μm^2) against MNP solution concentration, which is given in Figure 6. As the solution concentration of conjugated MNPs increases, the number of MNPs bound to the protein-modified surface undergoes a corresponding increase. Therefore, we can directly relate surface-bound MNP concentration as determined by AFM to MNP solution concentration.

XPS was also used to detect the presence of the captured MNP-modified antibodies as a function of MNP concentration. A portion of these results, obtained with the derivatized GMR-analog substrates, is presented in Figure 7, which covers the spectral region for the Fe(2p) spin orbit couplet, i.e., the Fe($2p_{3/2}$) at 711.1 eV and Fe($2p_{1/2}$) at 724.0 eV. These features are diagnostic of the bound MNPs, which are the only iron-containing component in the system. As the MNP surface concentration increases, the Fe$2p_{3/2}$ peak intensity (711.1 eV) increases, confirming the increase in magnetic material captured by the antibody-modified surface. The positions of the bands match well with literature values for Fe_2O_3, which is consistent with the general composition of the MNPs.[30-32] The integrated area, under the Fe($2p_{3/2}$) feature, for example, can be taken as the ratio of the area for the Au(4f) band of the underlying substrate as a means for assessing the change in the relative surface concentration of MNPs. A plot of the XPS-ratio intensities against the surface concentration of MNPs from the AFM characterization exhibits a linear correlation (data not shown), which substantiates the AFM-based quantification of MNP surface concentration.

AFM was also used to examine the specificity of the MNP binding with the capture surface. These tests exposed GMR-analog surfaces that were modified with rabbit IgG capture antibodies to antigen-coupled MNPs, serving as a negative control since the goat α-mouse IgG labeled MNPs should not specifically bind to the rabbit IgG surface. The non-specific binding of the goat α-mouse IgG labeled MNPs with the rabbit IgG surface was minimal. For example, the mouse IgG capture antibody surface bound 1.3 MNP/μm^2 from an 8-pM MNP solution. In comparison, the 8-pM solution gave an average surface concentration of 0.03 MNP/μm^2 for the rabbit IgG capture antibody surface which is only ~2.3% of that for the specific binding at the mouse IgG capture antibody surface. Taken

together, these results begin to substantiate that the observed response arises from the selective binding of the capture α-mouse IgG substrate with respect to the antigen-labeled MNP.

GMR Data

Figure 8 shows two examples of the GMR response in our magnetics-based immunosorbent assay. Figure 8a corresponds to the data obtained upon exposure of a chip to a 2.4-pM solution of conjugated MNPs, whereas the data in Figure 8b are the results for the exposure of a separate chip to a 13.3-pM solution. The responses for both chips prior to exposure to the MNP solution are also given. In all cases, the applied field was initially set at a value sufficient to saturate the response of the bridge. The current flow to the electromagnet was then scanned at 1 A/s until reaching a field of a similar magnitude but opposite direction that saturated the spins in the new direction of the applied field. This approach to data acquisition served two purposes. First, the response at saturation can be used as a baseline for determining the amplitude of the observed response (see below). Second, saturation "resets" the device and thereby results in a scan that can be analyzed without needing to account for hysteresis.

The responses yield two important qualitative observations. Most importantly, the change in the GMR response tracks with the solution concentration of conjugated MNPs. The response for the GMR exposed to the higher concentration of conjugated MNPs is much larger than that for the device incubated at the lower MNP concentration. Both responses are clearly larger than the corresponding blanks.

Moreover, the blank scans of the applied magnetic field at the two different GMR-based bridges show detectable values of E_1-E_2. With a perfectly balanced Wheatstone

bridge, there should be no detectable response owing to the equivalence of the resistances for each of the four GMRs in the bridge. The response of the GMRs, which was observed for all of the devices tested, is therefore diagnostic of an imbalanced bridge. We attribute the imbalance to subtle mismatches in the resistances of the two sense-GMRs with respect to the two reference-GMRs. That is, the resistances of the sense-GMRs are matched, and so are those for the two reference-GMRs. However, the resistances of the sense-GMRs differ from those of the reference GMRs. This imbalance is a consequence of the GMR layout. Since the sense GMRs are interdigitated and the reference GMRs are not, there is a difference in the heat dissipation that arises from Joule heating; the thicker BCB layer over the reference GMRs may also have a subtle effect. Furthermore, interdigitation also affects the resistances due to magnetic fields between neighboring strips that arise from I_{src} flow. These effects are all small, but when taken together can add up to the small imbalance in the bridge. We note that the observed blank responses reflect differences in the two sets of resistor pairs of less than 0.1%. The remainder of this section discusses the quantitative aspects of these tests by taking advantage of the imbalance in the Wheatstone bridge.

The analysis of the GMR response for quantitation is based on the expected difference in the bridge resistance as reflected by the voltage difference across the two legs of the bridge, E_1-E_2. At a given source voltage, V_{src}, the classical formulation for a Wheatstone bridge as configured in Figure 3b is

$$E_1 - E_2 = V_{src}\left[\frac{R_{S1}(R_{S2}+R_{R2}) - R_{R2}(R_{S1}+R_{R1})}{(R_{S1}+R_{R1})(R_{S2}+R_{R2})}\right] \qquad (1)$$

As noted earlier, however, the imbalance in the bridge is such that we can reasonably invoke the following two assumptions: 1) $R_{S1} \approx R_{S2}$ and $R_{R1} \approx R_{R2}$; and 2) $R_{S1} \neq R_{R1}$. Equation 1 therefore reduces to

$$E_1 - E_2 = V_{src}\left[\frac{R_S - R_R}{R_S + R_R}\right] \tag{2}$$

where R_S represents R_{S1} and R_{S2} and R_R denotes R_{R1} and R_{R2}.

If the sample and blank responses are then respectively defined as $(E_1\text{-}E_2)_S$ and $(E_1\text{-}E_2)_B$ and primed annotations are used to denote the response of the sense GMRs after exposure to the conjugated MNP solution, we can write

$$\frac{(E_1 - E_2)_S}{(E_1 - E_2)_B} = \frac{\left[\frac{R_S' - R_R}{R_S' + R_R}\right]}{\left[\frac{R_S - R_R}{R_S + R_R}\right]} \tag{3}$$

Equation 3 therefore normalizes the response of each GMR-based bridge. As a consequence, the landmarks in Figure 8 depict either ΔR_{MNP} (i.e., $(E_1\text{-}E_2)_S$) or ΔR_{Blank} (i.e., $(E_1\text{-}E_2)_{Blank}$), the ratio of which functions as the normalization given by Equation 3.

Figure 9 shows the GMR response as a function of both the MNP solution concentration and the MNP surface concentration from AFM imaging. Both plots exhibit a linear dependence, with their agreement validating that the response of the GMR-based bridge can be used as a quantitative test for bioassays that utilize protein-protein interactions. We attribute the small differences in offset and correlation largely to the uncertainty in reliably pipetting the solution of MNPs entirely onto the GMR sense pad.

The two sets of data can also be used to estimate different perspectives of the detection capabilities of GMR methodology. By using three times the regression of the

linear dependence of the plot of the normalized bridge response, a limit of detection of ~1 pM in MNP concentration can be projected. The same treatment yields an estimated limit of detection from the bridge response as a function of surface concentration of ~0.2 MNP/μm^2. These results further translate to a limit of detection with respect to surface coverage of ~0.06% when using a MNP diameter of 60 nm.

These results can also be examined by considerations of the total number of particles detected across the entire sense pad, assuming the active area of the sense pad is equivalent to its 215 × 315 μm footprint. At a limit of detection of ~0.2 MNP/μm^2, the treatment indicates that a total of ~13,500 MNPs are bound to the area encompassed by the sense pad.

Conclusions

Taken together, these results demonstrate the intriguing potential of GMR sensors as a readout tool for application in a range of areas in bioanalytical science, including early disease detection via biomarker profiling and homeland security. Approaches to multiplex detection also appear to be reasonable projections through the use of GMR arrays by taking advantage of the small footprint of individual sense pads. We are presently exploring approaches to extend this capability to lower limits of detection by employing MNPs with a higher magnetic susceptibility, by concepts aimed at reducing readout noise (e.g., phase-sensitive readout), and by testing the effectives of magnetic tunnel junctions as an alternative GMR format. Moreover, modeling has indicated that the sensitivity of a GMR is maximized when the particle diameter and GMR are comparable in size,[10, 11] suggesting a slightly different perspective for a route to improve performance with respect to most other surface-based assays. Work along each of these lines is underway.

Acknowledgements

Support from NSF's XYZ-on-a-Chip Initiative (#88241), the W. M. Keck Foundation, and DARPA's BioMagnetICs program is acknowledged. We also acknowledge James Anderegg for the XPS characterizations. The Ames Laboratory is operated for the U.S. Department of Energy by Iowa State University under contract W-7405-eng-82.

References

(1) Baibich, M.; Broto, J. M.; Fert, A.; Van Dau, N.; Petroff, F. *Phys. Rev. Lett.* **1988**, *61*, 2472-75.
(2) Prinz, G. A. *Science* **1998**, *282*, 1660-63.
(3) Zhang, Z.; Feng, Y. C.; Clinton, T.; Badran, G.; Yeh, N.-H.; Tarnopolsky, G.; Girt, E.; Munteanu, M.; Harkness, S.; Richter, H.; Nolan, T.; Ranjan, R.; Hwang, S.; Rauch, G.; Ghaly, M.; Larson, D.; Singleton, E.; Vas'ko, V.; Ho, J.; Stageberg, F.; Kong, V.; Duxstad, K.; Slade, S. *IEEE Trans. Magn.* **2002**, *38*, 1861-66.
(4) Vilkner, T.; Janasek, D.; Manz, A. *Anal. Chem.* **2004**, *76*, 3373-86.
(5) Miller, M. M.; Sheehan, P. E.; Edelstein, R. L.; Tamanaha, C. R.; Zhong, L.; Bounnak, S.; Whitman, L. J.; Colton, R. J. *J. Magn. Magn. Mater.* **2001**, *225*, 138-44.
(6) Schotter, J.; Kamp, P. B.; Becker, A.; Pühler, A.; Brinkmann, D.; Schepper, W. B., H.; Reiss, G. *IEEE Trans. Magn.* **2002**, *38*, 3365.
(7) Edelstein, R. L.; Tamanaha, C. R.; Sheehan, P. E.; Miller, M. M.; Baselt, D. R.; Whitman, L. J.; Colton, R. J. *Biosens. Bioelectron.* **2000**, *14*, 805-13.
(8) Graham, D. L.; Ferreira, H. A.; Freitas, P. P.; Cabral, J. M. S. *Biosens. Bioelectron.* **2003**, *18*, 483-88.
(9) Ferreira, H. A.; Graham, D. L.; Freitas, P. P.; Cabral, J. M. S. *J. Appl. Phys.* **2003**, *93*, 7281-86.
(10) Tondra, M.; Porter, M.; Lipert, R. J. *J. Vac. Sci. Technol., A* **2000**, *18*, 1125-29.
(11) Tondra, M.; Popple, A.; Jander, A.; Millen, R. L.; Pekas, N.; Porter, M. D. *J. Magn. Magn. Mater.* **2005**, *293*, 725-30.
(12) Melikhov, Y.; Lee, S. J.; Jiles, D. C.; Schmidt, D. H.; Porter, M. D.; Shinar, R. *J. Appl. Phys.* **2003**, *93*, 8438-40.
(13) He, W.; Lee, S. J.; Jiles, D. C.; Schmidt, D. H.; Porter, M. D.; Shinar, R. *J. Appl. Phys.* **2003**, *93*, 7459-61.
(14) Tondra, M.; Granger, M.; Fuerst, R.; Porter, M.; Nordman, C.; Taylor, J.; Akou, S. *IEEE Trans. Magn.* **2001**, *37*, 2621-23.
(15) Pekas, N.; Granger, M. C.; Tondra, M.; Popple, A.; Porter, M. D. *J. Magn. Magn. Mater.* **2005**, *293*, 584-88.

(16) Pekas, N.; Porter, M. D.; Tondra, M.; Popple, A.; Jander, A. *Appl. Phys. Lett.* **2004**, *85*, 4783-85.
(17) Daughton, J. M.; Bade, P. A.; Jenson, M. L.; Rahmati, M. M. M. *IEEE Trans. Magn.* **1992**, *28*, 2488-93.
(18) Grünberg, P.; Schreiber, R.; Pang, Y.; Brodsky, M. B.; Sowers, H. *Phys. Rev. Lett.* **1986**, *57*, 2442-45.
(19) White, R. L. *IEEE Trans. Magn.* **1992**, *28*, 2482-87.
(20) Inomata, K. *J. Electroceram.* **1998**, *2*, 283-93.
(21) Djayaprawira, D. D.; Tsunekawa, K.; Nagai, M.; Maehara, H.; Yamagata, S.; Watanabe, N.; Yuasa, S.; Suzuki, Y.; Ando, K. *Appl. Phys. Lett.* **2005**, *86*, 092502/1-02/3.
(22) Parkin, S. S. P.; Kaiser, C.; Panchula, A.; Rice, P. M.; Hughes, B.; Samant, M.; Yang, S.-H. *Nat. Mater.* **2004**, *3*, 862-66.
(23) Daughton, J. M. *J. Magn. Magn. Mater.* **1999**, *192*, 334-42.
(24) Rife, J. C.; Miller, M. M.; Sheehan, P. E.; Tamanaha, C. R.; Tondra, M.; Whitman, L. J. *Sens. Actuators, A* **2003**, *107*, 209-18.
(25) Jin, Z.; Bertram, H. N.; Dakroub, H. *IEEE Trans. Magn.* **2002**, *38*, 2265-67.
(26) Tondra, M.; Anderson, J. M. Magnetizable bead detector. U.S. Patent 6,743,639, June 1, 2004.
(27) Duhachek, S. D.; Kenseth, J. R.; Casale, G. P.; Small, G. J.; Porter, M. D.; Jankowiak, R. *Anal. Chem.* **2000**, *72*, 3709-16.
(28) Jones, V. W.; Kenseth, J. R.; Porter, M. D.; Mosher, C. L.; Henderson, E. *Anal. Chem.* **1998**, *70*, 1233-41.
(29) Grubisha, D. S.; Lipert, R. J.; Park, H.-Y.; Driskell, J.; Porter, M. D. *Anal. Chem.* **2003**, *75*, 5936-43.
(30) Oku, M.; Kirokawa, K. *J. Electron Spectrosc. Relat. Phenom.* **1976**, *8*, 475.
(31) Paparazzo, E. *J. Electron Spectrosc. Relat. Phenom.* **1987**, *43*, 97.
(32) Seyama, H.; Soma, M. *J. Electron Spectrosc. Relat. Phenom.* **1987**, *42*, 97.

Figure Captions

Scheme 1. Miniaturized immunosorbent assay approach.

Figure 1. Change in resistance of a single GMR as a function of applied magnetic field. The applied magnetic field is aligned with the plane of the multilayer structure and is scanned from 560 to –560 Oe and back to 560 Oe (see Experimental Section for further details).

Figure 2. Photomicrograph of GMR sensor and electrical and fluidic interconnects: (a) GMR sensor, 6-μm microfluidic channels, 1000-μm inlet/outlet reservoirs, electrical interconnects, and wire bonding pads. (b) Expanded view of the GMR sensor configured as a Wheatstone bridge. Two sensing resistors, R_{S1} and R_{S2} are interdigitated and positioned as a "sense pad" below a fluid reservoir, whereas the two reference resistors, R_{R1} and R_{R2}, are laid on either side of the sense pad.

Figure 3. GMR sensor schematic, with an abbreviated GMR path length for clarity. (a) The two interdigitated sensing resistors, R_{S1} and R_{S2}, are shown in blue and red. The two reference resistors, R_{R1} and R_{R2}, are shown in green and are positioned on either side of the sense pad; the yellow lines represent the wire interconnects. (b) All measurements are made in a Wheatstone bridge circuit by sourcing a 5-mA current at I_{src}. The observed change in resistance is measured across E_1 and E_2.

Figure 4. Schematic and photographs of the GMR detection setup. (a) The GMR chip is the small rectangle surrounded by the electromagnet. The probe card is connected to the break

out box, a digital voltmeter, and current source, and contacts the GMR chip through tungsten wires (b), which are lowered to the chip surface, along with the white-taped electromagnet (c) using the probe station mechanics (not shown).

Figure 5. AFM topographic images (10 × 10 μm) of Au-coated GMR sense pad after immobilization of goat α-mouse IgG-labeled MNP: (a) GMR surface before MNP exposure; (b) GMR surface after incubation with 7-pM solution of conjugated MNPs; and (c) GMR surface after incubation with 13-pM solution of conjugated MNPs. All dilutions used 0.3% BSA and 0.02% NaN_3 in high-purity water.

Figure 6. Surface concentration of MNPs as a function of MNP solution concentration. Each data point is for a different GMR substrate.

Figure 7. XPS characterization in the Fe(2p) binding energy region for GMR analogues exposed to solutions containing (a) 33 and (b) 11 pM of conjugated MNPs; (c) is the capture antibody-modified surface only, (i.e., no contact with conjugated MNPs).

Figure 8. GMR response of sense pad versus magnetic field. Plot of the changing voltage difference (E_1-E_2) of a GMR bridge versus the applied magnetic field. ΔR_{blank} was recorded after Au deposition but before immobilization of (a) 2.4 and (b) 13.3 pM of conjugated MNP. ΔR_{MNP} was recorded after MNP immobilization. The dashed lines in (b) illustrate the magnitude of ΔR_{MNP} and ΔR_{blank}. The dashed green line denotes the baseline response, which corresponds to the signal at saturation. The dashed red and dotted blue lines represent the

blank response and the response upon capture of labeled MNPs. The responses in (a) and (b) are for separate GMRs. GMR response is equal to $(\Delta R_{MNP} / \Delta R_{blank}) \times 100$: (a) 206 %; (b) 567 %.

Figure 9. GMR response versus both the solution concentration and the surface concentration of MNP, where the GMR response is equal to $(\Delta R_{MNP} / \Delta R_{blank}) \times 100$. Each data point is an individual GMR substrate. Regression of the GMR response versus surface concentration: $y=85.6x + 97.0$; $R^2=0.9980$. Regression of the GMR response versus solution concentration: $y=33.9x + 103.6$; $R^2=0.9675$.

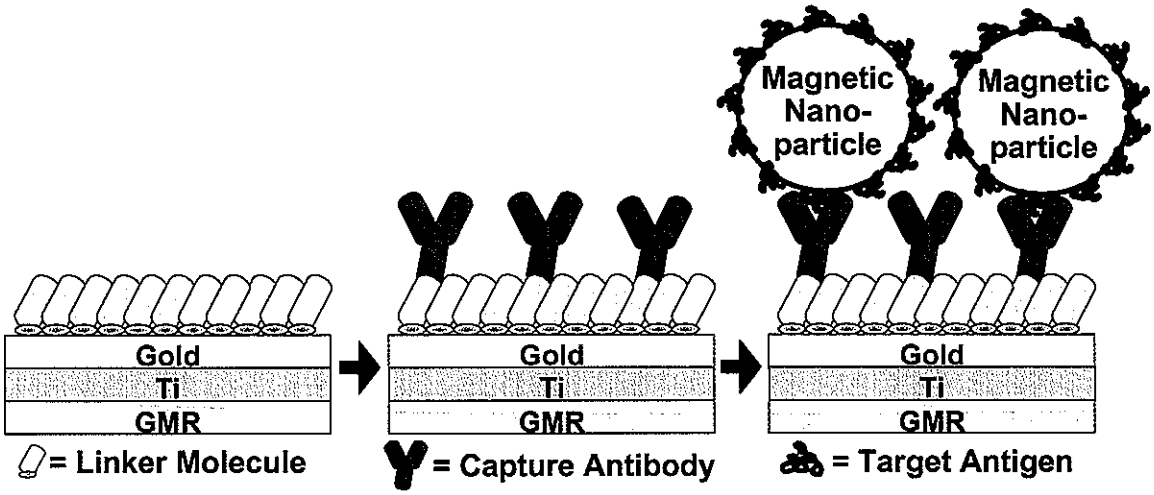
Magnetic Nano-particle
Magnetic Nano-particle
Gold
Ti
GMR
Gold
Ti
GMR
Gold
Ti
GMR
= Linker Molecule
= Capture Antibody
= Target Antigen

Scheme 1

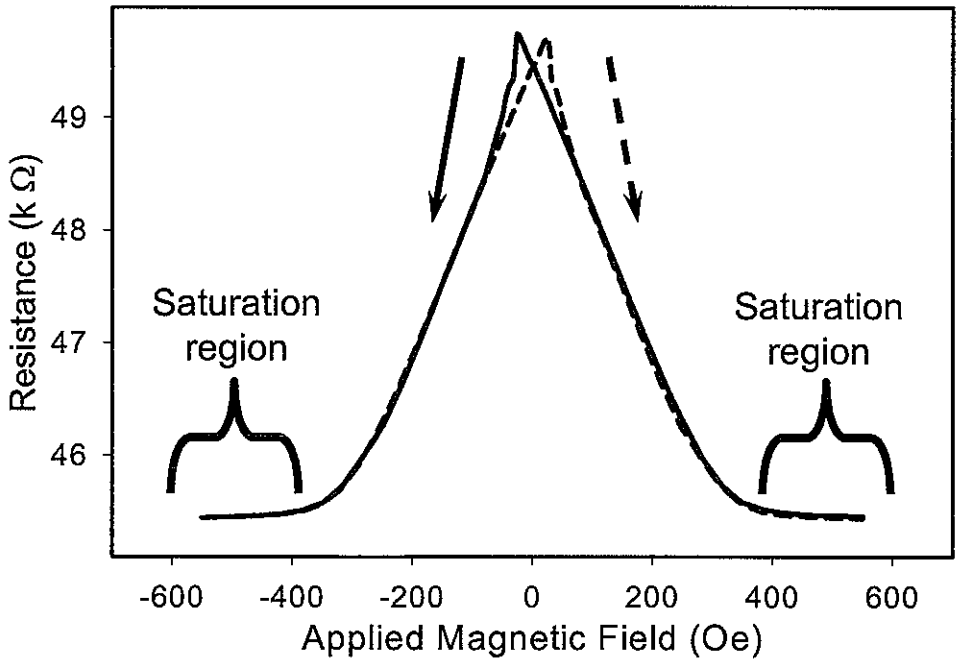
Resistance (k Ω)
49
48
47
46
Saturation region
Saturation region
-600
-400
-200
0
200
400
600
Applied Magnetic Field (Oe)

Figure 1

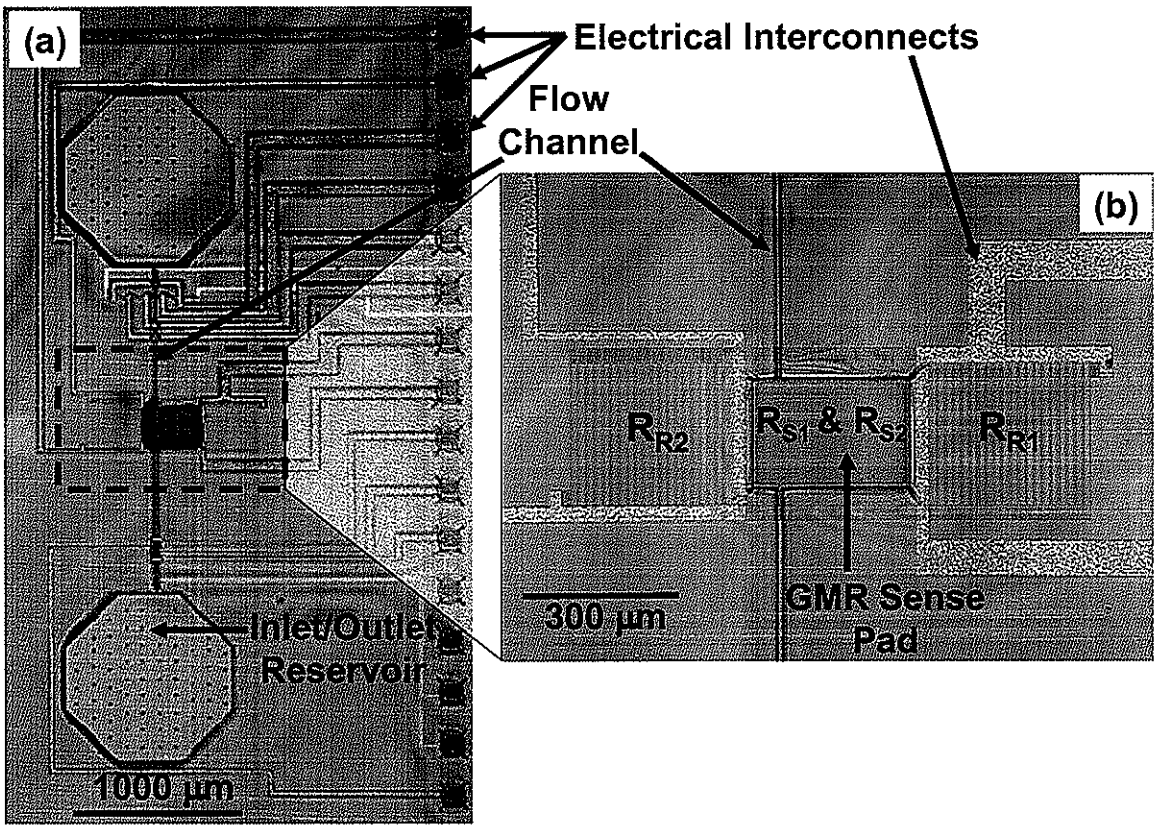
(a)
Electrical Interconnects
Flow
Channel
(b)
R_{R2}
R_{S1} & R_{S2}
R_{R1}
300 µm
GMR Sense
Pad
Inlet/Outlet
Reservoir
1000 µm

Figure 2

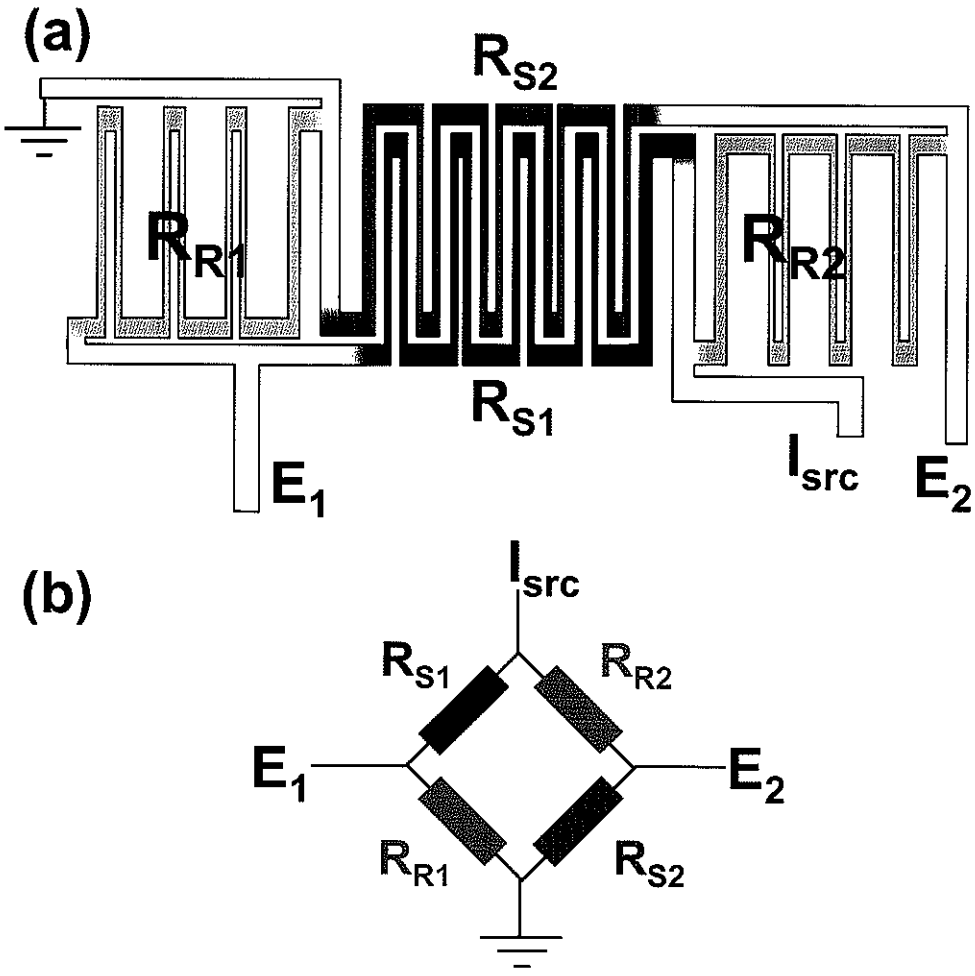

Figure 3

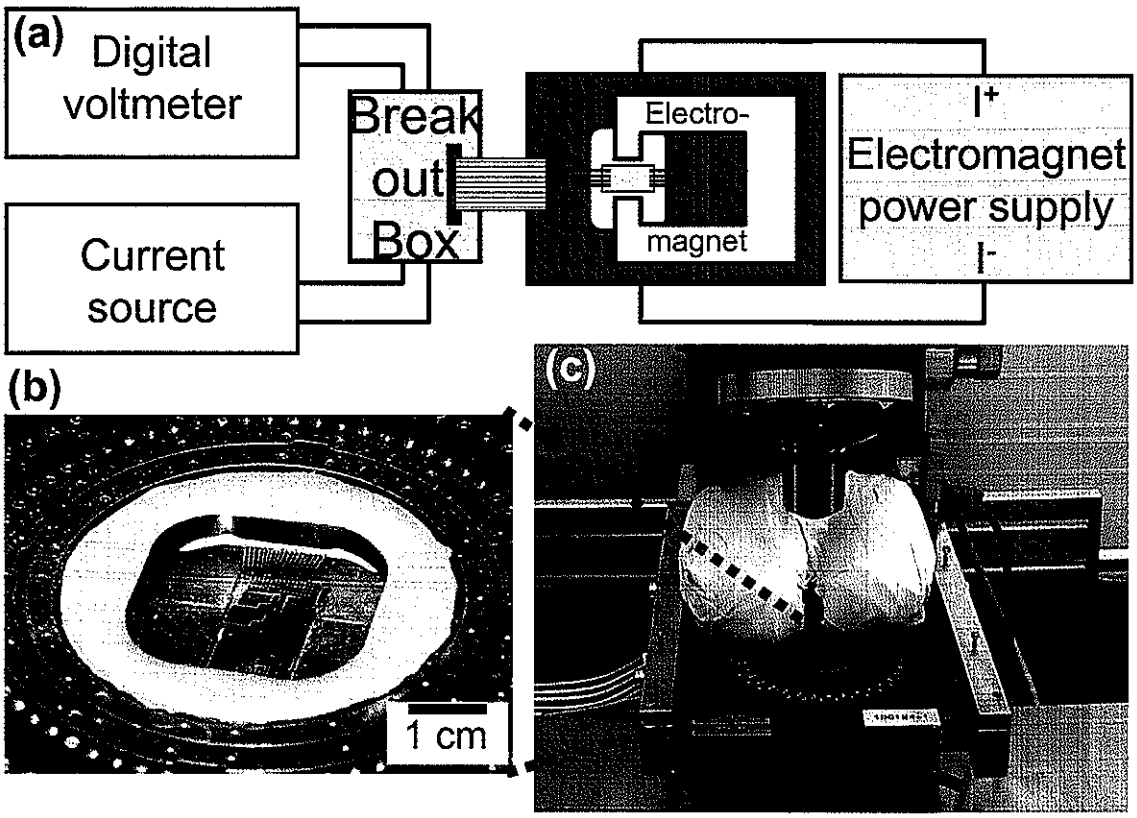
(a)
Digital voltmeter
Current source
Break out Box
Electro-
magnet
I+
Electromagnet power supply
I-
(b)
1 cm
(c)

Figure 4

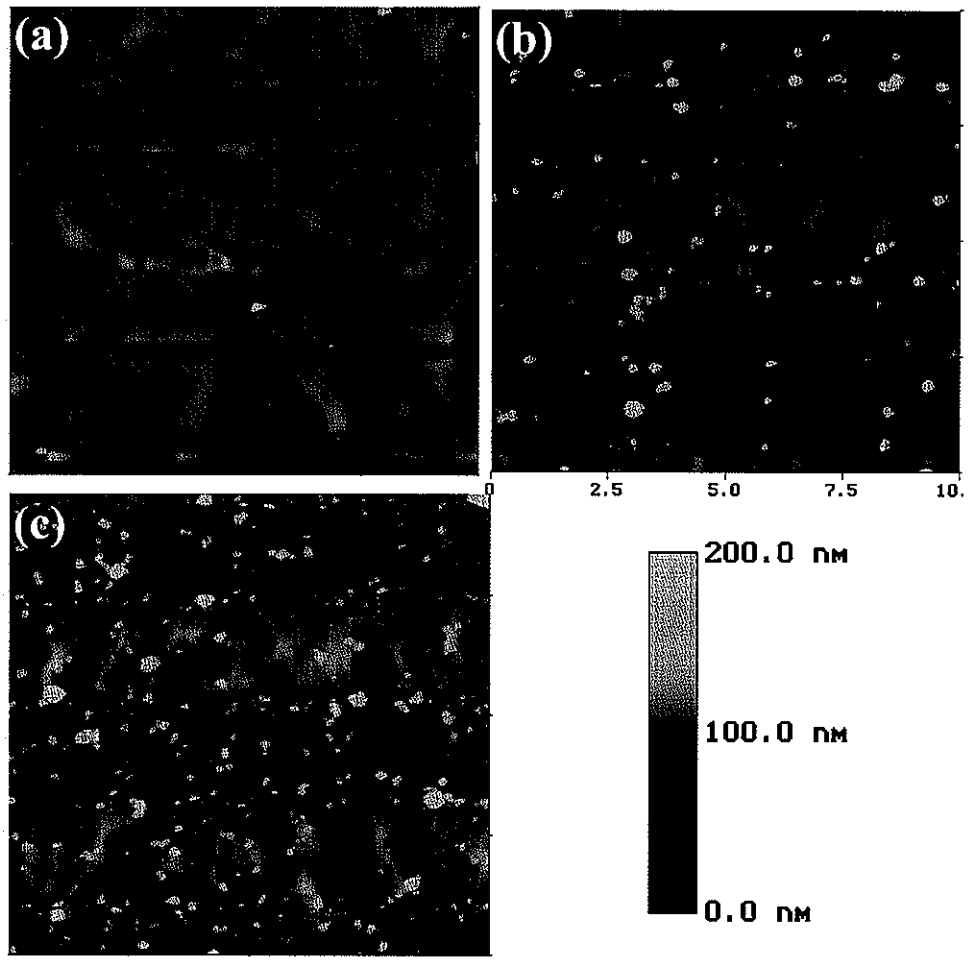

Figure 5

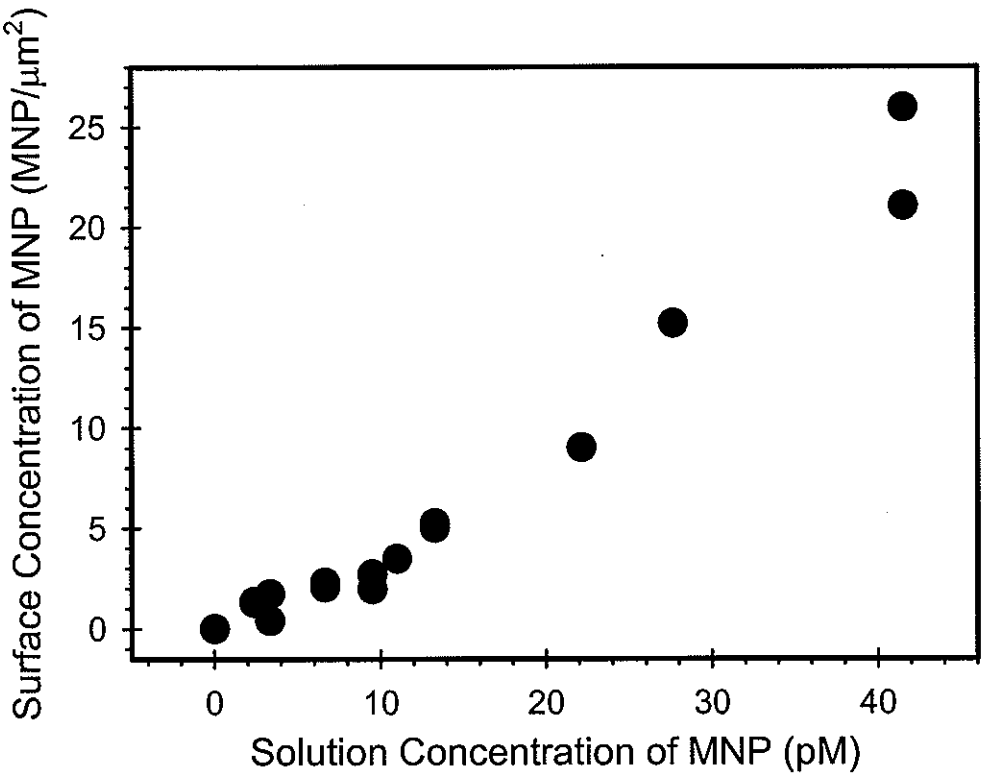
Surface Concentration of MNP (MNP/μm²)
25
20
15
10
5
0
0
10
20
30
40
Solution Concentration of MNP (pM)

Figure 6

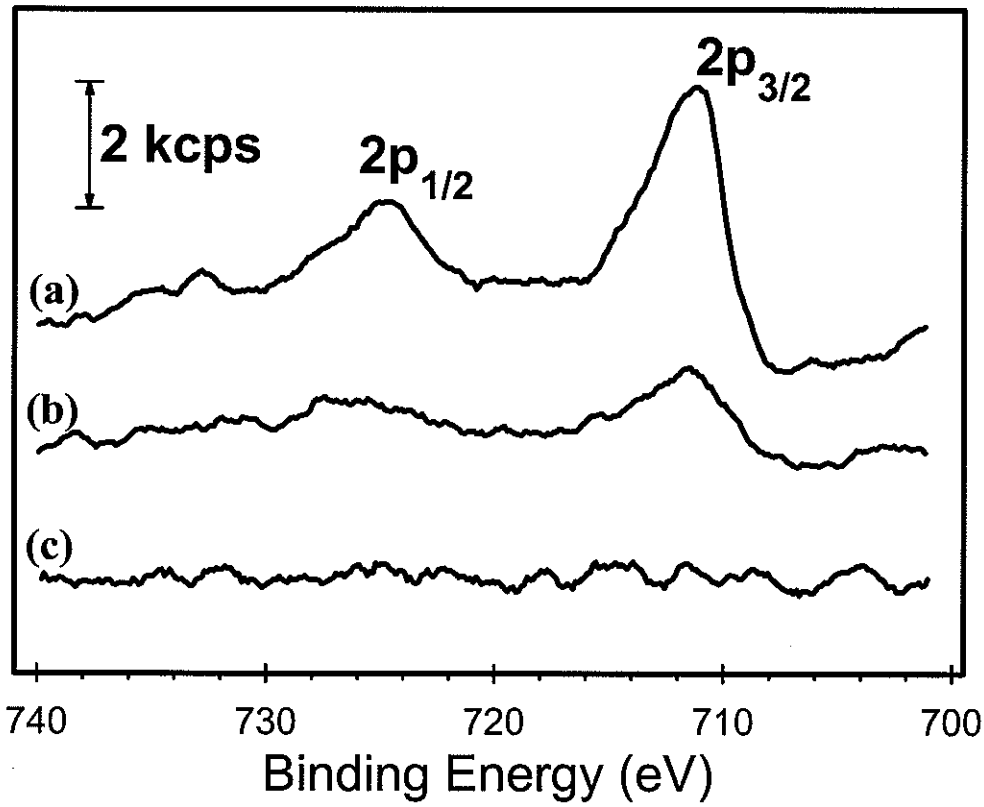

Figure 7

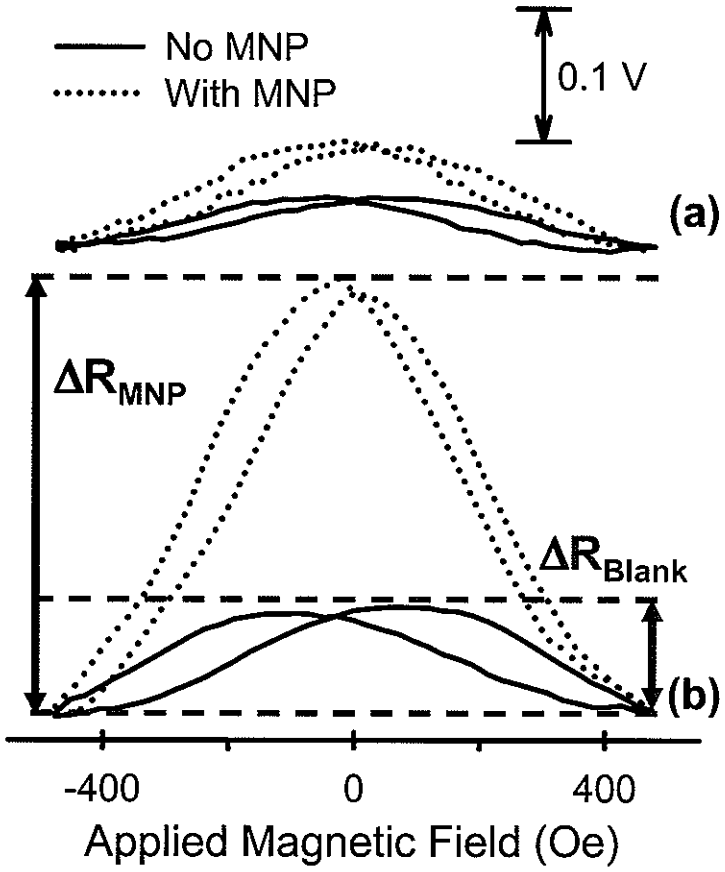
No MNP
With MNP
0.1 V
(a)
ΔR_MNP
ΔR_Blank
(b)
-400
0
400
Applied Magnetic Field (Oe)

Figure 8

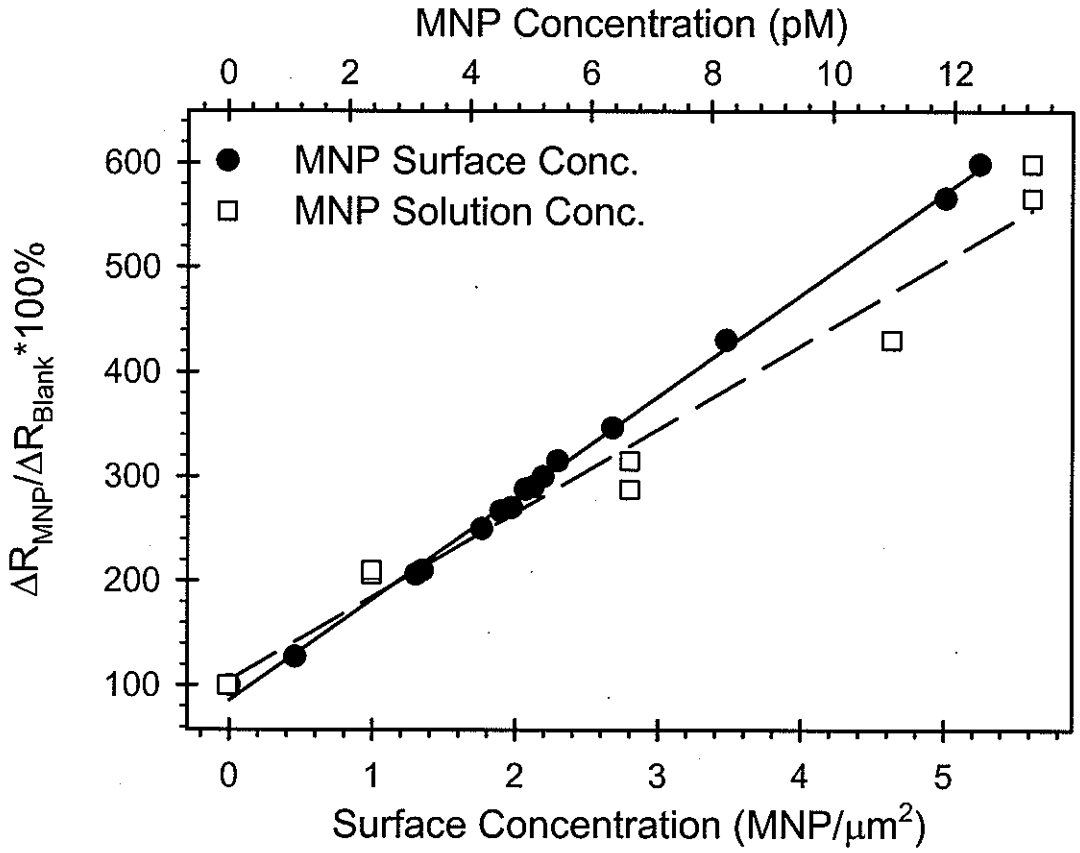
MNP Concentration (pM)
0
2
4
6
8
10
12
600
500
400
300
200
100
MNP Surface Conc.
MNP Solution Conc.
$\Delta R_{MNP}/\Delta R_{Blank}*100\%$
0
1
2
3
4
5
Surface Concentration (MNP/μm^2)

Figure 9

CHAPTER 2: GIANT MAGNETORESISTIVE SENSORS FOR CHIP-SCALE DETECTION OF BIORECOGNITION EVENTS USING SURFACE MODIFICATION AND MAGNETIC LABELS

A manuscript in preparation for submission to *Analytical Chemistry*

Rachel L. Millen, John Nordling, Heather A. Bullen, and Marc D. Porter

Department of Chemistry, Ames Laboratory-USDOE, and Institute for Combinatorial Discovery, Iowa State University, Ames IA 50011

Mark Tondra

NVE Corporation, Eden Prairie, MN 55433

Abstract

Microfabricated devices formed from alternating magnetic and non-magnetic layers (a few hundred nanometers in thickness) exhibit a phenomenon known as the giant magnetoresistance effect. The resistance of these giant magnetoresistors (GMRs) is dependent on the strength of an external magnetic field, a trait that dominates the computer data storage industry in the building of high speed, high data density storage drives. Sensitivity, small size, and speed are also attributes of portable bioanalytical sensors, suggesting that a merger of GMR technology and magnetic labeling strategies may potentially serve as one of the tools in a "point of use" detection strategy in the bioanalytical sciences.

This paper describes the utilization of GMRs for the detection of streptavidin-coated magnetic particles that are selectively captured by biotinylated gold addresses on a 3 × 0.2 cm sample stick. The GMR sensor is the readout method as the sample stick is scanned in a "credit-card" fashion over the sensor. Integrated on-chip magnetic reference addresses

remove any sensor-sample stick separation effects. The detection of streptavidin-coated magnetic particles lays the groundwork for their use as a universal label for antigen detection, e.g., in a sandwich-type immunoassay using biotinylated labels. The magnetic particle surface coverage at the limit of detection was determined to be ~2%. Issues related to mitigation of nonspecific adsorption will also be discussed.

Introduction

Several research laboratories are exploring the utility of giant magnetoresistors (GMRs)as a new tool in the bioanalytical sciences.[1] These efforts are attempting to exploit the attributes central to their widespread use in magnetic data storage as sensitive, high speed, and compact magnetic sensors in computer hard drives.[2, 3] There have been advances in the direction of GMR detection of DNA and proteins.[4-8] Our laboratory has been working with immunosorbent assays on the GMR surface[9], and also toward the use of GMRs in a magnetic flow cytometer.[10]

The magnetic detection capabilities of a GMR are due to their unusually large level of magnetoresistance, i.e., change in resistivity dependent on an applied magnetic field (H_{app}). A material that displays magnetoresistance has a resistivity dependent upon an external magnetic field. Typically materials exhibit small changes in resistance with H_{app} (<1%). GMRs however, can undergo a change in resistance up to 80% at room temperature.[11]

Since GMRs have already proven themselves portable in the computer industry, we are envisioning a credit-card type reader for biodetection. In this scheme, the capture and magnetic labeling of a bioanalyte would take place on a disposable sample stick that would

be scanned past a GMR sensor. The magnitude of the GMR sensor response would then be related to the amount of magnetically-labeled bioanalyte present on the sample stick.

The response of the GMR to magnetic material is distance dependent, in that small changes in the distance between the magnetic sample and the GMR affect the response.[12, 13] To compensate for this distance dependence, we have incorporated an on-chip magnetic reference. The signal from the magnetically-labeled bioanalyte can then be calibrated with the on-chip magnetic reference to give a signal free of effects from variations in sample-sensor distance, as well as the degree of sample-sensor parallelism. The method of scanning itself can also compensate for long-term drift of the GMR signal.[13]

This paper discusses the reaction scheme described in Figure 1 for modifying the sample stick. The bioactive regions of the sample stick are created from patterned gold, modified with an amine-terminated thiolate monolayer. This thiolate monolayer is then biotinylated to simulate a biotinylated biomarker, allowing the use of the same streptavidin-coated superparamagnetic magnetic particles (MPs) as a universal label for varied future assays (e.g., sandwich immunoassays, competitive immunoassays, DNA hybridization). In this work, the concentration of streptavidin-coated MPs reacted with the biotinylated bioactive regions is varied, and the resulting MP-modified sample stick is scanned over a multilayer GMR sensor.

Experimental Section

Surface Biotinylation and Capture of Magnetic Particles

Studies of the binding of streptavidin-modified MPs were accomplished using template-stripped gold (TSG)[14] as the supporting substrate. TSG was prepared by resistively

evaporating a 250-nm layer of gold (99.95% pure) onto a clean silicon (111) wafer at rates of 0.1 and 0.2 nm/s for the first 100 nm of gold and the remaining 150 nm of gold, respectively. After evaporation, a 1 x 1 cm clean glass slide was affixed to the gold film with 2-part epoxy (Epo-Tek), and then cured at 150 °C for 2 h. Next, the glass square was carefully detached from the silicon wafer, which exposes the surface of the gold film that was previously in contact with the silicon substrate.

Biotinylated addresses were created by microcontact printing. This process used a poly(dimethyl)siloxane (PDMS, Dow Corning) stamp with a centered, 3-mm diameter hole to define the active area on the TSG substrate.[15, 16] First, the stamp is inked by immersion into a 2-mM ethanolic solution (USP grade, AAPER) of octadecanethiol (ODT, Aldrich). The stamp is then dried in a high-purity nitrogen stream, placed in contact with the TSG substrate for ~30 s, and removed. The printed substrate is rinsed with ethanol, immersed for ~12 h in an ethanolic solution of 0.1-mM 11-amino-1-undecanethiol hydrochloride (AUT, Dojindo), rinsed again with ethanol, and dried with nitrogen. This step modifies the uncoated, 3-mm address of the stamped substrate with an amine-terminated adlayer.

The AUT-modified substrates were next exposed for ~12 h to a biotinylation buffer, which was prepared by dissolving 1 mg of *N*-hydroxysuccinimidobiotin (NHS-biotin, Pierce) in 1.0 mL of dimethyl sulfoxide (DMSO, Fisher), and subsequently mixed with 50 mL of an aqueous solution of sodium borate buffer (50 mM, Pierce). Finally, the substrates were rinsed with water and dried with nitrogen. All aqueous solutions were prepared with deionized water that was further purified by a Milli-Q system (Millipore).

The particle capture step entailed the exposure of the biotinylated substrates to 20 μL of superparamagnetic magnetic particles (MPs, 1.05-μm diameter) covalently coupled with

streptavidin (37% ferrites, Dynabeads MyOne Streptavidin, Dynal Biotech) for systematically varied amounts of time in a humidified environment. The as-received MPs have a concentration of 1×10^{10} MPs/mL. The presence of the MPs was detected using a JEOL 5910 scanning electron microscope (SEM). This procedure first coated the samples with a thin gold film in a Technics Hummer sputtering system for 2.5 min and 100 mTorr Ar. This step was required to minimize sample charging by the electron beam of the microscope. The surface concentration was determined by averaging the number of MPs at five different locations on each address, using an image size of 1,950 μm^2.

Sample Stick Fabrication

The design and layout of the sample stick, which consisted of alternating nickel and gold addresses, is detailed in Figure 2. Figure 2a shows the entire sample stick; it consists of five gold sample addresses, interspersed between six nickel reference addresses. A close-up of a gold address surrounded by two nickel reference addresses is given in Figure 2b. Both the nickel references and the gold addresses are 200 × 200 μm squares and are spaced 500 μm from each other.

The sample stick was created using photolithographic and metal lift-off techniques. First, a positive photoresist (AZ4330, Clariant) was coated onto 0.5-mm thick Pyrex wafers (University Wafer) at 2000 rpm for 30 s; these samples were then soft baked at 110 °C for 1 min. The photoresist-covered wafer was next exposed to UV light for 4 s using a mask with the pattern for the nickel reference addresses, post-exposure baked for 1 min at 110 °C, and immersed in developer (3:1 water:Shipley 351 developer) for 2 min. After emerging from the developer, the sample stick was coated with a 10-nm layer of nickel at a rate of 0.02–0.05 nm/s, followed by a 15-nm titanium protection layer deposited at 0.1 nm/s. Lift-

off of the nickel-coated photoresist was performed by sonication in acetone (Fisher), immediately followed with an ethanol rinse, and a drying step with a stream of high-purity nitrogen.

The gold addresses were coated onto the nickel-addressed sample sticks by a similar set of spin-coating, patterning, and developing steps, noting that the photomask was carefully positioned on the nickel-addressed sample stick with a mask aligner. In this case, the deposition of an 8-nm titanium adhesion layer (0.1 nm/s) preceded the deposition of a 75-nm film of gold (0.1 nm/s). The sample sticks were again sonicated in acetone, rinsed with ethanol, and dried with nitrogen. Finally, the sample sticks were diced into 2 by 0.3 cm sections by American Dicing.

Sample Stick Biotinylation and Capture of Superparamagnetic Particles

The procedure for the biotinylation of the gold addresses on the sample sticks is a modified version of that used for the TSG substrates described earlier. First, the sample sticks were cleaned in a 40-W Ar plasma for 10 min at 1 torr, immersed in AUT for ~12 h, rinsed with ethanol, and dried with high-purity nitrogen. In this case, the biotinylation solution was a 50/50 mixture (v/v) of the TSG biotinylation solution and glycerol. Using a fused silica capillary (24.0-μm I.D., 148-μm O.D.) and a 50-μL syringe, a droplet of the glycerol/biotinylation solution was placed on each of the gold addresses of the sample stick for 1 h in a humidified environment (Figure 2c); each droplet fully covered one address After rinsing with PBS, the sticks were immersed for ~16 h in 1% bovine serum albumin (BSA, Sigma) in 50 mM borate buffer, which served as a blocking agent. The sticks were again rinsed with PBS (Sigma).

The capture step for the magnetic particles used a 20-μL drop of MP solution that was applied to the entire surface of the sample stick for 2 h in a humidified environment. All the addresses on an individiual sample stick were therefore exposed to the same concentration of MPs. Following MP binding, the sample sticks were rinsed extensively with PBS, rinsed briefly with water to remove residual buffer salts, and dried with nitrogen. The surface concentration of captured MPs was again determined by SEM.

Layout and Production of GMR Chips

Details of the GMR multilayer structure, prepared by standard microfabrication techniques,[9, 17] are described in detail elsewhere.[9, 18] The sensor itself (Figure 3a) is composed of four GMRs arranged as the resistors in a Wheatstone bridge. Two of the GMRs function as sensing resistors and two as reference resistors (Figure 3b).[9] The sensing GMRs are interdigitated as a densely packed, 200 x 200 μm sense pad (R_{S1} and R_{S2}). The two reference GMRs (R_{R1} and R_{R2}) are also laid down in a serpentine pattern, but are positioned on opposite sides of the sensing area defined by the two interdigitated sensing GMRs. The sense and reference GMRs are separated by 30 μm. Each GMR consists of an 11,000 μm long strip that is 2 μm wide, with 2 μm separating the neighboring GMR strips. Each GMR chip is coated with a ~260-nm passivation layer of Si_3N_4, in order to insulate the device during subsequent processing and application steps.

GMR Instrumentation

Other features of the GMR setup are detailed in Figure 3. The GMR chip (Figure 3a) was wire-bonded to a printed-circuit board (Figure 3b) and connected to a current source (Keithley 220) and nanovoltmeter (Keithley 2182) through a breakout box (Figure 3c). The current source supplied 1.0 mA to the GMR-based Wheatstone bridge and the nanovoltmeter

determined the drop (E_1 - E_2) across the GMR bridge. The magnetic field is applied to the system by two electromagnetic coils arranged in a Helmholtz-type configuration, which are energized by a 400 W bipolar operational power supply (Kepco BOP 20-20M). The coils, custom manufactured by Nicollet Technologies, can reach a maximum field of ±550 Oe and can readily maintain the constant H_{app} of 150 Oe for long periods of time (±0.1 Oe in 1 h). The field strength at the GMR surface as a function of the current applied to the coils was verified with a Hall probe gaussmeter (F. W. Bell, Model 5070). The current source, nanovoltmeter, and electromagnet power supply were controlled through a GP-IB interface board by a LabWindows/CVI program that was written in-house.

A constant current of 1.0 mA (I_{src}) is applied to the bridge and the voltage difference (E_1 - E_2) is measured across the bridge to track the change in the resistance of R_{S1} and R_{S2} that arises from the screening of H_{app} by captured superparamagnetic particles. These experiments applied 150 Oe across the GMR platform to magnetize the superparamagnetic labels. This field was also selected based on a characterization of the response of the device as a function of H_{app}; these tests indicated that the device displayed its largest sensitivity to H_{app} at ~150 Oe.[13]

The sample stick, described in Figure 2, is scanned parallel to H_{app} as shown in Figure 3. Each gold address and nickel reference address passes directly over the sense resistor area of the GMR-based bridge at a separation of ~50 μm. In actuality, the GMR-based bridge is moved and the sample stick is held stationary, but for simplicity, we refer to this procedures as "scanning the sample". In recent work, we have shown that the incorporated nickel references effectively compensate for variations in the distance between the sample stick and

sensor up to ~200 μm.[13] Further details of the probe station and the mechanics of scanning the sample stick have been recently described.[13]

Infrared Reflection Spectroscopy (IRS)

The substrates for IRS characterizations were prepared by the resistive evaporation of 225 nm of gold onto a 5-nm titanium adhesion layer previously coated onto 3 x 1 in glass slides. The creation of the AUT-derived monolayer and the subsequent biotinylation reaction followed the procedure described previously. All IRS data were acquired with a Nicolet 850 FT-IR spectrometer, equipped with a liquid nitrogen-cooled HgCdTe detector and under a constant purge with boil-off from liquid nitrogen. Spectra were obtained using *p*-polarized light incident at 80° with respect to the surface normal. The spectra were recorded as $\log(R/R_0)$, where R is the sample reflectance and R_0 is the reflectance of an octadecanethiolate-d_{37} monolayer-coated gold reference substrate. The spectra are an average of 512 sample and reference scans, collected at 4-cm^{-1} resolution with Happ-Genzel apodization.

Results and Discussion

Infrared Spectroscopy Characterization

Biotinylation of the AUT-derived monolayer on gold was verified by IRS. The spectra in Figure 4a is that of the AUT-derived monolayer on gold. The bands at 2922 and 2853 cm^{-1} are diagnostic of the polymethylene chains of the adlayer, whereas the much weaker features around 1600 cm^{-1} are likely due to a combination of N-H bending and C-N bending modes.[19, 20] Moreover, and in accordance to the infrared surface selection rule operative at highly reflective metallic surfaces,[21] the absence of a detectable N-H stretching

mode, which is observed at ~3416 cm^{-1} when AUT is dispersed in KBr,[22] suggests that the N-H linkages are aligned close to the surface parallel.

The adlayer spectrum undergoes a marked change after biotinylation. This result is shown in Figure 4b. Several features emerge that confirm the formation of a biotin terminal group. These bands include the N-H stretch at 3255 cm^{-1}, the overlapped C=O stretch and amide I bands at 1706 cm^{-1}, the amide II band at 1554 cm^{-1}, and the overlapped amide III and biotin ring bands at 1267 cm^{-1}. The increases in the methylene stretching modes and methylene scissors mode (1464 cm^{-1}) are also consistent with the expected changes. Collectively, these spectra confirm the successful completion of the surface modification steps.[23]

MP Incubation Time and Concentration

To determine the time required for the capture step, the surface concentration of the MPs was monitored as a function of binding time at two different MP concentrations on the biotin-modified TSG substrates (Figures 5 and 6). SEM images of TSG substrates exposed to a solution of MPs for 0.5, 1.0, and 2.0 h at concentrations of 0.4 and 17 pM are presented in Figure 5. These images show not only an increase in MP surface concentration with binding time, but also the monodispersity of the MPs, which have diameters (~1 μm) consistent with manufacturer specifications. The images also reveal that the MPs have a tendency to cluster into small domains.

This tendency is likely due to the sedimentation rate of the magnetic particles, which do not remain fully suspended throughout the course of the reaction time. The gravity deposition of the particles described by the ballistic deposition model likely accounts for the non-random particle adsorption.[24, 25] According to the model, the MPs would have a net

gravitational drift toward the substrate surface. When an MP collides with a biotinylated surface free from obstruction, it binds, which is a reasonable conclusion due to the exceptionally strong interaction of biotin and streptavidin. However, if a drifting particle (MP_D) strikes a surface-bound MP (MP_S), the MP_D rolls down the surface of MP_S and binds in close proximity to the attached MP_S, provided space permits. As more MPs accumulate on the surface, the space becomes constricted and the MPs begin to form multiple layers. However, these subsequent MP layers are formed by weak interactions and are removed when the surface is rinsed. In fact, the presence of MP multilayers was not observed in any of the ~350 images analyzed over the course of this work, which further confirms the specificity of the MP surface capture reaction.

The evolution of the number of bound MPs with time in the two sets of experiments is summarized by the plots of MP surface concentration versus time shown in Figure 6. At both solution concentrations, the surface concentrations of captured MPs rise steeply for ~1 h, and then begin to level off. The surface concentration of the 0.4-pM solution of MP appears to saturate at ~0.35 MP/μm^2, while that for the 17-pM solution approaches a plateau at ~0.49 MP/μm^2. These two limits reflect the difference in the absolute numbers of MPs in the two different solutions. Importantly, the number of particles in a 20-μL volume of the 0.4-pM solution (~5×10^6) is very close to that required to pack the surface of the capture substrate at the jamming limit (0.53 MPs/μm^2), assuming the standard ballistic deposition model (i.e., 61% surface coverage).[26, 27] Although the actual surface coverage is not at the jamming limit, the large formation constant for the biotin-streptavidin complex (2.5×10^{13}),[28] coupled with its diffusion limit reaction kinetics in solution,[28] suggests that if an MP contacts the biotinylated surface, it should bind. This idea is further supported by the observation of

the MP surface clusters predicted by the ballistic deposition model, which assumes that binding to the surface is irreversible. However, the MP surface concentration below that expected by the ballistic model, even when considering the plateau approached by the 17-pM solution (0.49 MP/μm^2). In fact, the 20-μL solution of 17 pM MP contains over 40 times the theoretical maximum surface concentration. We attribute the discrepancy to the loss of particles by adsorption to locations beyond the areas defined by address (see Figure 2c) and/or the possible existence of weakly held secondary particle layers. Based on these data, a reaction time of 2 h was selected for use in the binding of MPs to the biotinylated sample sticks (see below).

We also carried out an investigation of the propensity of the labeled MPs to nonspecifically bind to the biotinylated TSG samples. These tests placed 20- and 40-μL of a 80-ng/mL streptavidin solution in PBS buffer onto the biotinylated substrates, in order to competitively block the biotin sites on the TSG surface prior to exposure to solutions of MPs. After ~12 h, these samples were rinsed with PBS buffer and then exposed to a 20-μL drop of a 0.4-pM MP solution for 3 h. Imaging with SEM yielded MP surface concentrations for the 20- and 40-μL streptavidin aliquots of 0.010 MP/μm^2 and 0.006 MP/μm^2, respectively. In the absence of the blocking step, a 20-μL droplet of MPs has a MP surface concentration of 0.357 MP/μm^2. In other words, these tests indicate a fairly low level (2-3%) of non-specific MP binding.

GMR Sample Sticks

After characterization of the biotinylation and MP binding on the TSG substrates, the next experiments applied the same reaction scheme to the sample sticks and subsequent readout by the GMR-based sensor bridge. The results of these experiments are summarized

in Figures 7-9. Figure 7 shows the SEM images of a nickel reference (Figure 7a) and gold addresses (Figure 7b-d), the latter images from three different sample sticks. Figure 8 presents the responses obtained from the GMR scans of the sample sticks, and Figure 9 summarizes the results by plotting the GMR response with respect to both the MP solution and surface concentrations.

The entire nickel reference address is shown in Figure 7a. The presence of only a few particles shows that the of non-specific binding on the reference address is minimal. The images of the gold addresses were obtained for sample sticks exposed to 0.7, 3.0, and 17.0 pM solutions of the MPs. Again, the number of particles tracks with the increase in the MP solution concentration. The corresponding surface concentrations for Figure 7b-d are 0.18, 0.40, and 0.48 MP/μm^2, respectively.

Figure 8 presents the GMR responses obtained when biotinylated sample sticks that were exposed to a 17-pM (Figure 8a) and 3-pM (Figure 8b) solution of streptavidin-modified MPs, were scanned across the GMR bridge. As detailed previously,[10, 13] the response from the passage of a gold sample address (or nickel reference address) exhibits a complex shape. Qualitatively, the response represents the superposition of the magnetic field originating from the moving address material with that of the externally applied magnetic field. Prior to contact with the field from an address, the response reflects only the presence of the constant external field, H_{app}, which is aligned along the long axis of the GMR strips. As the address approaches the sense GMRs, the magnetic field undergoes a decrease as a consequence of the constructive superposition of the field for the address with H_{app}. This situation leads to an increase in the resistance of the sense GMRs. As the edge of the address progresses past the sense GMRs, the total field undergoes a rapid decrease and then a sign change. The sense

GMRs therefore exhibit a rapid decrease in resistance. The pattern then reverses itself as the trailing edge of the addresses moves across the sense GMRs.

The shapes of the profiles in Figure 8 can then be understood by recognizing the effect of having the GMRs wired in a Wheatstone bridge configuration. As such, the observed voltage of the GMR bridge at a fixed applied field can be written according to the diagram in Figure 3b as

$$E_1 - E_2 = I_{src}\left[\frac{R_{R1}R_{R2} - R_{S1}R_{S2}}{R_{S1} + R_{S2} + R_{R1} + R_{R2}}\right] \qquad (1)$$

However, as detailed previously,[9] the resistances of the GMR bridge are imbalanced in that the resistances of the two sense GMRs differ from those of the two reference GMRs. This imbalance arises from the layout of the bridge. The GMRs that function as sensors are interdigitated, whereas those that act as references are not. As a consequence, there is a difference in the dissipation of heat from Joule heating. Interdigitation may also affect the resistance because of the cross-talk between the magnetic fields of neighboring GMR strips that arises from the flow of source current. These effects, while leading to less than 0.1% difference in the two sets of resistances,[9] nevertheless play an important role in formalizing the analytical treatment of the observed response.

Based on this situation, Equation 1 can be recast by invoking: (1) $R_{S1} \approx R_{S2}$, $R_{R1} \approx R_{R2}$, and (2) $R_{S1} \neq R_{R1}$, and by defining $\Delta E = E_1 - E_2$, $R_S = R_{S1}$, $R_R = R_{R1}$. Equation 1 then simplifies to

$$\Delta E = \frac{I_{src}}{2}\left[R_R - R_S\right] \qquad (2)$$

Lastly, in order to quantitatively correlate the responses at different addresses on the same or different sample sticks, the response of a gold sample address is normalized to the responses of the nickel reference addresses on both sides of the sample address. Thus, the "reference-normalized" response ($\Delta E^N_{S,i}$) for a sample address i with respect to those of the two neighboring nickel reference addresses can be written as

$$\Delta E^N_{S,i} = \frac{2\Delta E_{S,i}}{\Delta E_{R,i-1} + \Delta E_{R,i+1}} \qquad (3)$$

where ΔE_R represents the response of the two neighboring nickel reference addresses at i - *1* and i + *1*. As we recently reported,[13] this approach to reference-normalization not only serves as a highly effective means to compare the responses of samples located at different positions on a sample stick, but also those obtained for scans of different sample sticks.

Using Equation 9, the reference-normalized GMR response is plotted as a function of both the surface and solution concentration of MPs in Figure 9 for a series of measurements with sample sticks exposed to MP solutions ranging from 0.4 to 17 pM. As is evident, $\Delta E^N_{S,i}$ exhibits a rapid increase as the MP solution concentration increases, approaching a limiting MP surface concentration that is slightly less than the value found for the 17-pM MP solution in Figure 6. As importantly, $\Delta E^N_{S,i}$ increases linearly with the MP surface concentration, which indicates that there is no detectable cross-talk between neighboring particles and simplifies the quantitative treatment of the results.

Using the data in Figure 9, a plot of MP surface concentration versus MP solution concentration (not shown) can be used to determine a dissociation constant for the biotin-streptavidin interaction of 2×10^{-12}, compared to the reported dissociation constant of

4×10^{-14}.[28] We attribute the difference in the values to the effect the ballistic deposition and bulk of the particles had on the reaction.

The limit of detection for the number of MPs that can be realized using this readout format can be estimated by taking three times the average residual of the linear regression line for the plot of $\Delta E_{S,i}^{N}$ with respect to MP surface concentration. This analysis yields a limit of detection of ~0.02 MP/μm^2. For a 200 × 200 μm sensor, this value corresponds to a total of ~800 MPs. To provide further perspective in terms of this level of performance, a limit of detection of 0.02 MP/μm^2 translates to a surface coverage of 2%. This treatment, albeit not a rigorous "apples to apples" comparison is similar to that found with X-ray photoelectron spectroscopy in the surface science arena.

Lastly, the performance can also be put in rough perspective by assuming that every bound particle corresponds to a single antigen binding event. In other words, the presence of one MP is attributed to the labeling of one antigen, for example, in a sandwich-styled immunoassay. In this case, the ability to detect 800 MPs corresponds to 800 binding events or 1.3 zeptomoles of antigen on a single 200 × 200 μm gold address. While recognizing that these estimations do not account for limitations associated with non-specific binding, cross-reactivity, sample contamination, or specific binding affinity, these projections nevertheless highlight the potential merits in coupling GMRs, our internally referenced sample sticks, and a magnetic labeling strategy as an exciting new tool in the bioanalytical sciences.

Conclusions

In this paper, the value of the GMR in the detection of bioactive magnetic particles has been demonstrated. A new scanning method of detection has also been shown to be an

effective means of utilizing the GMR sensor. This method takes advantage of a new sample stick design which includes an on-chip magnetic reference. The potential of the GMR sensors for use as a readout tool for bioanalytes in settings from the clinical laboratory to the battlefield are exciting.

Furthermore, the streptavidin-modified MPs can be used as a universal magnetic label, which moves the system one step closer to a portable and user-friendly device. We are also exploring methods to detect multiple analytes simultaneously by taking advantage of the small size of the gold addresses. Further improvements to the methodology are also being examined. For example, experiments to balance the size (which has an impact on particle binding) and the magnetic susceptibility (which has a strong effect on the detection of a particle) could lower the limit of detection by increasing magnetic signal and MP binding, while reducing the amount of non-specific binding. Phase-sensitive readout to decrease noise, and also the utilization of other GMR materials and structures are other avenues of exploration for the improvement of the GMR detection setup. Work along each of these lines is underway.

Acknowledgements

Support from NSF's XYZ-on-a-Chip Initiative (#88214), the W. M. Keck Foundation, and DARPA's BioMagnetICs program is gratefully acknowledged. The Ames Laboratory is operated for the U.S. Department of Energy by Iowa State University under contract W-7405-eng-82.

References

(1) Graham, D. L.; Ferreira, H. A.; Freitas, P. P. *Trends Biotechnol.* **2004**, *22*, 455-62.
(2) Baibich, M.; Broto, J. M.; Fert, A.; Van Dau, N.; Petroff, F. *Phys. Rev. Lett.* **1988**, *61*, 2472-75.
(3) Prinz, G. A. *Science* **1998**, *282*, 1660-63.
(4) Ferreira, H. A.; Graham, D. L.; Freitas, P. P.; Cabral, J. M. S. *J. Appl. Phys.* **2003**, *93*, 7281-86.
(5) Schotter, J.; Kamp, P. B.; Becker, A.; Pühler, A.; Brinkmann, D.; Schepper, W. B., H.; Reiss, G. *IEEE Trans. Magn.* **2002**, *38*, 3365.
(6) Schotter, J.; Kamp, P. B.; Becker, A.; Pühler, A.; Reiss, G.; Brückl, H. *Biosens. Bioelectron.* **2004**, *19*, 1149-56.
(7) Miller, M. M.; Sheehan, P. E.; Edelstein, R. L.; Tamanaha, C. R.; Zhong, L.; Bounnak, S.; Whitman, L. J.; Colton, R. J. *J. Magn. Magn. Mater.* **2001**, *225*, 138-44.
(8) Edelstein, R. L.; Tamanaha, C. R.; Sheehan, P. E.; Miller, M. M.; Baselt, D. R.; Whitman, L. J.; Colton, R. J. *Biosens. Bioelectron.* **2000**, *14*, 805-13.
(9) Millen, R. L.; Kawaguchi, T.; Granger, M. C.; Porter, M. D.; Tondra, M. *Anal. Chem.* **2005**, *77*, 6581-87.
(10) Pekas, N.; Porter, M. D.; Tondra, M.; Popple, A.; Jander, A. *Appl. Phys. Lett.* **2004**, *85*, 4783-85.
(11) Daughton, J. M. *J. Magn. Magn. Mater.* **1999**, *192*, 334-42.
(12) Tondra, M.; Porter, M.; Lipert, R. J. *J. Vac. Sci. Technol. A* **2000**, *18*, 1125-29.
(13) Nordling, J.; Millen, R. L.; Bullen, H. A.; Tondra, M.; Porter, M. D. **2005**, Manuscript in preparation.
(14) Stamou, D.; Gourdon, D.; Liley, M.; Burnham, N. A.; Kulik, A.; Vogel, H.; Duschl, C. *Langmuir* **1997**, *13*, 2425-28.
(15) Kumar, A.; Whitesides, G. M. *Appl. Phys. Lett.* **1993**, *63*, 2002-04.
(16) Kumar, A.; Biebuyck, H. A.; Whitesides, G. M. *Langmuir* **1994**, *10*, 1498-511.
(17) Tondra, M.; Anderson, J. M. Magnetizable bead detector. U.S. Patent 6,743,639, June 1, 2004.
(18) Rife, J. C.; Miller, M. M.; Sheehan, P. E.; Tamanaha, C. R.; Tondra, M.; Whitman, L. J. *Sens. Actuators, A* **2003**, *107*, 209-18.
(19) Snyder, R. G.; Maroncelli, M.; Strauss, H. L.; Halknark, C. A. *J. Phys. Chem.* **1986**, *90*, 5623-30.
(20) Bellamy, L. J. *The Infrared Spectra of Complex Molecules*, 2nd ed.; Chapman and Hall: London, 1980.
(21) Greenler, R. G. *J. Chem. Phys.* **1966**, *44*, 310-15.
(22) Wallwork, M. L.; Smith, D. A.; Zhang, J.; Kirkham, J.; Robinson, C. *Langmuir* **2001**, *17*, 1126-31.
(23) Riepl, M.; Enander, K.; Liedberg, B.; Schaferling, M.; Kruschina, M.; Ortigao, F. *Langmuir* **2002**, *18*, 7016-23.
(24) Faraudo, J. *Phys. Rev. Lett.* **2002**, *89*, 276104.
(25) Talbot, J.; Ricci, S. M. *Phys. Rev. Lett.* **1992**, *68*, 958-61.
(26) Evans, J. W. *Rev. Mod. Phys.* **1993**, *65*, 1281-329.
(27) Senger, B.; Voegel, J.-C.; Schaaf, P. *Colloids Surf. A* **2000**, *165*, 255-85.

(28) Green, N. M. In *Methods in Enzymology: Avidin-Biotin Technology*; Wilchek, M., Bayer, E. A., Eds.; Academic Press: New York, 1990; Vol. 184, pp 54-55.

Figure Captions

Figure 1. Reaction schematic (not to scale). The process first exposes NHS-biotin to a gold surface coated with a monolayer formed from AUT, which couples biotin to the adlayer and yields N-hydroxy succinimide as the leaving group. After modification, the sample is exposed to a solution of streptavidin-conjugated MPs which are then captured by the substrate via streptavidin-biotin coupling.

Figure 2. Sample stick micrographs. (a) The 2 × 0.3 cm sample stick was created using photolithography procedures to consist of alternating 200 × 200 μm nickel reference and gold sample addresses. (b) An expanded view (1.8 × 0.7 mm) of two nickel reference addresses neighboring a gold sample address. (c) Example of the placement of a sample droplet onto a biotinylated gold sample address.

Figure 3. Photomicrographs and instrumentation schematic of the GMR reader. (a) The 200 × 200 μm GMR sensors (R_{S1} and R_{S2}) are wired in a Wheatstone bridge format (b) with two similarly sized reference GMRs (R_{R1} and R_{R2}). The external magnetic field (H_{app}) is applied along the long axis of the GMR sensor strips. (c) The GMR chip is wire-bonded to a green printed-circuit board, which is connected to a breakout box through a larger circuit board interconnect. (d) The breakout box is then connected to a digital voltmeter and current source. The electromagnet power supply is connected to two electromagnet coils (not shown) in a Helmholtz configuration set on either side of the GMR sensor. The sample is scanned back and forth across the sensor, parallel to the direction of H_{app}.

Figure 4. Infrared reflectance spectra of the AUT-derived monolayer on gold before biotinylation, showing the peaks due to the alkyl stretch at 2800 and 2750 cm^{-1} (a), and after (b) reaction with NHS-biotin to form a biotin-terminated surface. The new bands (3255 (N-H stretch), 1706 (C=O stretch, biotin; amide I shoulder), 1554 (amide II), 1464 (CH_2 scissors deformation), and 1267 cm^{-1} (amide III & biotin ring) confirm the presence of biotin on the surface.

Figure 5. SEM images of TSG substrates displaying bound streptavidin-modified MP. The TSG substrates were incubated with two solution concentrations of MP, 0.4 (a-c) and 17 pM (d-f). With increasing reaction time (images from left to right at 0.5, 1.0, and 2.0 h) the MP surface concentration observably increases at a MP solution concentration of 0.4 pM; however, with a MP solution concentration of 17 pM, little change is observed after 1 h. MP surface concentrations in MP/μm^2: (a) 0.15, (b) 0.30, (c) 0.34, (d) 0.37, (e) 0.48, and (f) 0.48 MP/μm^2.

Figure 6. Plot of MP surface concentration versus time. The surface concentration of the 17-pM solution of MP saturates near 0.5 MP/μm^2, while the 0.4 pM solution reaches a plateau at ~0.35 MP/μm^2.

Figure 7. SEM images of sample sticks exposed to streptavidin-modified MP. A nickel reference square (a) and MP bound to a gold bioactive address (b) from a sample stick exposed to 0.7 pM MP are shown. Bound MP from sample sticks exposed to 3 pM MP (b) and 17 pM MP (c) are also shown, displaying the decrease in the number of bound MP with

decreasing MP concentration. Surface concentrations of MP from the entire address, of which a portion is displayed in (b), (c), and (d) are 0.176, 0.404, and 0.478 MP/μm^2, respectively.

Figure 8. Plots of the GMR response (ΔE) of a biotinylated sample stick exposed to 17 pM (a) and 3 pM (b) streptavidin-coated MP. Each reference and sample address evokes a complex response from the GMR sensor with two maxima and a minimum for each square. The asterisks highlight the response from the gold addresses. The aberrant signal from the fourth gold address in (b) is due to the mechanical issues during sample stick creation.

Figure 9. Plot of normalized GMR response ($\Delta E_{S,i}^{N}$) versus MP solution concentration and MP surface concentration. Each data point is a single gold address. The line plots the regression of the referenced GMR signal versus the MP surface concentration ($y = 2.1x + 0.009$, $R^2 = 0.9988$). The error was propagated from the error of the GMR responses of the gold and nickel addresses before reference-normalization, and the error bars are approximately the size of the data points.

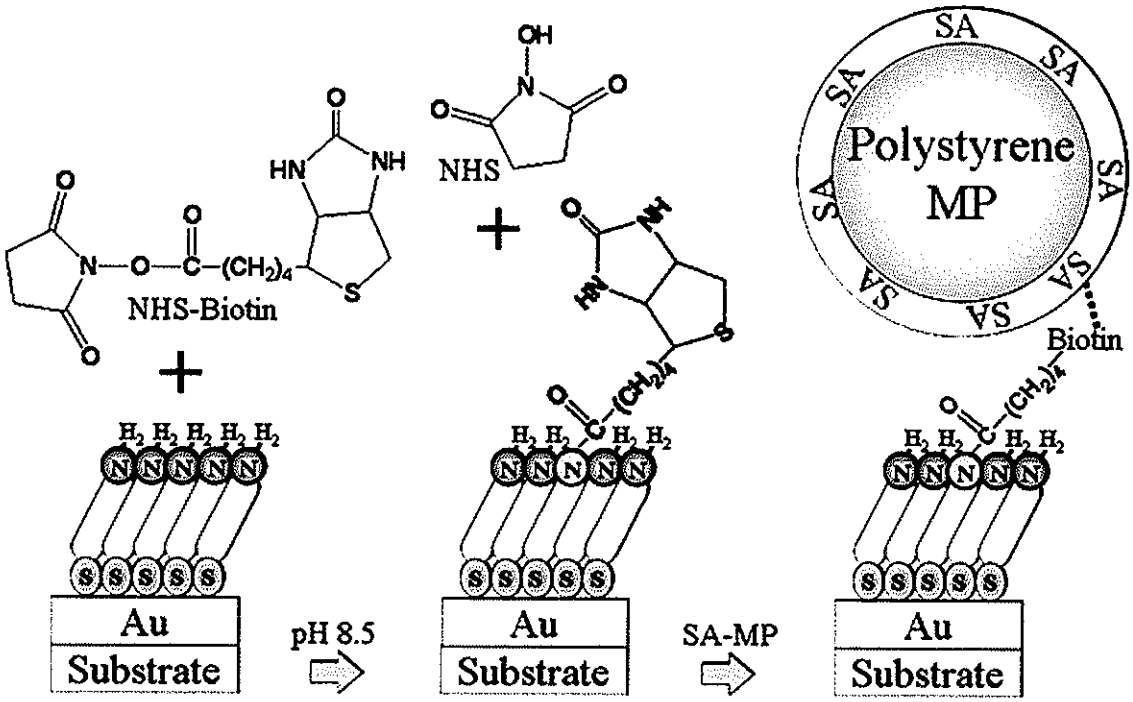
NHS-Biotin
NHS
pH 8.5
SA-MP
Au
Substrate
Polystyrene
MP
SA
Biotin

Figure 1

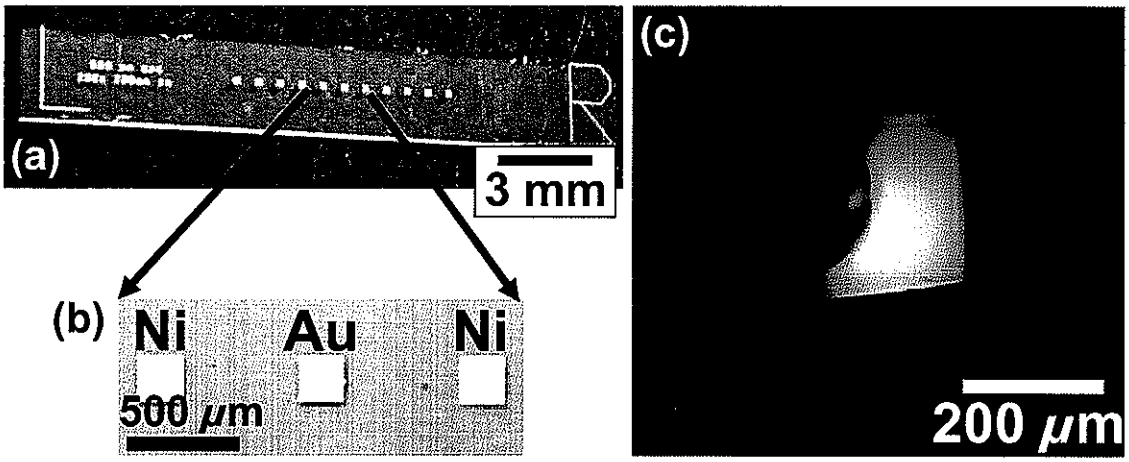

Figure 2

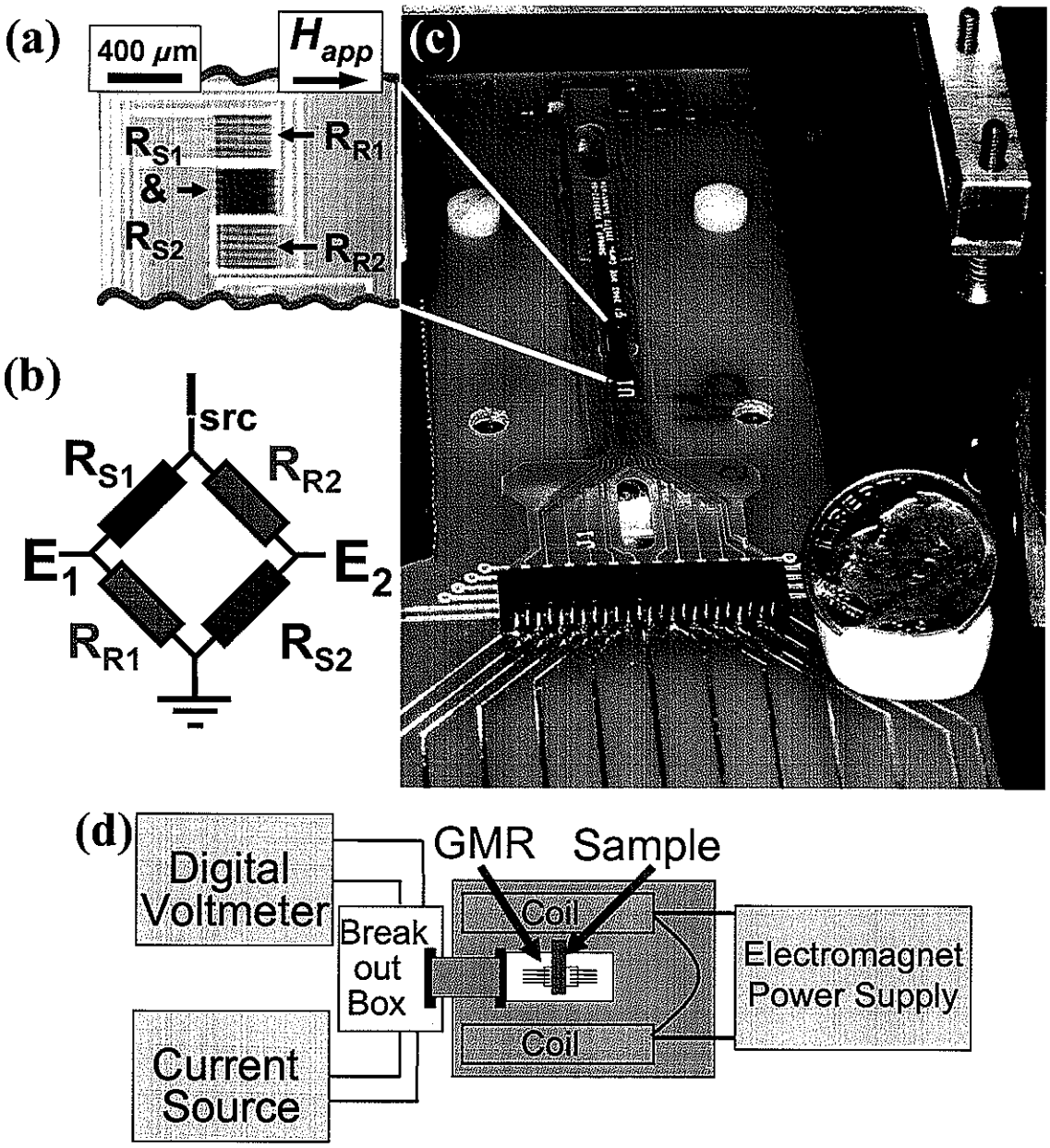
(a)
400 μm
H_{app}
R_{S1}
R_{R1}
&
R_{S2}
R_{R2}
(b)
src
R_{S1}
R_{R2}
E_1
E_2
R_{R1}
R_{S2}
(c)
(d)
Digital Voltmeter
Break out Box
Current Source
GMR
Sample
Coil
Coil
Electromagnet Power Supply

Figure 3

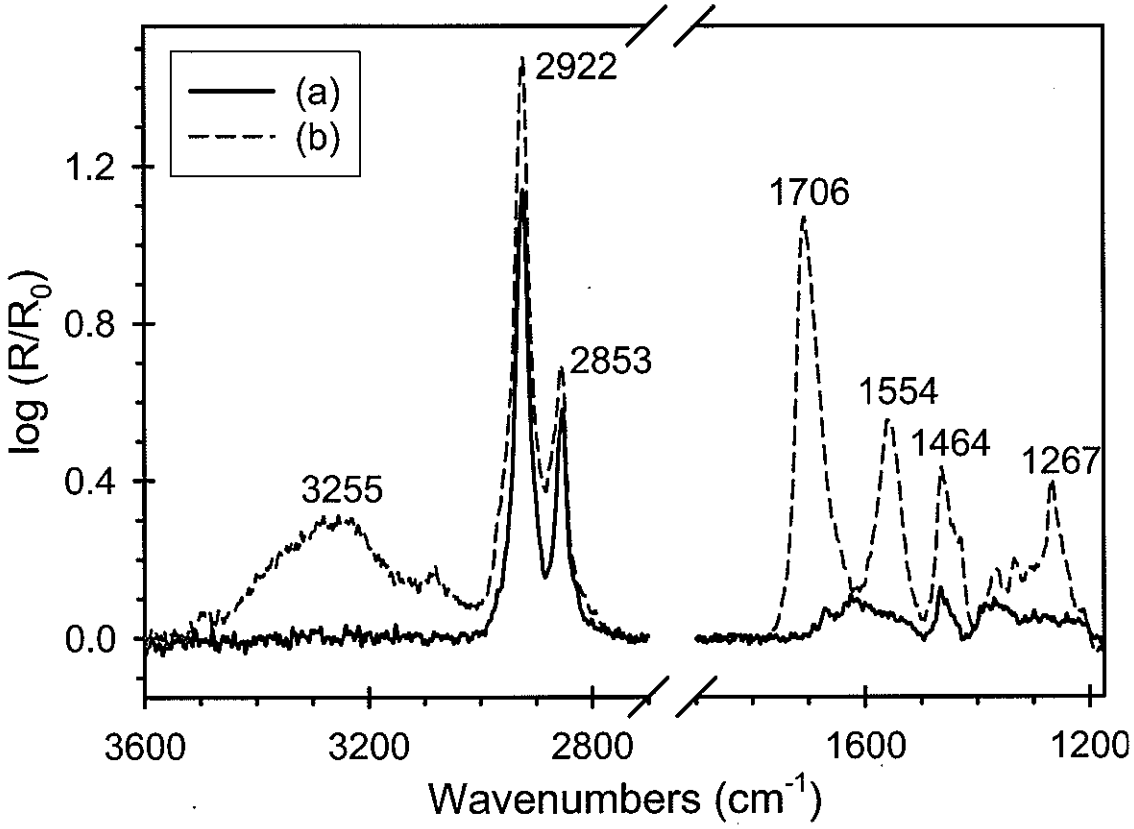
(a)
(b)
2922
1706
2853
1554
1464
1267
3255
1.2
0.8
0.4
0.0
log (R/R0)
3600
3200
2800
1600
1200
Wavenumbers (cm-1)

Figure 4

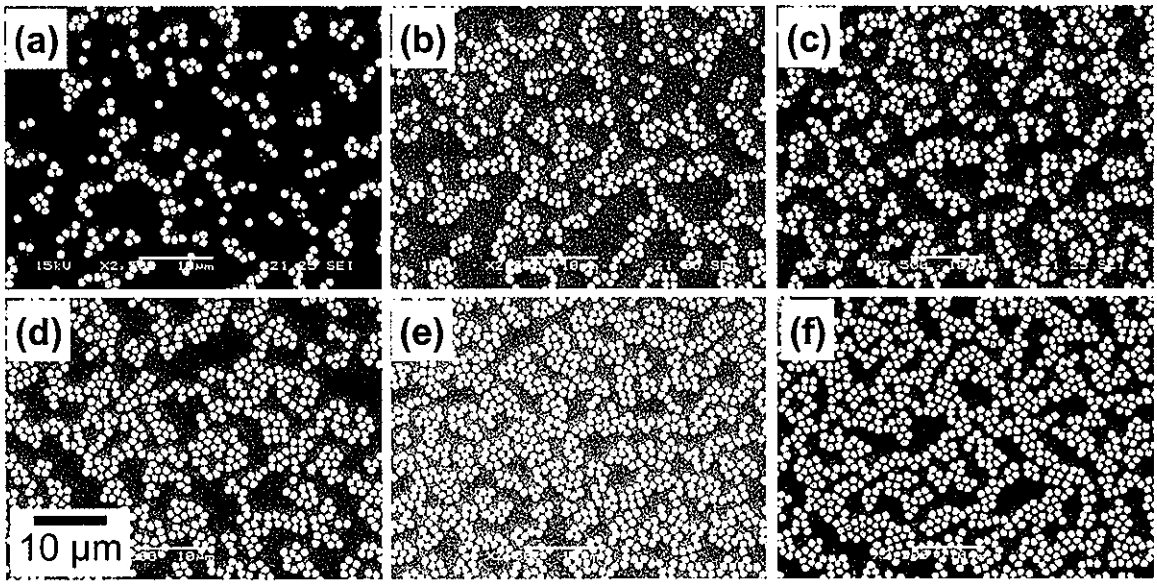

Figure 5

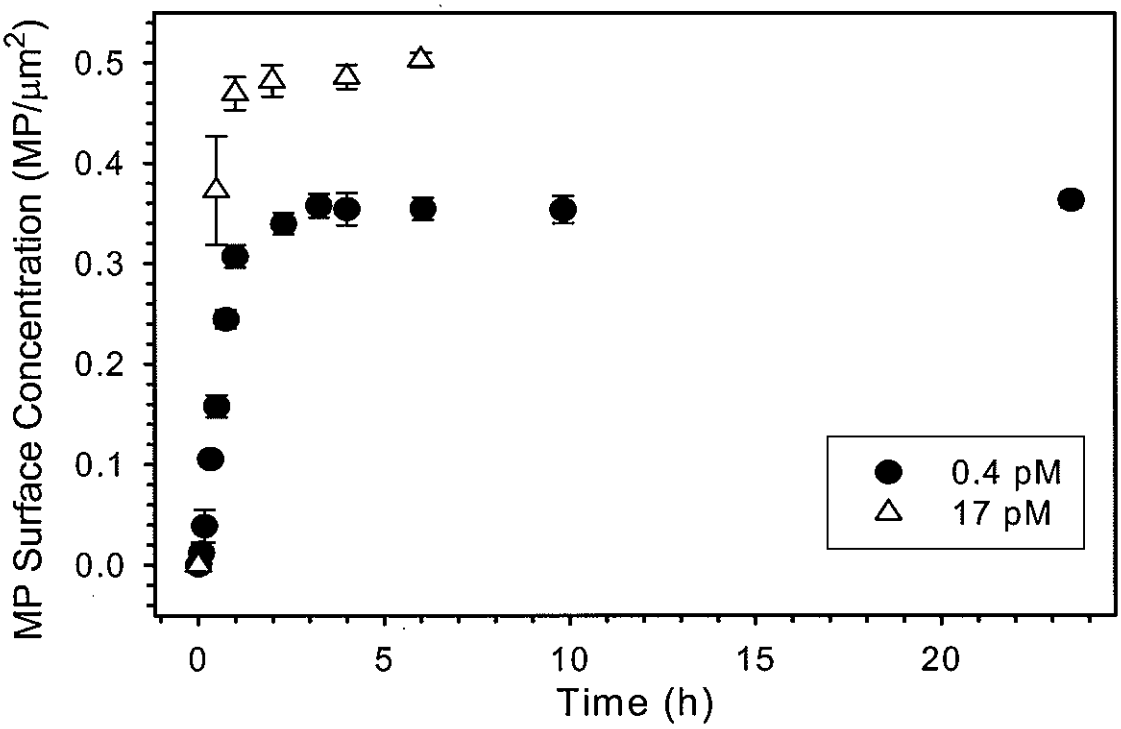
MP Surface Concentration (MP/μm²)
0.0
0.1
0.2
0.3
0.4
0.5
0
5
10
15
20
Time (h)
0.4 pM
17 pM

Figure 6

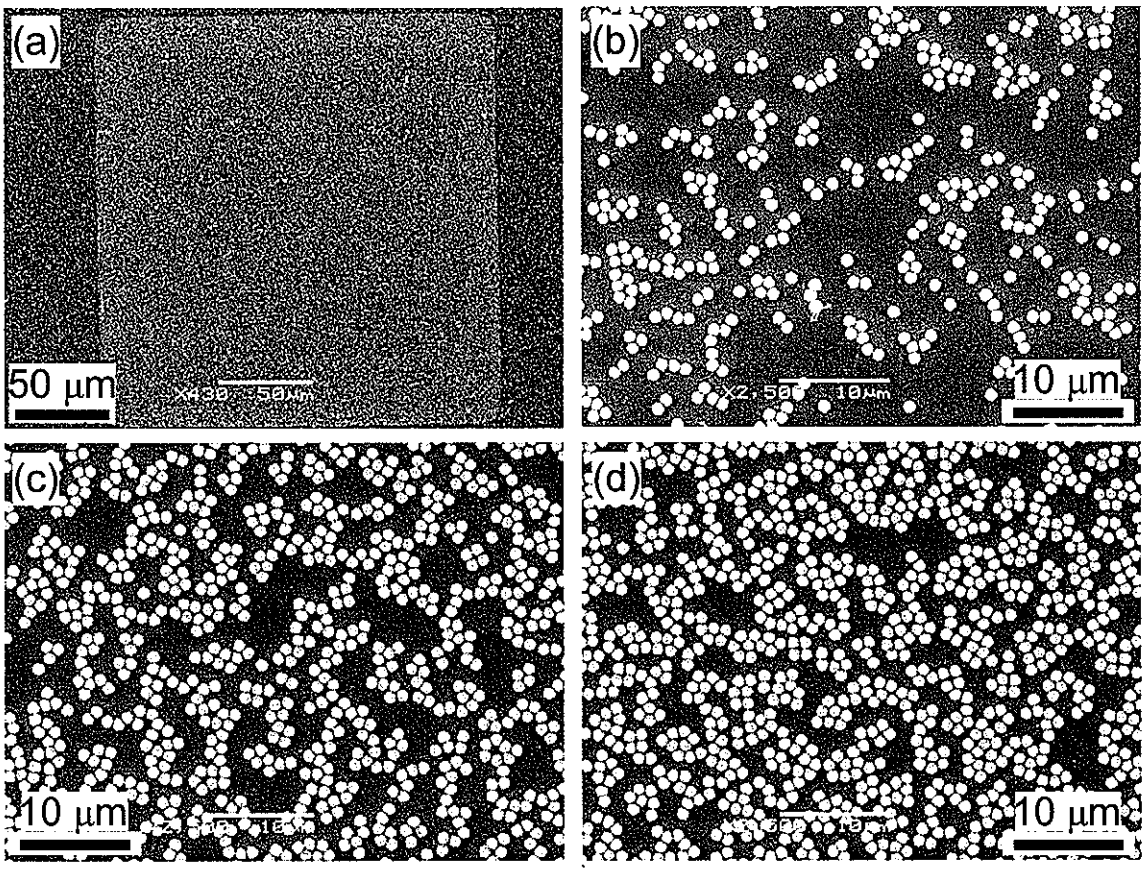

Figure 7

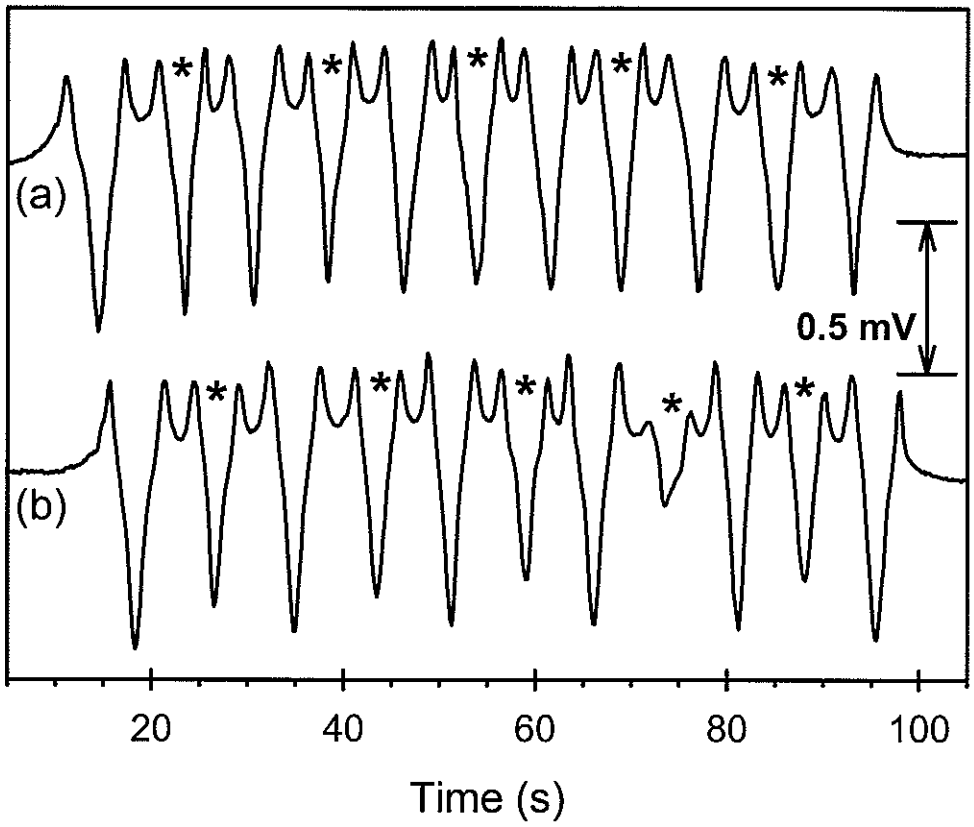

Figure 8

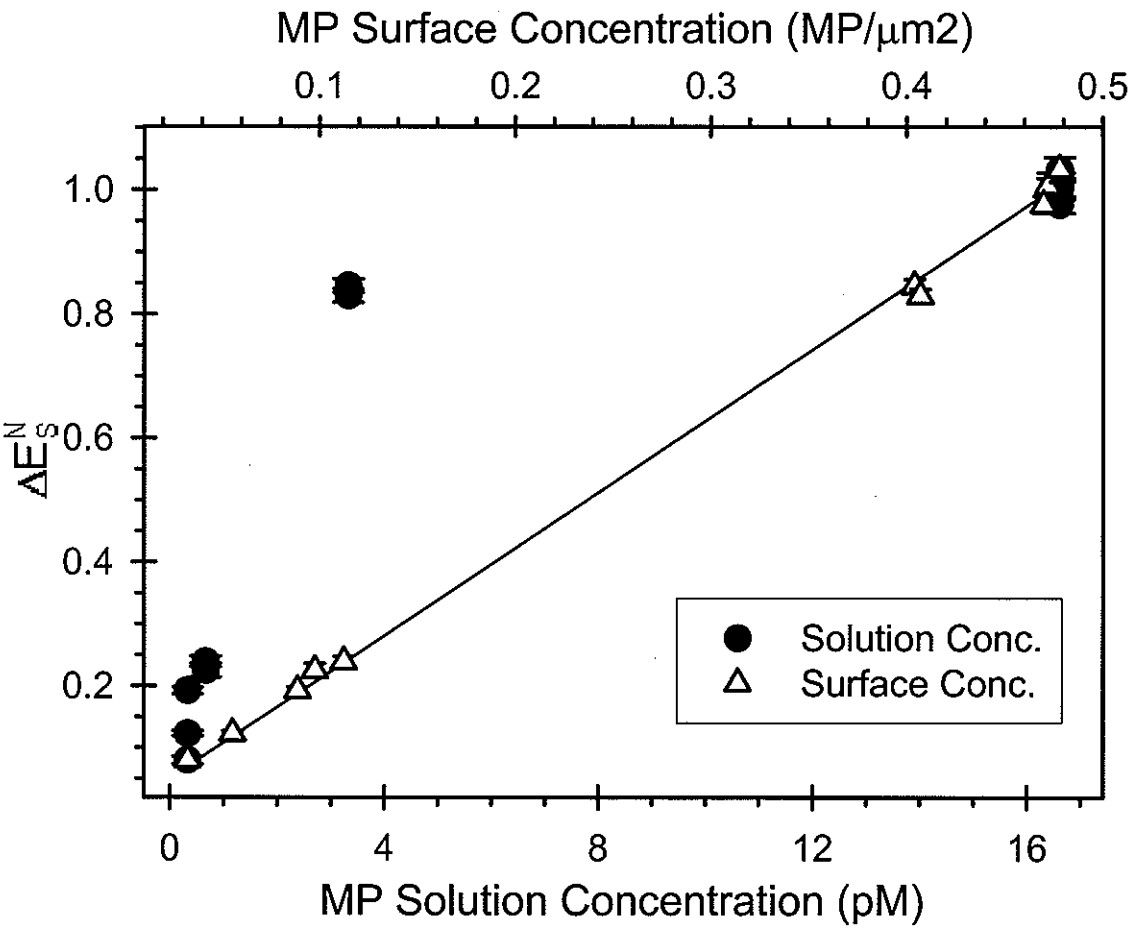
MP Surface Concentration (MP/μm2)
0.1
0.2
0.3
0.4
0.5
1.0
0.8
0.6
0.4
0.2
ΔE_S^N
Solution Conc.
Surface Conc.
0
4
8
12
16
MP Solution Concentration (pM)

Figure 9

CHAPTER 3: CHIP-SCALE DETECTION OF ANTIBODY-ANTIGEN RECOGNITION EVENTS OF RABBIT IgG USING GIANT MAGNETORESISTIVE SENSORS, MAGNETIC LABELS, AND AN INTEGRATED MAGNETIC REFERENCE

A manuscript in preparation for submission to *Nano Letters*

Rachel L. Millen, John Nordling, Heather A. Bullen, and Marc D. Porter

Department of Chemistry, Ames Laboratory-USDOE, and Institute for Combinatorial Discovery, Iowa State University, Ames IA 50011

Mark Tondra

NVE Corporation, Eden Prairie, MN 55433

Abstract

Giant magnetoresistance is a phenomenon used by the computer data storage industry for the creation of high speed, high data density storage drives. The microfabricated giant magnetoresistors (GMRs) are constructed of alternating nonmagnetic and magnetic layers (a few hundred nanometers in thickness), the resistance of which depends on the strength of an external magnetic field. The features of these sensors (i.e., sensitivity, small size, and speed) are desirable features of portable bioanalytical sensors. A strategy to combine GMR sensor readout with magnetic labeling of biomolecules may be used to form a bioanalytical toolbox.

This paper describes the merger of GMR technology, biotin-streptavidin magnetic labeling strategies, and the creation of a disposable, self-referenced sample stick for the detection of immunoassay binding events. Specifically, the presence of rabbit IgG was detected using a sandwich assay conformation. Bioactive addresses on the disposable sample stick were labeled with capture antibody and reacted with antigen, which is labeled with a

biotinylated protein. The labeled protein was then reacted with streptavidin-coated magnetic particles. The sample stick was scanned over the GMR sensor for readout in a "credit-card" type fashion, and the GMR signal was equated to the amount of magnetically labeled rabbit IgG captured on the surface of the sample stick and referenced to the incorporated on-stick reference addresses. Issues related to the small size of the capture antibody address, assessments of GMR detection capabilities, and potential applications are described.

Introduction

Since the first report in 1962 by Clark and Lyons,[1, 2] there has been an ever-increasing interest in the clinical and field application of biosensors. There are many methods that exist for the determination of biolytes, all of which have their own set of strengths and limitations. Some of the more common techniques are enzyme-linked immunosorbent assays (ELISA),[3] cell culture methods,[4] PCR,[5] and fluorescence spectroscopy.[6]

In the data storage industry, a different revolution began with the discovery of the giant magnetoresistance effect in 1988.[7, 8] Giant magnetoresistors (GMRs) are now utilized in virtually all read/write heads in computer hard-drives for compact, high-density, and high-speed information retrieval and storage.

In the search for a novel biosensor with the preferred traits of sensitivity, small size, speed, and a potential for multiplexing, the detection of magnetically-labeled bioanalytes with a GMR sensor is particularly intriguing in view of its attributes already exploited by the computer industry. GMR sensors and magnetic labels have been used to detect DNA hybridization events,[9-13] and streptavidin-biotin binding.[14, 15] Our group has also been exploring the GMR sensor and magnetic properties in general. Fluidic actuation devices

(i.e., pumps),[16, 17] sample and label diverters,[18, 19] and the detection of flowing magnetic particles[20] have been studied within microfluidic channels. The GMR as a platform for immunosorbent assays has been initially investigated both on a functionalized GMR sensor[21] and in a scanning "credit-card type" GMR reader.[22] The mechanism and theory of the scanning GMR reader and an integrated on-chip magnetic reference have also been examined.[23]

Many materials display some form of magnetoresistance, which is the dependence of material resistivity on an external magnetic field (H_{app}). Usually this resistivity change is less than 1%, but when the magnitude of the change is much larger, up to 80%, the dependence is labeled giant magnetoresistance. The structures which display giant magnetoresistance are constructed from layers of alternating magnetic and nonmagnetic materials, the number and composition of which determine the type of GMR. The layers are thin, with thicknesses on the order of the mean free path of an electron.[24] This unique construction leads to the quantum mechanical GMR effect caused by the spin-polarized transport of electrons within the GMR. Explanation of the theoretical underpinnings of this effect can be found elsewhere,[25-27] but in brief, the GMR sensor resistance change with an external magnetic field is due to the changing alignment of the magnetic moments of the magnetic layers.

This paper expands upon the earlier work that laid the groundwork for the scanning GMR reader by characterizing the response of the GMR to ferromagnetic thin films and magnetic particles (MP), as well as describing the function of ferromagnetic thin films as an integrated reference.[22, 23] The current work utilizes the immunosorbent assay scheme described in Figure 1 (not drawn to scale in order to display all components clearly). The

sample stick, a linear array of alternating on-chip nickel reference and gold addresses, is modified so that the gold address is coated with a capture antibody capable of binding an unknown concentration of antigen. The antigen is further reacted with biotinylated label antibody, followed by streptavidin-modified magnetic particles (MP). The sample stick is then scanned directly over the GMR sensor, and the change in resistance that arises from each address as it passes over the GMR is recorded. The resistance change caused by the scanning of the gold address is compared to that from the nickel reference addresses in order to compensate for sample to sample variations in distance between the GMR and the address. This paper reports on the creation of a sample stick with gold addresses modified with goat α-rabbit IgG as the capture antibody for the detection of the antigen rabbit IgG through labeling with biotinylated goat α-rabbit IgG and streptavidin-modified MP. The normalized GMR response is then correlated with the concentration of the rabbit IgG antigen. Two different types of MP are compared and contrasted. Issues related to the complications of mass transport to small capture addresses, assessments of GMR detection capabilities, and potential applications are also discussed.

Experimental Section

Sample Stick Fabrication

The sample stick of alternating nickel and gold addresses, shown in Figures 2a and 2b, was created using photolithographic and metal lift-off techniques. Each sample stick consists of eleven 200 × 200 μm alternating nickel reference addresses and gold sample addresses, with 500 μm separating neighboring addresses. Some sample sticks were also created with circular gold addresses (200-μm diameter); their use will be specified in the

results. The first step in creation of the sample sticks coated a positive photoresist (AZ4330, Clariant) onto Pyrex wafers (0.5 mm thick, University Wafer) at 2000 rpm for 30 s, which was followed by a 1 min soft bake at 110 °C. A 4-s UV exposure time was used to pattern the photoresist using a mask with open areas in the location of the nickel reference addresses. The samples were then post-exposure baked for 1 min at 110 °C, and immersed in developer (3:1 water:Shipley 351 developer) for 2 min. A thin film of nickel (10 nm) was deposited on the samples at a rate of 0.02–0.05 nm/s, followed by the deposition of a 15-nm titanium layer (0.1 nm/s) to protect the nickel film. Lift-off was performed by sonication in acetone. The samples were then rinsed with ethanol and dried with a nitrogen stream. The spin-coating, patterning—this time with a carefully aligned mask for the gold addresses of the samples—and developing steps were repeated on the nickel-patterned samples. An 8-nm titanium adhesion layer was deposited on the patterned samples at 0.1 nm/s, followed by a 75-nm gold film deposited at 0.1 nm/s. For lift-off, the samples were sonicated in acetone, rinsed with ethanol, and dried with nitrogen. The samples were diced into 2 × 0.3 cm sample sticks by American Dicing. All metal deposition used resistive evaporation with an Edwards Auto 306 coating system.

Covalent Immobilization of Capture Protein on Sample Sticks

The sample sticks were prepared for use as a capture substrate by the selective application of capture antibodies to the gold addresses. This process began by cleaning the sample sticks in a 40-W Ar plasma at 1.0 torr for 10 min. The sample sticks were then completely immersed in an ethanolic 0.1 mM dithiobis(succinimidyl propionate) (DSP) solution ~12 h. Next, as shown in Figure 2c, small droplets of 200 μg/mL goat α-rabbit IgG capture antibody in 40% glycerol (v/v) in 50 mM sodium borate buffer (pH 8.5) were applied

to the gold addresses using a fused silica capillary (24.0-μm I.D., 148-μm O.D.), a syringe, and micromanipulators. To combat non-specific binding, a 200-μg/mL solution of bovine serum albumin (BSA) in 40% glycerol and borate buffer was applied to the nickel addresses, and the sample sticks were left undisturbed for 30 min in a humidified environment. After the covalent binding of the antibody to the succinimidyl end group of the DSP-derived monolayer,[28-30] the sample sticks were rinsed four times with 10 mM phosphate-buffered saline (PBS) by volume displacement, and placed in 1% BSA in borate buffer ~12 h as a blocking step to further minimize non-specific binding.

Antigen Application and Labeling Steps

The antigen (rabbit IgG) was diluted in PBS to differing concentrations before binding to the capture antibody surface. The antigen was applied in 20-μL drops to the entire sample stick, held in a humidified environment for a given incubation time (see below), and then rinsed with PBS buffer. The label was a solution of 2 μg/mL biotinylated goat α-rabbit IgG in PBS, and was also applied as a 20-μL drop to the sample stick in a humidified environment for ~12 h. The volume and concentration of label antibody were chosen to be one-hundred times in excess of that necessary to saturate the five 200-μm gold squares.

Streptavidin-modified superparamagnetic particles were applied as 20-μL drops to the entire sample stick for 3 h in a humidified environment. The majority of the experiments used 1.05-μm MP coated with streptavidin (~1×10^{10} MP/mL, 37% ferrites, MyOne Streptavidin Dynabeads, Dynal Biotech). MP binding was characterized qualitatively with optical microscopic images (Olympus BX5OWI Epi-fluorescence microscope). However, some experiments used the 145-nm diameter streptavidin-conjugated Captivate™ ferrofluid (FF) available from Molecular Probes.

Layout and Production of GMR Chips

The GMR is a multilayered structure of alternating magnetic and nonmagnetic layers, created using standard microfabrication practices.[31] Specifics of the thicknesses, number of layers, and composition are presented elsewhere.[32] The sensor area of the chip (Figure 3a) is actually four GMRs arranged as the resistors in a Wheatstone bridge (Figure 3b), which has also been described in detail.[21] The 200 × 200 μm GMR sensing area consists of two GMRs (R_{S1} and R_{S2}), interdigitated in a serpentine pattern to form a densely packed sensing region. The two reference GMRs (R_{R1} and R_{R2}) are positioned on either side of the GMR sensing area, and are also formed in a serpentine pattern. There is a 30-μm separation between the sense and reference GMRs, which are each 11,000 μm long strips that are 2-μm wide. The strips in R_{S1} and R_{S2} are separated from each other by 2 μm; whereas there is a 6-μm separation between the R_{R1} and R_{R2} stripes. A ~260-nm Si_3N_4 passivation layer is coated on the GMR chips to protect the sensor from harm during further processing and application steps.

Changes in the GMR resistance of the sense GMRs that are caused by the screening of the magnetic field by the magnetic bioanalyte labels are monitored by measuring the voltage drop ($E_1 - E_2$) across the bridge when sourcing a current of 1.0 mA (I_{src}). A constant H_{app} of 150 Oe was used to magnetize the superparamagnetic labels and to operate the sensor in the previously determined optimum sensitivity regime.[23]

GMR Scanning of the Sample Sticks

The sample stick, pictured in Figure 2 and shown suspended over the GMR sensor in Figure 3c, is scanned in a direction parallel to H_{app}. Each gold sample and nickel reference address intersects the GMR chip directly over the sense resistors, with a distance of ~50 μm

between the GMR sensor and sample stick. Although the GMR sensor is moved and the sample stick is stationary, we refer to this process as "scanning the sample".

Data Analysis

The voltage drop ($E_1 - E_2$) across the GMR-based Wheatstone bridge at a fixed applied field can be written according to the diagram in Figure 3b as

$$E_1 - E_2 = I_{src}\left[\frac{R_{R1}R_{R2} - R_{S1}R_{S2}}{R_{S1} + R_{S2} + R_{R1} + R_{R2}}\right] \qquad (1)$$

However, as detailed previously,[21] the GMR bridge is imbalanced in that the resistances of the two sense GMRs differ from those of the two reference GMRs. This imbalance is a result of the difference in the layout of the two sense GMRs with respect to the two reference GMRs of the bridge. That is, the GMRs that function as the two sensors are interdigitated, whereas those that act as the two references are not. This situation leads to a difference in the dissipation of any heat that arises from Joule heating. Interdigitation may also affect resistance because of cross-talk between neighboring GMR strips due to magnetic fields caused by the flow of source current. These effects result in no more than a 0.1% difference in the two sets of resistances.[21] This difference, nonetheless, is central in formulating the analytical treatment of the observed response.

Recognizing this difference, Equation 1 can be recast by invoking: (1) $R_{S1} \approx R_{S2}$, $R_{R1} \approx R_{R2}$, and (2) $R_{S1} \neq R_{R1}$. Equation 1 therefore simplifies to

$$\Delta E = \frac{I_{src}}{2}\left[R_R - R_S\right] \qquad (2)$$

where $\Delta E = E_1 - E_2$, R_R represents R_{R1} and R_{R2}, and R_S equals R_{S1} and R_{S2}.

The last step in the data treatment involves the use of the response of nickel reference addresses. As detailed and validated in earlier reports,[22, 23] the nickel reference addresses effectively compensate for small variations in the separation between the sample stick and the GMR sensor for addresses located on the same sample stick, but also for those obtained for scans of different sample sticks. The reference-normalized GMR signal ($\Delta E^N_{S,i}$) for a given sample address *i* is determined by dividing the GMR response from the gold address ($\Delta E_{S,i}$) by the average of the response from the nickel references on either side of the gold address, as shown in Equation 1.

$$\Delta E^N_{S,i} = \frac{2\Delta E_{S,i}}{\Delta E_{R,i-1} + \Delta E_{R,i+1}} \qquad (3)$$

Here, ΔE_R represents the response of the two neighboring nickel reference addresses at $i - 1$ and $i + 1$. We add that when the signal from the gold address is less than or equal to the peak-to-peak noise of the measurement, (i.e., the PBS blank), the peak-to-peak noise of the system (~20 μV) is used in place of the GMR response when normalizing the response.

GMR Instrumentation

The magnetic probe station used in these experiments is presented in Figure 3, and described in greater detail elsewhere.[23] A printed-circuit board (Figure 3c) and wire-bonding was used to connect the GMR chip to the current source and voltmeter via a breakout box (Figure 3d). A Keithley 220 current source supplied the 1.0-mA I_{src} and the voltage drop across the GMR bridge ($E_1 - E_2$) was measured with a Keithley 2182 nanovoltmeter. The magnetic field is applied by two electromagnetic coils arranged in an approximate Helmholtz configuration powered by a 400-W bipolar operational power supply (Kepco BOP 20-20M). The custom-manufactured electromagnets (Nicollet Technologies) can reach a maximum

field of ±550 Oe when scanning the applied magnetic field, and can sustain the constant H_{app} of 150 Oe for periods of time much longer than the length of a set of experiments (±0.1 Oe in 1 h). A Hall probe gaussmeter (F. W. Bell, Model 5070) was used to calibrate the magnetic field strength at the position of the GMR sensor with respect to the current applied to the electromagnets. A LabWindows/CVI program written in-house and interfaced through a GP-IB board was used to control the current source, nanovoltmeter, and electromagnet power supply.

Reagents

The sodium borate buffer packets (50 mM) were purchased from Pierce and used as received. The PBS packets (10 mM), BSA (essentially IgG free), DSP, and biotin goat α-rabbit IgG were purchased from Sigma. All dilutions used distilled water that was further purified by passage through a Millipore Milli-Q system. Acetone (ACS grade) was from Fisher, ethanol (USP grade) from Aaper Alcohol & Chemical Co., and the goat α-rabbit IgG (H & L, cross-adsorbed) and rabbit IgG (affinity purified) from USBiological.

Results and Discussion

Antigen Binding Time and MP-labeled Immunoassay

To begin the exploration of GMR response as a function of antigen concentration, sample sticks were exposed to solutions of rabbit IgG which varied in concentration from 0 to 200 ng/mL. Two sets of experiments were carried out, using incubation times of either 6 or 22 h. The circular gold addresses were used in this experiment in order to better correlate to the evolution of the theory described below. After completion of all the steps in the assay, the GMR response due to the magnetically labeled antigen was determined. Figure 4 shows

the raw GMR voltage readout that was obtained from scanning the sample and reference addresses of two sample sticks. Figure 4a is the response for a sample stick incubated for 6 h with a 200-ng/mL antigen solution, whereas that in Figure 4b is for a sample stick exposed to a 50-ng/mL antigen solution for the same period of time. Both plots represent the response of six nickel reference addresses interwoven with those of five gold sample addresses; the response for the gold sample addresses are highlighted by an asterisk at the signal minimum. As is evident, the profile at each address has a complex shape, and exhibits two maxima and one minimum. The profile represents the superposition of the magnetic field of an address on H_{app}.[20, 23] In other words, the field from an address that is vertically separated from the sense GMRs by ~50 μm first adds to H_{app} as the edge of the address approaches the sense GMRs. The field from the address then rapidly decreases as the address moves directly over the sense GMRs, and changes its direction to interfere with H_{app}. This profile reverses itself as the back portion of the address passes across the sense GMRs. Since the magnitude of the contribution by the address field is directly proportional to the amount of magnetic material at each address and the separation between the address and GMR sensor, the signal from an address can be determined as the difference between the minimum in the response and the average of the two maxima.[22, 23]

The results in Figure 4 contain three important observations. First, the relative magnitude of the sample address signals with respect to the reference address signals are markedly larger at the sample sticks exposed to the 200 ng/mL solution of rabbit IgG (scan a). This difference is consistent with the expectation that an increase in the antigen concentration in turn leads to uptake of the magnetically labeled particles. Second, the absolute magnitude of the profile for the reference addresses is smaller in scan b than scan a.

This difference arises from the dependence of the response on the separation between the sample stick and GMR sensor, and reflects a larger separation in scan b with respect to scan a. Third, the overall profiles undergo a small, but observable shift in the baseline as the two scans proceed. This shifting reflects subtle differences in the magnetic field from scanning the GMR, but again is accounted for by the measurement method.

The normalized GMR responses of the gold addresses from sample sticks incubated with varied antigen concentrations are plotted versus rabbit IgG concentration in Figure 5 for the experiment that used the 6- (filled circles) and 22-h (open circles) incubation time. The standard deviation for each data point was determined from the five gold sample addresses on each sample stick. Comparatively, the 6-h binding time curve undergoes a slow change at low concentrations that then rises to a plateau at ~100 ng/mL rabbit IgG. The value of $\Delta E_{S,i}^{N}$ at the plateau is ~1.5. The 22-h binding time curve also shows an increase with antigen concentration, but shows a much more rapid increase by reaching a limiting value for $\Delta E_{S,i}^{N}$ at ~50 ng/mL. The value for $\Delta E_{S,i}^{N}$ at the plateau is also ~1.5. These differences clearly have important implications to the application of this detection platform, suggesting that the mass transport of materials at low concentrations (e.g., the analyte) to the small capture address of particular concern.[33]

The underlying basis for the difference in the two experiment sets becomes more apparent when examining the optical microscopy images of the two sets of gold addresses shown in Figure 6. Each image is a gold address from an individual sample stick. Figures 6a-c are images for 6-h incubations at respective antigen concentrations of 10, 50, and 100 ng/mL, whereas images for the 22-h exposures are given in Figures 6d-f for antigen

levels of 1.0, 10, and 50 ng/mL. At 6 h, there is minimal particle binding at 10 ng/mL rabbit IgG (Figure 6a). In fact, the image is indistinguishable from that of a PBS blank (data not shown). At 50 ng/mL rabbit IgG (Figure 6b), a much larger number of MPs are evident. The distribution of particles, however, is highly skewed. The density of particles near the edge of the address is significantly greater than that closer to the center of the address, forming a ring of ~15-25 μm in width. Ring-shaped patterns are also observed in assays using square-shaped gold addresses (data not shown). In completing this data set, Figure 6c shows that the coverage of MPs becomes much more uniform and much denser across the entire address at an antigen concentration of 100 ng/mL. According to the $\Delta E_{S,i}^{N}$ plot in Figure 5, this image is close to an antigen concentration in which the response dependence reaches a plateau.

A somewhat similar evolution of MP surface coverage was observed when the antigen was allowed to bind for 22 h (Figures 6d-f), although the range of concentrations for the changes in the patterns occurred at lower values. Addresses exposed to 1.0 ng/mL of rabbit IgG are indistinguishable from PBS blank addresses by both optical microscopy (data not shown) and GMR-based readout (Figure 5). The presence of "ring formation" is also observed in this set of experiments, but at an antigen concentration of 10 ng/mL. Furthermore, the sample address in Figure 6f, which was incubated with 50 ng/mL rabbit IgG antigen for 22 h, appears to be slightly more dense and uniform in coverage of MPs with respect to that for the 6-h exposure to 100 ng/mL in Figure 6c.

In speculating on the reasons for this ring formation phenomenon, we considered the issue of antigen diffusion to the gold address. Sheehan and Whitman have already addressed this issue for diffusion to a flat disk in a flat surface.[33] The solution for the "Weber's disk" problem in electrostatics is similar to that for the diffusion to a disk,

$$j(r) = \frac{2DN_A c_0}{\pi\sqrt{a^2 - r^2}} \tag{4}$$

where j is the flux at the disk, D represents the diffusion coefficient, N_A is Avogadro's number, c_0 is the initial solution concentration, a is the radius of the disk, and r is the distance from the center of the disk. From Equation 4, it can be observed that the flux increases near the edge of the disk, and is at a maximum when $a \approx r$. This formulation neglects the effect of the initial exposure of the disk to solution, and considers only the flux after reaching a steady-state. That is, the model considers only radial-type diffusion, and not the linear process that contributes at short immersion times. In order to determine the accumulation of molecules on the disk (N) at an accumulation time t, Equation 4 is first integrated from 0 to a with respect to r over the surface of the disk to find J (total flux to the disk) as follows:[33]

$$J = \int_0^a \frac{2DN_A c_0}{\pi\sqrt{a^2 - r^2}} (2\pi r) dr \tag{5}$$

Since

$$\int \frac{r}{\sqrt{a^2 - r^2}} dr = -\left(a^2 - r^2\right)^{1/2} \tag{6}$$

evaluation of Equation 5 from 0 to a yields

$$J = 4DN_A c_0 a \tag{7}$$

Further integration of Equation 7 with respect to time leads to

$$N(t) = 4DN_A c_0 at \tag{8}$$

For all further calculations, a diffusion coefficient of 5×10^{-7} cm^2/s is assumed for the antigen.[34] The following discussion also makes the assumption that MP binding correlates directly to the location and amount of antigen binding.

Since the flux of the antigen to the gold address is larger at the outer edge of the disk, one can speculate that binding of the antigen to the surface will also occur from the outside edge of the address inward. If enough time is given for binding, the antigen should eventually fill in the entire address. However, if the binding time is fixed at a relatively short time (i.e., 6 h), as the antigen concentration decreases, less of the center of the address is filled in. The results from the 22-h binding time confirm the proposal. With the increased binding time, the antigen limitation which causes the ring formation occurs at a lower concentration of antigen, as can be seen in both Figure 5 and Figure 6.

For example, the amount of IgG to completely coat a gold address can be estimated to be $\sim 3 \times 10^8$ antigen molecules by using the area of the address and the approximate surface area of an IgG ($\sim$120 nm^2).[35] The accumulation of IgG calculated for the gold addresses (a = 100 μm) with a binding time of 6 h and an initial concentration of 100 ng/mL is $\sim 1.7 \times 10^8$ antigen molecules, calculated from Equation 9. Experimentally, this is enough antigen to cover the address with MP during the labeling step. The ring formation occurs at half the antigen concentration, 50 ng/mL. Since $N(t)$ and c_0 are directly proportional, the address will accumulate half the previously calculated antigen, e.g. $\sim 8.7 \times 10^7$ antigen. This is not enough antigen to coat the address, neither experimentally, since the ring formation is observed, nor theoretically when compared to calculated coverage values. This is when the particular characteristics of the flux described by Equation 4 become important, since as c_0 decreases, fewer antigens diffuse to the center of the address.

In closing this section, the detection limit for the two sets of assays is estimated by linearly extrapolating a line between 10 and 50 ng/mL for the 6-h binding time. By including three times the normalized signal from the PBS blank into the equation, a limit of detection of 35 ng/mL, or ~230 pM, in rabbit IgG can be approximated. In comparison, the extrapolation of a line between 1.0 and 10 ng/mL with the plot of the data with the 22-h binding time yields a limit of detection of ~2 ng/mL, which corresponds to ~13 pM.

Preliminary Studies of Ferrofluid-labeled Immunoassay

In addition to the investigations with the micrometer-size magnetic particles, preliminary studies of the same sample system were conducted using a different type of magnetic particles, 145-nm FF particles conjugated with streptavidin, that were described in the experimental section. The results of this experiment, which used a 6-h binding time, are summarized in Figure 7 as a plot of $\Delta E_{S,i}^{N}$ as a function of rabbit IgG concentration. With the FF label, there is no detectable signal change from the 1 ng/mL sample. However, the signal then rises and appears to approach a plateau above ~100 ng/mL. If the data from 1-10 ng/mL are treated as indicative of a linear response, a limit of detection of ~6 ng/mL (40 pM) can be estimated using these nanoparticles.

The small size of the FF is interesting, since the small size should increase the diffusion rate of the FF in comparison to the MP, and possibly decrease the binding time to the biotin labels on the address surface. Work is needed to more fully understand the capture of the FF by the biotinylated protein label. Comparison studies of the MP and FF on sample sticks with identical nickel references are needed to determine which particle type gives a better magnetic response from the GMR.

Conclusions

In this paper, the value of the GMR sensor for the detection of proteins using a self-referenced sample stick has been demonstrated. The scheme described could be used for the detection of proteins, bacteria, or viruses. While the current detection limit shows the promise of the system, methods are needed to reduce the assay time (e.g. elevated temperatures,[36] or increased mass transfer[37]). However, readout time is fast, as a measurement of five gold sample addresses and six nickel reference addresses in ~120 s. The current scan rate of ~55 μm/s could be further improved with scan automation. Further work also needs to be done to select the optimal magnetic particle, with the best balance of labeling efficiency, size, and magnetic character of the particle. We are also currently working toward lowering readout noise by using phase-sensitive detection. The reaction scheme described is also well suited for multiplexing. By modifying each gold address with a different capture antibody, simultaneous detection of multiple analytes is possible. Patterns of gold addresses could be designed to match the pen positions of microarray spotters, rapidly creating sample sticks for multianalyte detection. Sample scanning can also be automated for better reproducibility and ease of use. Work toward these goals is in progress.

Acknowledgements

Support from NSF's XYZ-on-a-Chip Initiative (#88214), the W. M. Keck Foundation, and DARPA's BioMagnetICs program is thankfully acknowledged. The Ames Laboratory is operated for the U.S. Department of Energy by Iowa State University under contract W-7405-eng-82.

References

(1) Clark Jr., L. C.; Lyons, C. *Ann N Y Acad. Sci.* **1962**, *102*, 29-45.
(2) D'Orazio, P. *Clin. Chim. Acta* **2003**, *334*, 41-69.
(3) Christopoulos, T. K.; Diamandis, E. P. *Immunoassay*; Academic Press: New York, 1996.
(4) Lagally, E. T.; Mathies, R. A. *J. Phys. D: Appl. Phys.* **2004**, *37*, 245-61.
(5) Roper, M. G.; Easley, C. J.; Landers, J. P. *Anal. Chem.* **2005**, *77*, 3887-94.
(6) Zhang, J.; Campbell, R. E.; Ting, A. Y.; Tsien, R. Y. *Nat. Rev. Mol. Cell Biol.* **2002**, *3*, 906-18.
(7) Baibich, M.; Broto, J. M.; Fert, A.; Van Dau, N.; Petroff, F. *Phys. Rev. Lett.* **1988**, *61*, 2472-75.
(8) Binasch, G.; Grunberg, P.; Saurenbach, F.; Zinn, W. *Phys. Rev. B* **1989**, *39*, 4828-30.
(9) Schotter, J.; Kamp, P. B.; Becker, A.; Pühler, A.; Reiss, G.; Brückl, H. *Biosens. Bioelectron.* **2004**, *19*, 1149-56.
(10) Edelstein, R. L.; Tamanaha, C. R.; Sheehan, P. E.; Miller, M. M.; Baselt, D. R.; Whitman, L. J.; Colton, R. J. *Biosens. Bioelectron.* **2000**, *14*, 805-13.
(11) Miller, M. M.; Sheehan, P. E.; Edelstein, R. L.; Tamanaha, C. R.; Zhong, L.; Bounnak, S.; Whitman, L. J.; Colton, R. J. *J. Magn. Magn. Mater.* **2001**, *225*, 138-44.
(12) Schotter, J.; Kamp, P. B.; Becker, A.; Pühler, A.; Brinkmann, D.; Schepper, W. B., H.; Reiss, G. *IEEE Trans. Magn.* **2002**, *38*, 3365.
(13) Graham, D. L.; Ferreira, H. A.; Feliciano, N.; Freitas, P. P.; Clarke, L. A.; Amaral, M. D. *Sens. Actuators, B* **2005**, *107*, 936-44.
(14) Ferreira, H. A.; Graham, D. L.; Freitas, P. P.; Cabral, J. M. S. *J. Appl. Phys.* **2003**, *93*, 7281-86.
(15) Graham, D. L.; Ferreira, H. A.; Freitas, P. P.; Cabral, J. M. S. *Biosens. Bioelectron.* **2003**, *18*, 483-88.
(16) He, W.; Lee, S. J.; Jiles, D. C.; Schmidt, D. H.; Porter, M. D.; Shinar, R. *J. Appl. Phys.* **2003**, *93*, 7459-61.
(17) Melikhov, Y.; Lee, S. J.; Jiles, D. C.; Schmidt, D. H.; Porter, M. D.; Shinar, R. *J. Appl. Phys.* **2003**, *93*, 8438-40.
(18) Pekas, N.; Granger, M. C.; Tondra, M.; Popple, A.; Porter, M. D. *J. Magn. Magn. Mater.* **2005**, *293*, 584-88.
(19) Tondra, M.; Granger, M.; Fuerst, R.; Porter, M.; Nordman, C.; Taylor, J.; Akou, S. *IEEE Trans. Magn.* **2001**, *37*, 2621-23.
(20) Pekas, N.; Porter, M. D.; Tondra, M.; Popple, A.; Jander, A. *Appl. Phys. Lett.* **2004**, *85*, 4783-85.
(21) Millen, R. L.; Kawaguchi, T.; Granger, M. C.; Porter, M. D.; Tondra, M. *Anal. Chem.* **2005**, *77*, 6581-87.
(22) Millen, R. L.; Nordling, J.; Bullen, H. A.; Porter, M. D. *Manuscript in preparation.*
(23) Nordling, J.; Millen, R. L.; Bullen, H. A.; Tondra, M.; Porter, M. D. **2005**, Manuscript in preparation.
(24) Daughton, J. M.; Bade, P. A.; Jenson, M. L.; Rahmati, M. M. M. *IEEE Trans. Magn.* **1992**, *28*, 2488-93.
(25) Prinz, G. A. *Science* **1998**, *282*, 1660-63.

(26) Johnson, M. *J. Phys. Chem. B* **2005**, *109*, 14278-91.
(27) White, R. L. *IEEE Trans. Magn.* **1992**, *28*, 2482-86.
(28) Duhachek, S. D.; Kenseth, J. R.; Casale, G. P.; Small, G. J.; Porter, M. D.; Jankowiak, R. *Anal. Chem.* **2000**, *72*, 3709-16.
(29) Wagner, P.; Hegner, M.; Kernen, P.; Zaugg, F.; Semenza, G. *Biophys. J.* **1996**, *70*, 2052-66.
(30) Jones, V. W.; Kenseth, J. R.; Porter, M. D.; Mosher, C. L.; Henderson, E. *Anal. Chem.* **1998**, *70*, 1233-41.
(31) Tondra, M.; Anderson, J. M. Magnetizable bead detector. U.S. Patent 6,743,639, June 1, 2004.
(32) Rife, J. C.; Miller, M. M.; Sheehan, P. E.; Tamanaha, C. R.; Tondra, M.; Whitman, L. J. *Sens. Actuators, A* **2003**, *107*, 209-18.
(33) Sheehan, P. E.; Whitman, L. J. *Nano Lett.* **2005**, *5*, 803-07.
(34) Starr, T. E.; Thompson, N. L. *J. Phys. Chem. B* **2002**, *106*, 2365-71.
(35) Silverton, E. W.; Navia, M. A.; Davies, D. R. *PNAS* **1977**, *74*, 5140-44.
(36) Johnstone, R. W.; Andrew, S. M.; Hogarth, M. P.; Pietersz, G. A.; McKenzie, I. F. C. *Mol. Immunol.* **1990**, *27*, 327-33.
(37) Glaser, R. W. *Anal. Biochem.* **1993**, *213*, 152-61.

Figure Captions

Figure 1. Reaction scheme. The sample stick consists of alternating Ni references and bioactive gold addresses. A DSP-derived monolayer is formed on the gold addresses and reacted with the capture antibody. After blocking the remaining areas of the sample stick with BSA, the stick is exposed to antigen, followed by the biotinylated label antibody. Streptavidin-coated magnetic particles are applied, and the GMR signal from the magnetically-labeled antigen is compared to the nickel references and quantified.

Figure 2. Sample stick photographs. (a) Photolithography procedures were used to craft the 2 × 0.3 cm sample stick, which consists of 200 × 200 μm features of alternating nickel reference and gold addresses. (b) The bioactive gold addresses and reference Ni squares are aligned with the 200 × 200 μm GMR sensing area when it is scanned across the sensor. (c) The capture antibody is applied to the gold DSP-modified region using a capillary.

Figure 3. GMR sensor pictures and instrumentation schematic. (a) The GMR sensors (200 x 200 μm, R_{S1} and R_{S2}) are fabricated in a Wheatstone bridge circuit (b). The two GMRs used as references (R_{R1} and R_{R2}) are of an equivalent size and lie on either side of the intertwined sense resistors. H_{app} is the direction of the applied magnetic field. (c) A green printed-circuit board is used to connect to the GMR chip through wire bonds. The schematic in (d) draws out the further connections from the circuit board to the breakout box, which is further connected to the current source and digital nanovoltmeter. Two electromagnets are configured in an approximate Helmholtz configuration to produce a uniform H_{app} through and around the GMR sensor. The sample stick, shown in (c) attached to a glass slide holder,

and schematically in (d) is scanned back and forth across the sensor, parallel to the direction of H_{app}.

Figure 4. GMR response to scanned sample sticks. (a) The GMR response to a sample stick previously incubated with a 200-ng/mL solution of rabbit IgG, labeled with biotinylated α-rabbit IgG, and exposed to streptavidin-coated MP. (b) A similar response scan from a similarly processed sample stick, with the exception of the rabbit IgG concentration, which in this case was 50 ng/mL. Asterisks highlight the minimum from the three-point signal from each gold address.

Figure 5. Normalized GMR response as a function of rabbit IgG concentration using MP labels. Rabbit IgG antigen binding time was 6 h (closed circles) and 22 h (open circles). Both plots rise to a plateau at a normalized GMR response of ~1.5, although the plateau begins at lower concentration with the 22-h antigen binding time. Each data point is an individual sample stick.

Figure 6. Optical microscopic images of circular gold sample stick addresses after bioassay and labeling with MP. Images (a), (b), and (c) show the results from 6 h of rabbit IgG binding time with concentrations of 10, 50, and 100 ng/mL respectively. Images (d), (e), and (f) show the results from 22 h of rabbit IgG binding time with concentrations of 1.0, 10, and 50 ng/mL respectively. The same trend of minimal binding at the low concentration, the formation of a MP ring, and saturation of the surface can be observed from the sets of data

from both binding times; however, the ring formation occurs at a lower antigen concentration for the longer binding time.

Figure 7. Reference-normalized GMR response ($\Delta E_{S,i}^{N}$) as a function of rabbit IgG concentration using 145-nm FF labels on square gold addresses. The rabbit IgG antigen binding time was 6 h. Each data point is the average of an individual sample stick.

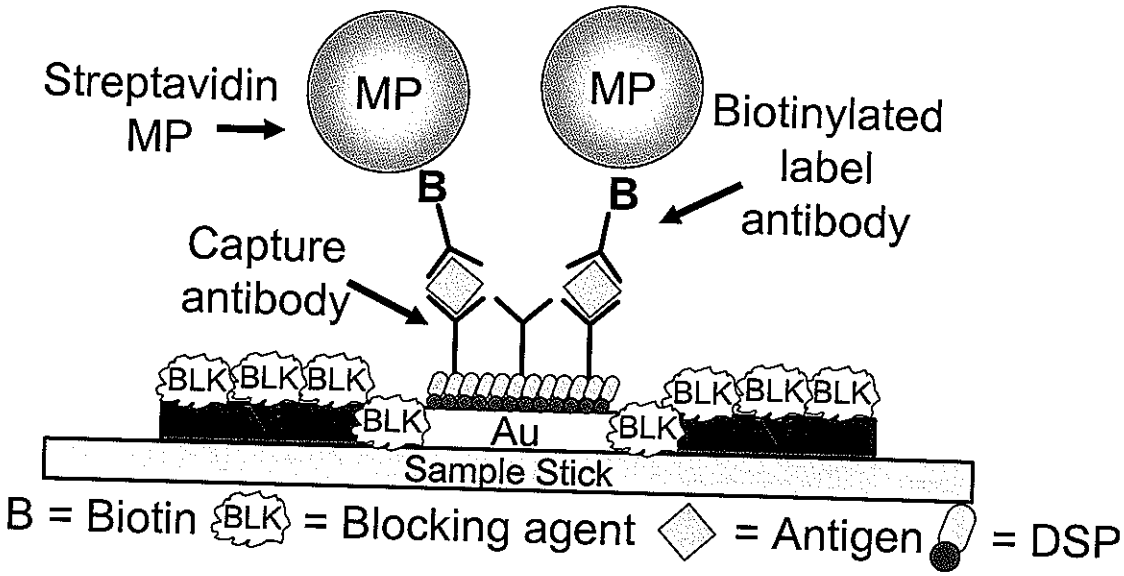
Streptavidin MP
MP
MP
Biotinylated label antibody
B
B
Capture antibody
BLK
BLK
BLK
BLK
Au
BLK
BLK
BLK
BLK
Sample Stick
B = Biotin
BLK
= Blocking agent
= Antigen
= DSP

Figure 1

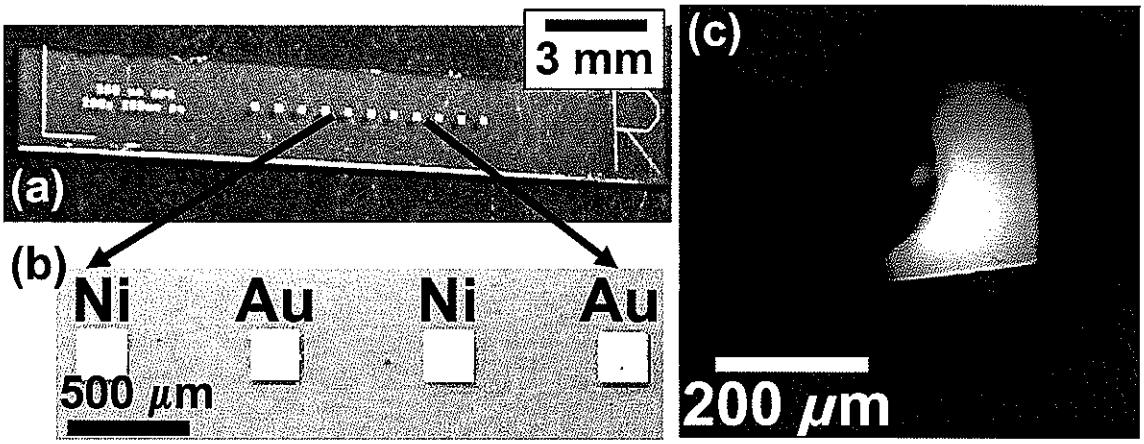

Figure 2

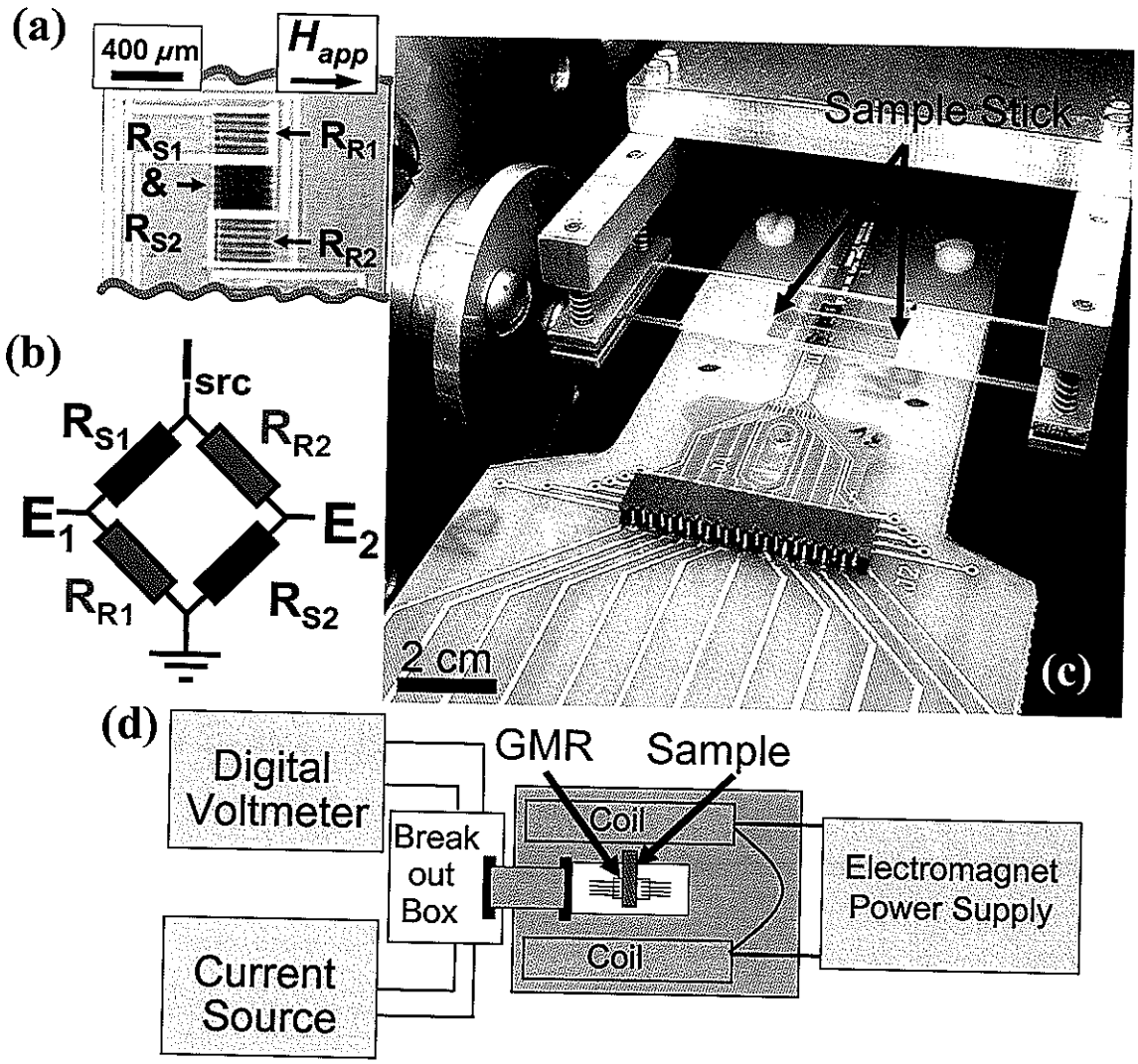
(a)
400 μm
H_{app}
R_{S1}
&
R_{S2}
R_{R1}
R_{R2}
(b)
src
R_{S1}
R_{R2}
E_1
E_2
R_{R1}
R_{S2}
Sample Stick
2 cm
(c)
(d)
Digital Voltmeter
Break out Box
Current Source
GMR
Sample
Coil
Coil
Electromagnet Power Supply

Figure 3

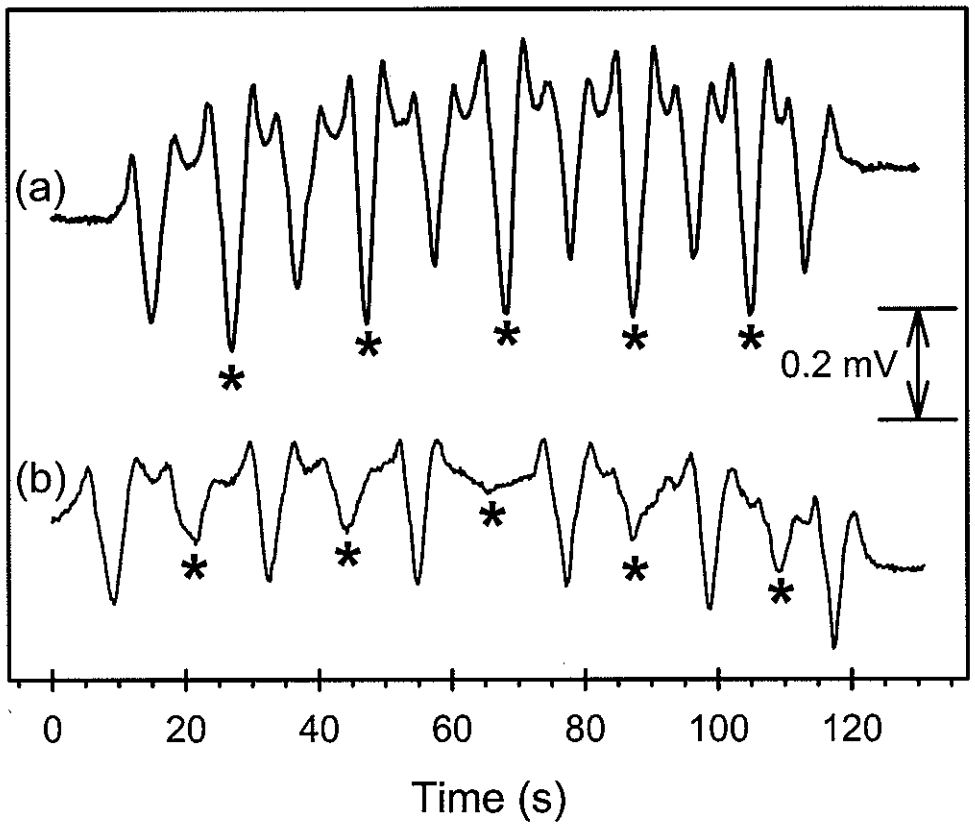

Figure 4

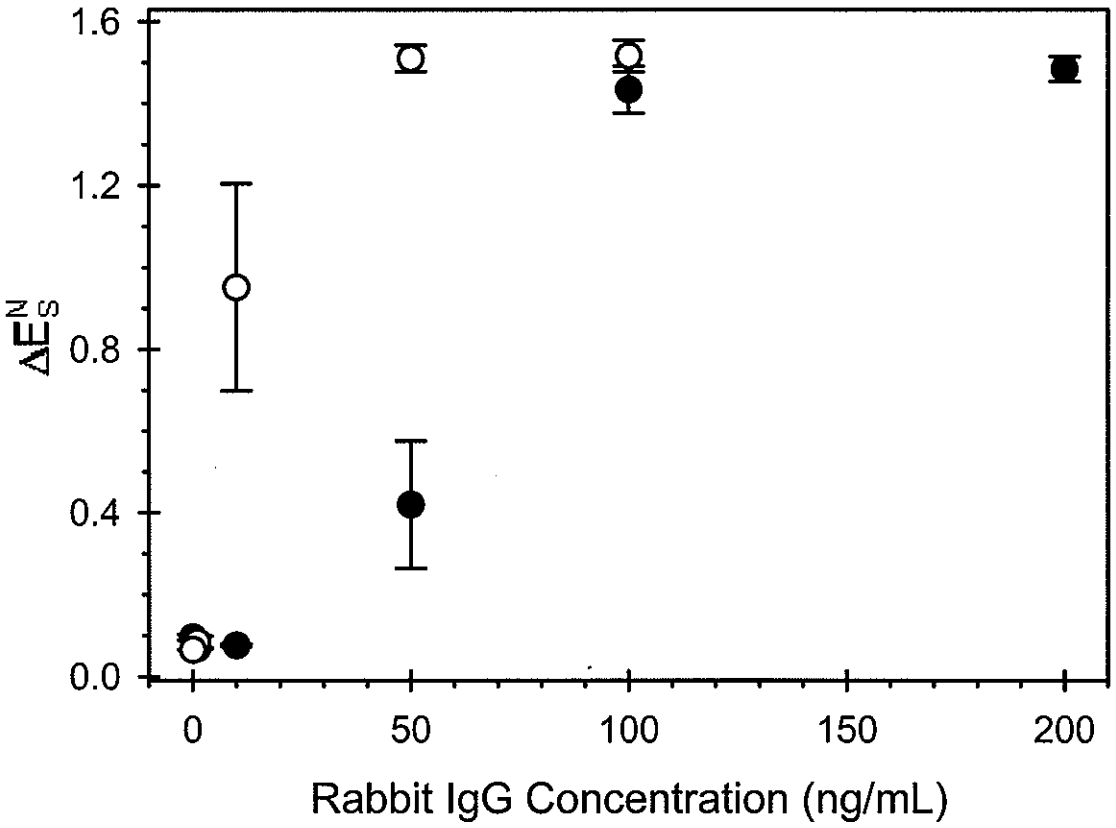
1.6
1.2
0.8
0.4
0.0
ΔE_S^N
0
50
100
150
200
Rabbit IgG Concentration (ng/mL)

Figure 5

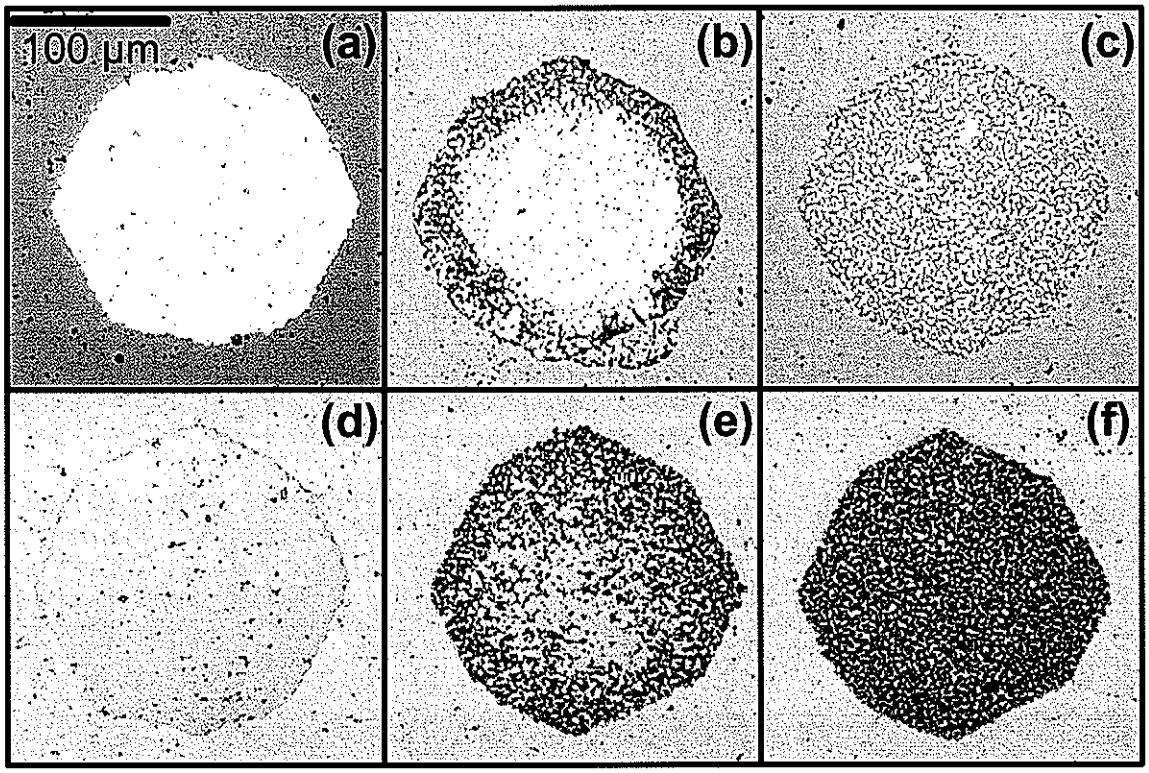

Figure 6

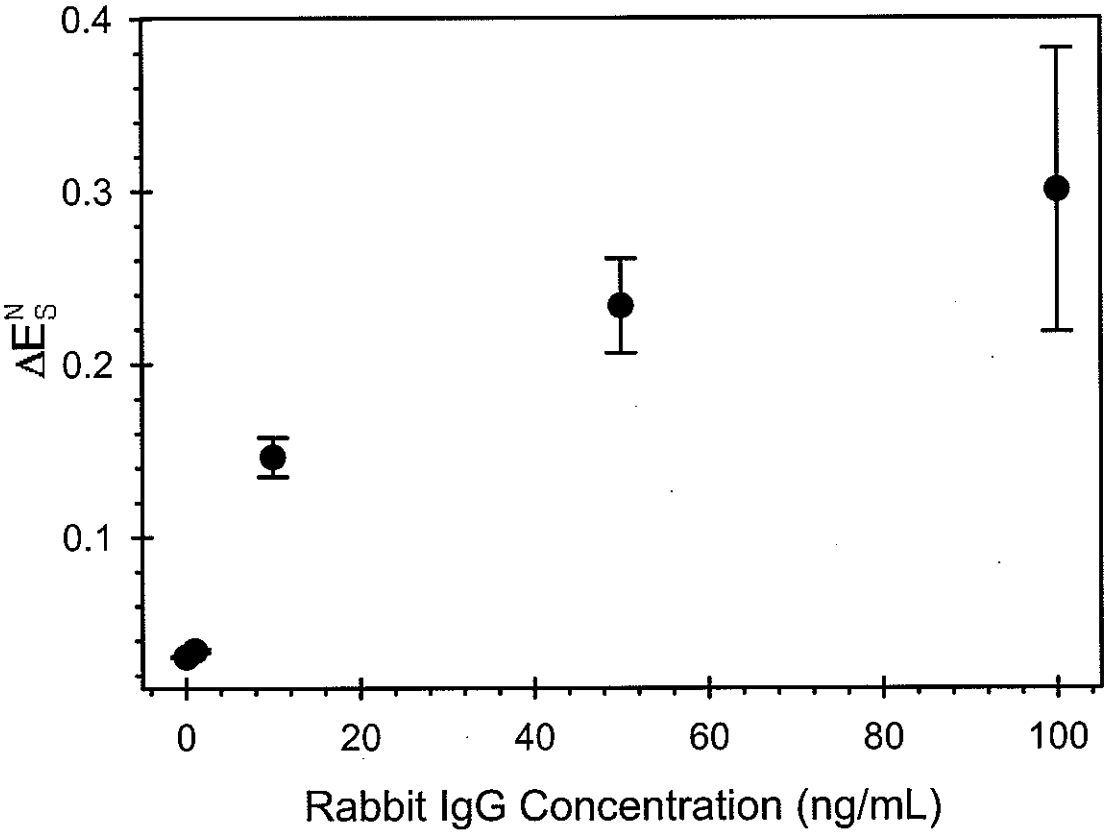
0.4
0.3
0.2
0.1
ΔE_S^N
0
20
40
60
80
100
Rabbit IgG Concentration (ng/mL)

Figure 7

CHAPTER 4: GIANT MAGNETORESISTIVE SENSORS FOR SIMULTANEOUS CHIP-SCALE DETECTION OF MULTIPLE IgG PROTEINS

A manuscript in preparation for submission to *Analytical Chemistry* (correspondence)

Rachel L. Millen, John Nordling, and Marc D. Porter

Department of Chemistry, Ames Laboratory-USDOE, and Institute for Combinatorial Discovery, Iowa State University, Ames IA 50011

Mark Tondra

NVE Corporation, Eden Prairie, MN 55433

Abstract

This paper describes the continued development of pathways to apply giant magnetoresistor (GMR) technology to the bioanalytical chemistry. GMRs are extensively used for magnetic sensing in computer hard drives. This work merges the sensitivity, high-speed, and small size of the GMR sensor with magnetic labeling techniques and a disposable self-referenced sample stick in order to simultaneously detect the presence of three IgG proteins. Briefly, gold addresses on the sample sticks are first coated with a thiolate monolayer that acts as a coupling agent for the covalent linkage of capture antibodies specific to the target antigens. Utilizing a sandwich assay procedure, the sample sticks are exposed to any or all of the three antigens (rabbit, rat, and human IgG) followed by labeling with a biotinylated protein and the final step of immersing the sample stick in a solution of streptavidin-modified magnetic particles (MP). The MPs interact with the biotinylated labels and reveal the presence of the antigen when the sample stick is read by a scan over the GMR sensor. The GMR response is internally calibrated with the on-chip reference address, and

the location and magnitude of the GMR signals with respect to the magnetic references is related to antigen concentration. Methods of decreasing non-specific binding are also briefly discussed.

Introduction

The giant magnetoresistive effect, discovered in 1988,[1, 2] is the phenomenon behind the giant magnetoresistive sensors used for the detection of magnetic data in practically all computer hard drives. These giant magnetoresistors (GMRs) have recently branched from their heavy utilization by the computer industry out into the bioanalytical arena.[3] The GMR traits of speed, small size, and sensitivity are being applied to the initial efforts toward the detection of DNA hybridization,[4-7] and streptavidin-biotin binding.[8, 9]

Our group has also been active in this field, investigating magnetic pumps[10, 11] and diverters,[12, 13] as well as the detection of a flowing magnetic ferrofluid within microfluidic channels.[14] Immunosorbent assays have also been explored by our group, beginning with an assay built on the modified surface of a GMR[15] This was expanded upon by the introduction of a disposable self-referenced sample stick, scanned across the GMR sensor as a readout method,[16] and initially utilized for the detection of protein interactions.[17, 18] This paper describes our preliminary efforts for the creation of a multiplexed immunoassay utilizing the GMR as a readout method of the self-referenced sample stick modified for the detection of three different IgG proteins.

The resistivity of most metals varies (usually less than 1%) with the application of an external magnetic field (H_{app}). This magnetoresistance is magnified greatly in some microfabricated multilayered structures, which is then called giant magnetoresistance. These

unique devices are a few hundred micrometers in thickness, and are constructed from multiple alternating layers of magnetic and nonmagnetic conductors that are each a few nanometers thick, i.e., a thickness on the order of the mean free path of an electron.[19] The GMR effect is a quantum mechanical consequence of the unique composition of the GMR sensors. Briefly, the magnetic layers of the structure align magnetically in an anti-parallel fashion through exchange coupling; however, under the influence of a magnetic field the magnetic alignment becomes more parallel with increasing H_{app}. As electron scattering is more probable in the GMR sensor with the antiparallel magnetization alignment and therefore more resistive, increasing magnetic field decreases the resistivity of the multilayered structure.[19-22] Consequently, the GMR sensor is very sensitive to magnetism, with some GMRs showing a change in resistance up to 80% at room temperatures.[23] In these experiments, we apply a constant H_{app} to the sensor and detect the perturbation to the constant H_{app} from the presence of both the magnetic reference addresses and the magnetic labels used on the bioassays.

In our experimental approach for the creation of a multiplexed assay utilizing GMR readout, we will create a sample stick for multiple biorecognition events, as shown schematically in Figure 1. The sample stick consists of alternating squares of magnetic references and gold addresses. The gold addresses are modified with a thiolate monolayer containing an end group capable of coupling with an antibody. A capture antibody, specific to different antigens, is bound to each bioactive gold address. Figure 1a illustrates this concept using three analytes. Each gold address is labeled with a single type of capture antibody, each specific to antigen 1, 2, or 3. The theoretical number of gold sample addresses, n, is theoretically unlimited, although this work only employs three antigens and

five sample addresses. The entire sample stick is immersed in a blocking agent to reduce non-specific binding and then exposed to the antigen solution. After incubation, the sample stick is submerged in a solution containing biotinylated label antibodies specific to 1, 2, or 3, creating a sandwich immunoassay. Finally, streptavidin-coated magnetic particles (MP) are bound to each address through biotin-streptavidin chemistry when the antigen and therefore the selective tag are present.

The completed sample stick is then scanned across the GMR sensor, and the GMR response from each gold address is analyzed and compared to the surrounding magnetic references. Further details on the magnetic referencing format can be found elsewhere.[16] Therefore, the GMR response can be equated the presence of antigen, and the signal with respect to the address location can be used to identify the antigen. Future directions and applications in the detection of multiple analytes are also discussed.

Experimental Section

Sample Stick Fabrication

The combination of photolithography and metal lift-off procedures used to create the sample sticks of alternating nickel and gold squares (Figure 2a-b) have formerly been described in detail.[18] Each sample stick consists of eleven 200 × 200 μm alternating magnetic references and gold addresses, with 500 μm separating each square on a 0.3 × 2 cm Pyrex substrate. A 10-nm thick nickel square, protected with a 15-nm titanium layer, served as the magnetic reference material, while a 75-nm thick gold square (with an 8-nm titanium adhesion layer) functioned as the modification ready gold address.

Covalent Immobilization of Capture Protein

The sample sticks were prepared for use as an assay capture substrate by the selective application of capture antibody to the gold squares. This process began with the cleaning of the sample sticks in a 40-W Ar plasma at 1.0 torr for 10 min. The sample sticks were then completely immersed in an ethanolic 0.1 mM dithiobis(succinimidyl propionate) (DSP) solution overnight. Small drops of 200 μg/mL capture antibody in 40% glycerol (by volume) in 50 mM sodium borate buffer (pH 8.5) were applied to the gold addresses using a fused silica capillary (24.0-μm I.D., 148-μm O.D.), a syringe, and micromanipulators. Individual capillaries and syringes were used for each capture antibody. To combat non-specific binding, 200 μg/mL bovine serum albumin (BSA) in 40% glycerol in borate buffer was applied to the nickel squares, and the capture antibody- and BSA-labeled sample sticks were left undisturbed for 30 min in a humidified environment. After the covalent binding of the antibody to the succinimidyl end group of the DSP-derived monolayer,[24-26] the sample sticks were rinsed four times with 10 mM phosphate-buffered saline (PBS) by volume displacement, and placed in 1% BSA in borate buffer overnight as a blocking step to further minimize non-specific binding.

Antigen Application and Labeling Steps

All antigen solutions were prepared in PBS, with each analyte present at a concentration of 100 ng/mL. The antigen was applied in 20-μL drops to the entire sample stick, held in a humidified environment for 6 h, and then rinsed with PBS buffer. All dilutions to the antigen concentration were in PBS. The label was a solution of 2 μg/mL biotinylated goat α-rabbit IgG, 2 μg/mL biotinylated goat α-rat IgG, and 2 μg/mL biotinylated goat α-human IgG in PBS, also applied as a 20-μL drop to the sample stick in a

humidified environment overnight. The chosen volume and concentration of label antibody were calculated as the amount of protein necessary for 100-fold saturation of the five 200-μm gold squares.

The final assay step labeled the biotinylated antibody with streptavidin-coated magnetic particles through the application of 20-μL drops to the each of the sample sticks, which were then maintained under the MP solution for 2 h in a humidified environment. The MPs used were 1.05-μm in diameter and covalently coupled with streptavidin (~10 × 10^9-MP/mL MyOne Streptavidin Dynabeads from Dynal Biotech). The magnetic character of the MP arises from their 37% ferrite content.

SEM was used to determine the number of address-bound MPs on the sample sticks. Images were taken with a JEOL 5910 of sample sticks previously coated with a thin layer of gold to reduce charging of the sample during microscopy.

Layout and Production of GMR Chips

GMR sensors are complex structures made of alternating magnetic and nonmagnetic layers. The makeup of these multilayered structures varies widely; however, the specifications for the GMRs used herein have previously been described.[27] A GMR sensor (Figure 3a) consists of four GMRs arranged as the component resistors of a Wheatstone bridge (Figure 3b).[15] Each of the four GMRs is a 2-μm wide, 11,000-μm long strip of multilayered material. Two of the GMRs (R_{S1} and R_{S2}) are intertwined in a close formation (2-μm separation distance) to form the GMR sensing area. The pattern of layout is repeated for the two reference GMRs (R_{R1} and R_{R2}), but has one reference GMR on either side of the GMR sensing area that is separated from the sensor by 30 μm. Standard microfabrication techniques were used to manufacture the GMR chips (NVE Corp.).[28] The GMR bridge is

wire-bonded to a printed-circuit board (Figure 3c), through which connections are made to the current source and voltmeter.

As diagrammed in Figure 3b, a current (I_{src}, 1.0 mA) is sourced to the bridge, while a voltmeter measuring the voltage across the GMR bridge detects the fluctuation of the magnetic field from the perturbation of the magnetic addresses and labels. As explained in previous work,[16] 150 Oe was chosen as H_{app}, both for the magnetization of the superparamagnetic labels, and due to the highly sensitive response of the GMR sensor at this field.

GMR Scanning of the Sample Sticks

The sample stick described in Figure 2a is scanned parallel to H_{app}, as shown in Figure 3a. The sample stick is optically aligned so that the nickel reference and gold addresses pass directly above the GMR sensing area, with ~50 μm separating the parallel GMR sensor and sample stick. With the configuration of our test station, the GMR sensor is translated and the sample stick is stationary; however, this is referred to as "scanning the sample" for simplicity.

Data Analysis

The GMR response is measured by monitoring the voltage drop (E_1 - E_2) across the GMR-based Wheatstone bridge at a constant H_{app}. Using the nomenclature assigned in Figure 3b, the voltage drop can be written as

$$E_1 - E_2 = I_{src}\left[\frac{R_{R1}R_{R2} - R_{S1}R_{S2}}{R_{S1} + R_{S2} + R_{R1} + R_{R2}}\right] \qquad (1)$$

However, this equation can be simplified due to the imbalance in the GMR-based Wheatstone bridge. As previously discussed,[15] there are differences in the resistance of the

two sense resistors with respect to the two reference resistors. These differences arise from the on-chip configuration of the GMR-based bridge. Differences in the dissipation of Joule heating arise from the close proximity and interdigitation of the sense resistors versus the neighboring reference resistors. Also, cross-talk from the magnetic fields produced from the current flow through the GMRs may differ with the spacing of the reference and sense resistors. While these consequences amount to only a 0.1% resistance difference between the sense and reference resistors, these effects must be considered in analyzing the GMR response.

The imbalance leads to the assumptions that $R_{S1} \approx R_{S2}$, $R_{R1} \approx R_{R2}$, and $R_{S1} \neq R_{R1}$, which can be applied to Equation 1 as follows ($\Delta E = E_1 - E_2$):

$$\Delta E = \frac{I_{src}}{2}\left[R_R - R_S\right] \tag{2}$$

where R_S represents the two sense resistors (R_{S1} and R_{S2}) and R_R represents the two reference resistors (R_{R1} and R_{R2}).

Since the GMR response is sensitive to differences in separation distance between the addresses and GMR sensor, a method of compensating for both sample tilt and sample stick loading height is necessary. The GMR signals from the nickel reference addresses (ΔE_R) permit the normalization of the signals from a gold address i, $\Delta E_{S,i}$, through the following equation:

$$\Delta E_{S,i}^{N} = \frac{2\Delta E_{S,i}}{\Delta E_{R,i-1} + \Delta E_{R,i+1}} \tag{3}$$

where the reference-normalized GMR signal ($\Delta E_{S,i}^{N}$) is divided by the average of the signal from the surrounding nickel reference addresses (at *i-1* and *i+1*). Further explanation of the reference-normalization process can be found in earlier work.[16]

When there is little to no MP binding to the modified gold addresses on the sample stick (i.e., the PBS blank), there is no observable signal. In these cases the signal from the gold address was set at 20 μV, which is the approximate peak-to-peak noise of the measurement between scans, allowing for signal normalization of the signals.

GMR Instrumentation

A modified probe station (previously described) was used for the magnetic scanning experiments in this work.[16] A nanovoltmer (Keithley 2182) was used to measure the voltage difference across the Wheatstone bridge, while a Keithley 220 current supply sourced the required I_{src}. Two coiled electromagnets set in an approximate Helmholtz configuration provided the magnetic field. The custom-made coils (Nicollet Technologies) were driven by a Kepco BOP 20-20M 400-W bipolar operational power supply. A Hall probe gaussmeter (F. W. Bell, Model 5070) was used to calibrate the magnetic field strength versus the current from the electromagnet power supply, as well as to quantify the field stability (±0.1 Oe in 1 h). All the instrumentation (e.g., current source, nanovoltmeter, and electromagnet power supply) was controlled through a GP-IB interface board by a LabWindows/CVI program written in-house.

Reagents

The sodium borate buffer packets (50 mM) were purchased from Pierce. The PBS packets (10 mM), BSA (essentially IgG free), DSP, and biotin goat α-rabbit IgG were purchased from Sigma. The ethanol (USP grade) was from Aaper Alcohol & Chemical Co.

The goat α-rabbit IgG (H & L, cross-adsorbed), goat α-rat IgG (H & L, cross-adsorbed), goat α-human IgG (H & L, cross-adsorbed), biotinylated goat α-human IgG (H & L), biotinylated goat α-rat IgG (H & L), rat IgG (affinity purified), human IgG (affinity purified) and rabbit IgG (affinity purified) from USBiological. All dilutions used distilled water that was more thoroughly purified by passage through a Millipore Milli-Q system.

Results and Discussion

SEM Sample Stick Characterization

The binding of MPs to the sample stick addresses, and therefore the success of the sandwich assay, was examined using SEM. Five gold addresses are present on the sample sticks, and were modified with three different capture antibodies. Addresses 1-5 were coated with goat α-rat IgG, goat α-rabbit IgG, goat α-human IgG, goat α-rat IgG, and goat α-rabbit IgG, respectively, on all the sample sticks. The sample sticks were exposed to four types of antigen solutions after blocking: (1) rabbit IgG, (2) rat IgG, (3) human IgG, or (4) an equal mixture of all three IgGs. Finally, the sample sticks were exposed to the mixture of the biotinylated tagging antibody, followed by the solution of streptavidin-coated MP labels.

Figure 4 shows SEM images of the gold addresses from three different sample sticks. Two different magnifications of an address modified with goat α-human IgG capture antibody is shown in Figures 4a-b. The sample stick was incubated with rabbit IgG; therefore, any MPs on the address surface are due to non-specific binding. It can be seen in Figures 4a-b that non-specific binding is minimal. When compared with the maximum coverage of specifically-bound MPs, the non-specific binding is typically less than 1% of the observed coverage from exposure to antigen.

Specific binding of rabbit IgG to a goat α-rabbit IgG capture address is demonstrated in Figure 4c. The MPs evenly cover the gold address, attached by the specific interaction pathway of the streptavidin-MP, biotinylated label, antigen, and surface-bound capture antibody. There are 0.51 MPs/μm^2 in this image, which was calculated from the average of five 1,950-μm^2 SEM images. Of the ~20,000 MPs on this address, only eight MP are larger than the company-specified 1-μm diameter, an indication of a high level of monodispersity.

A higher magnification image of MPs binding to the biotinylated label, this time of a rat IgG sandwich assay, is presented in Figure 4d. When examining the image closely, the MPs do not appear to be adsorbed on the surface in a completely random fashion. A random adsorption model assumes that diffusion is the main factor in particle movement.[29] However, the MPs in these experiments do not stay suspended for the entire 2-h reaction time, and therefore, there is a net movement of MPs toward the surface of the sample stick due to gravity. The ballistic deposition model is likely applicable in this situation, which assumes both gravitational drift of particles toward the substrate, and no particle diffusion after surface impact.[30, 31] One can envision an MP resting on the surface after coupling. If a second MP drifting toward the surface lands on the first MP, it can then roll down the side of the first MP. These steps are repeated as more MPs approach the surface, creating clusters. During this process, MPs resting on available biotin sites bind to the surface. However, any MPs (e.g., in a multilayer) not held in place by biotin-streptavidin interactions are removed during the rinse-step.

GMR Sample Stick Readout

The scanning of the sample stick over the GMR sensor gave a varied response, depending on the antigen solution with which the sample stick was incubated. Figure 5

displays the raw data from the GMR response to three different sample sticks. A sample stick incubated with only human IgG was scanned across the GMR to give the response shown in Figure 5a. The signals from the six nickel references are marked with asterisks on the graph to differentiate from the signals due to the MP bound to the gold addresses, which are numbered. The asterisk is positioned at the minimum of the signal from each reference address. The large peak at address #3 is due to the specific binding of MP to the human IgG sandwich assay positioned on the center gold address. The other numbers correspond to the remaining gold addresses, which are labeled with goat α-rat IgG and goat α-rabbit IgG capture antibody. The non-specific binding of MP to the four remaining gold addresses is minimal, and no GMR signal can be observed.

In comparison, the GMR signal from a sample stick exposed to only rat IgG is exhibited in Figure 5b. There are two addresses modified with goat α-rat IgG capture antibody on this sample stick – address #1 and address #4. The signal from the presence of MP is again evident for the specifically-bound MP and not present for the addresses labeled with capture antibody not specific to the applied antigen. When comparing the response of the GMR to the nickel references, the magnitude of the nickel reference signal from Figure 5a is less than that in Figure 5b. This is due to the sensitivity of the GMR response to the distance separating the sensor and the sample stick. Since the nickel references are equivalent from sample stick to sample stick, the distance effects can be effectively accounted for by the procedures described in the experimental section and earlier work.[16]

The plot response profile in Figure 5c is the results from scanning the sample stick incubated with a solution mixture of rat IgG, rabbit IgG, and human IgG. In this case, the antigen for every biomodified address is present in the antigen solution, and therefore, every

address should be capped with MP, as is evident by the presence of a GMR response for all five gold addresses.

Reference-normalized GMR Response

Figure 6 compares the reference-normalized GMR response for each gold address. Each set of columns represents address 1-5, with each axis label naming the capture antibody immobilized on that address. Each bar color is a single sample stick that has been incubated with either a single antigen, a solution of all three antigens, or PBS to serve as a blank. Though not extremely well tested, reproducibility from address to address on a single sample stick is reasonably high. For example, the normalized GMR responses for the complementary gold address on the rat IgG only sample stick are 2.55 and 2.46.

Furthermore, the reproducibility of the normalized GMR responses for similarly modified gold addresses is compared for all the sample sticks used in Figure 7, which is the combined data from 11 sample sticks (55 gold addresses). Each column is the average of the normalized GMR responses for the specific binding of the antigen denoted in the column label. For example, the rat IgG column is the response from the α-rat IgG-modified gold addresses on any sample incubated either with rat IgG only, or rat IgG in combination with rabbit and human IgG antigen. The "No Specific Antigen" is the reference-normalized GMR response from any non-specific binding on addresses with no complement present in the applied antigenic solution, which is a measure of the lack of cross-reactivity between antigens. The "PBS" data column is the averaged $\Delta E_{S,i}^{N}$ from sample sticks exposed to PBS in place of an antigen solution, which demonstrates the low amount of MPs non-specifically bound to the surface. Taken together, the high specificity to the target antigens, low cross-

reactivity, low non-specific binding, and rapid readout begin to demonstrate the potential of the assay strategy as a new and exciting readout tool in the bioanalytical arena.

Conclusions

These results illustrate the potential for the utilization of the GMR reader as a biosensor. The detection of three proteins utilizing the self-referenced sample stick and GMR readout was demonstrated in this work. However; the number of gold addresses, antigens, and even GMR sensors can be increased for the concurrent capture and readout of many more antigens. In theory, the number is unlimited, although cross-reactivity will somewhat limit the number. Nevertheless, care in the choice of antigens and reaction conditions should remove many issues related to cross-reactivity.

Furthermore, sample readout with this technique is quick. Currently, one scan requires ~120 s, and this number can even be increased with automation of the sample scanning system. Sample stick arrays could be made for the scanning multiple rows of addresses past a column of GMRs. The reaction time itself can be decreased using methods to increase mass transport,[32] as well as optimizing the reaction temperature,[33] to create both a rapid reaction and quick readout format.

Acknowledgements

Support from NSF's XYZ-on-a-Chip Initiative (#88214), the W. M. Keck Foundation, and DARPA's BioMagnetICs program is gratefully acknowledged. The Ames Laboratory is operated for the U.S. Department of Energy by Iowa State University under contract W-7405-eng-82.

References

(1) Baibich, M.; Broto, J. M.; Fert, A.; Van Dau, N.; Petroff, F. *Phys. Rev. Lett.* **1988**, *61*, 2472-75.

(2) Binasch, G.; Grunberg, P.; Saurenbach, F.; Zinn, W. *Phys. Rev. B* **1989**, *39*, 4828-30.

(3) Graham, D. L.; Ferreira, H. A.; Freitas, P. P. *Trends Biotechnol.* **2004**, *22*, 455-62.

(4) Schotter, J.; Kamp, P. B.; Becker, A.; Pühler, A.; Reiss, G.; Brückl, H. *Biosens. Bioelectron.* **2004**, *19*, 1149-56.

(5) Edelstein, R. L.; Tamanaha, C. R.; Sheehan, P. E.; Miller, M. M.; Baselt, D. R.; Whitman, L. J.; Colton, R. J. *Biosens. Bioelectron.* **2000**, *14*, 805-13.

(6) Miller, M. M.; Sheehan, P. E.; Edelstein, R. L.; Tamanaha, C. R.; Zhong, L.; Bounnak, S.; Whitman, L. J.; Colton, R. J. *J. Magn. Magn. Mater.* **2001**, *225*, 138-44.

(7) Graham, D. L.; Ferreira, H. A.; Feliciano, N.; Freitas, P. P.; Clarke, L. A.; Amaral, M. D. *Sens. Actuators, B* **2005**, *107*, 936-44.

(8) Graham, D. L.; Ferreira, H. A.; Freitas, P. P.; Cabral, J. M. S. *Biosens. Bioelectron.* **2003**, *18*, 483-88.

(9) Ferreira, H. A.; Graham, D. L.; Freitas, P. P.; Cabral, J. M. S. *J. Appl. Phys.* **2003**, *93*, 7281-86.

(10) He, W.; Lee, S. J.; Jiles, D. C.; Schmidt, D. H.; Porter, M. D.; Shinar, R. *J. Appl. Phys.* **2003**, *93*, 7459-61.

(11) Melikhov, Y.; Lee, S. J.; Jiles, D. C.; Schmidt, D. H.; Porter, M. D.; Shinar, R. *J. Appl. Phys.* **2003**, *93*, 8438-40.

(12) Pekas, N.; Granger, M. C.; Tondra, M.; Popple, A.; Porter, M. D. *J. Magn. Magn. Mater.* **2005**, *293*, 584-88.

(13) Tondra, M.; Granger, M.; Fuerst, R.; Porter, M.; Nordman, C.; Taylor, J.; Akou, S. *IEEE Trans. Magn.* **2001**, *37*, 2621-23.

(14) Pekas, N.; Porter, M. D.; Tondra, M.; Popple, A.; Jander, A. *Appl. Phys. Lett.* **2004**, *85*, 4783-85.

(15) Millen, R. L.; Kawaguchi, T.; Granger, M. C.; Porter, M. D.; Tondra, M. *Anal. Chem.* **2005**, *77*, 6581-87.

(16) Nordling, J.; Millen, R. L.; Bullen, H. A.; Tondra, M.; Porter, M. D. **2005**, Manuscript in preparation.

(17) Millen, R. L.; Nordling, J.; Bullen, H. A.; Porter, M. D. *Manuscript in preparation* **2005**.

(18) Millen, R. L.; Nordling, J.; Bullen, H. A.; Porter, M. D. *Manuscript in preparation.*

(19) Daughton, J. M.; Bade, P. A.; Jenson, M. L.; Rahmati, M. M. M. *IEEE Trans. Magn.* **1992**, *28*, 2488-93.

(20) Prinz, G. A. *Science* **1998**, *282*, 1660-63.

(21) White, R. L. *IEEE Trans. Magn.* **1992**, *28*, 2482-86.

(22) Inomata, K. *J. Electroceram.* **1998**, *2*, 283-93.

(23) Daughton, J. M. *J. Magn. Magn. Mater.* **1999**, *192*, 334-42.

(24) Duhachek, S. D.; Kenseth, J. R.; Casale, G. P.; Small, G. J.; Porter, M. D.; Jankowiak, R. *Anal. Chem.* **2000**, *72*, 3709-16.

(25) Wagner, P.; Hegner, M.; Kernen, P.; Zaugg, F.; Semenza, G. *Biophys. J.* **1996**, *70*, 2052-66.

(26) Jones, V. W.; Kenseth, J. R.; Porter, M. D.; Mosher, C. L.; Henderson, E. *Anal. Chem.* **1998**, *70*, 1233-41.
(27) Rife, J. C.; Miller, M. M.; Sheehan, P. E.; Tamanaha, C. R.; Tondra, M.; Whitman, L. J. *Sens. Actuators, A* **2003**, *107*, 209-18.
(28) Tondra, M.; Anderson, J. M. Magnetizable bead detector. U.S. Patent 6,743,639, June 1, 2004.
(29) Evans, J. W. *Rev. Mod. Phys.* **1993**, *65*, 1281-329.
(30) Faraudo, J. *Phys. Rev. Lett.* **2002**, *89*, 276104.
(31) Talbot, J.; Ricci, S. M. *Phys. Rev. Lett.* **1992**, *68*, 958-61.
(32) Glaser, R. W. *Anal. Biochem.* **1993**, *213*, 152-61.
(33) Johnstone, R. W.; Andrew, S. M.; Hogarth, M. P.; Pietersz, G. A.; McKenzie, I. F. C. *Mol. Immunol.* **1990**, *27*, 327-33.

Figure Captions

Figure 1. Schematic of the utilization of a sample stick for the simultaneous detection of multiple antigens. (a) Alternating nickel reference and gold addresses on a sample stick are modified with a blocking agent and capture antibody covalently linked to the gold, respectively. Each gold address may be coated with a different capture antibody, in this case, antibodies active against antigens 1, 2, and 3. The sample stick is exposed to the antigen solution, which may contain antigen 1, 2, and/or 3. A solution containing a mix of biotinylated label antibodies raised against the antigens of interest is incubated with the sample sticks, followed by a solution of streptavidin-coated magnetic particles (MPs). The presence of the MPs is readout by scanning the sample stick across a GMR sensor, and the signal from the sensor, after reference-normalization from the nickel sample, is used to quantify the antigens. (b) Importantly, the number of gold addresses, n, is theoretically unlimited. Therefore, an unlimited number of antigens could be screened simultaneously.

Figure 2. Micrographs of the sample stick. (a) The sample stick consists of a straight line of nickel reference and gold addresses on a 2 × 0.3 cm Pyrex substrate. (b) The alternating nickel reference and gold addresses are 200 × 200 μm squares created by using standard photolithography procedures.

Figure 3. Photomicrographs and wiring diagram of the GMR readout device. (a) The GMR sensor consists of four GMRs wired in a Wheatstone bridge configuration (b), with two sense resistors (R_{S1} and R_{S2}) forming a 200 × 200 μm sensing area, and two reference resistors (R_{R1} and R_{R2}) on either side of the sensing area. The sample stick is scanned over the sensing area

of the GMR reader, in the direction of H_{app}. (c) The GMR chip is wire-bonded to a green printed-circuit board, which serves as the connector to the supporting instrumentation, and surrounded by two electromagnet coils in a Helmholtz configuration.

Figure 4. SEM images of gold addresses from sample sticks exposed to a mixed solution of three biotinylated label antibodies (goat α-rabbit IgG, goat α-rat IgG, and goat α-human IgG) followed by a solution of streptavidin-coated MP. (a) The gold address was modified with goat α-human IgG capture antibody, and then incubated with rabbit IgG. Any MP binding in this case is non-specific. (b) A magnified image of the sample address in (a). (c) The gold address shown here used a goat α-rabbit IgG capture surface and rabbit IgG antigen. A regular distribution of specifically-bound MP can be seen, as well as a few oversized MPs. The MP surface concentration of this address is 0.51 MP/μm^2. (d) A higher magnification image of the streptavidin-MPs on a goat α-rat IgG capture surface exposed to the complementary antigen rat IgG, displaying a MP surface concentration of 0.48 MP/μm^2.

Figure 5. GMR response from three scanned sample sticks. Each plot shows the signal from the six nickel reference addresses marked with asterisks. The numbers 1-5 correspond to the scanned position of the five gold addresses, each modified with a capture antibody as follows: (1) goat α-rat IgG, (2) goat α-rabbit IgG, (3) goat α-human IgG, (4) goat α-rat IgG, and (5) goat α-rabbit IgG. The samples were then exposed to consecutive solutions containing antigen, the mixture of biotinylated label antibodies, and finally streptavidin-coated MP. Of the three sample sticks, (a) was exposed to the human IgG antigen solution,

(b) to the rat IgG antigen solution, and (c) to a solution containing a mixture of the human, rat, and rabbit IgG solutions.

Figure 6. The reference-normalized GMR responses ($\Delta E_{S,i}^{N}$) from the gold addresses of five sample sticks. The five sample sticks have five gold addresses apiece, labeled identically from stick to stick. Each column grouping is an address labeled with the name of the particular capture antibody as follows: (1) goat α-rat IgG, (2) goat α-rabbit IgG, (3) goat α-human IgG, (4) goat α-rat IgG, and (5) goat α-rabbit IgG. The responses from the sample sticks are displayed for each address, where a single color corresponds to an individual sample stick. The black, red, green, yellow, and blue columns represent the signals from single sample sticks exposed to antigen solutions containing PBS only, rat IgG, rabbit IgG, human IgG, and a mixture of rat, rabbit, and human IgG, respectively.

Figure 7. A comparison of $\Delta E_{S,i}^{N}$ from 11 sample sticks containing 55 gold sample addresses. The columns labeled "Rat IgG", "Rabbit IgG", and "Human IgG" show the averaged responses from the specific interaction of the antigens with their respective gold address complements. The "No Specific Antigen" column displays the reference-normalized response of any gold address exposed to a non-complementary antigen, and the "PBS Blank" column contains the GMR response from the gold addresses of sample sticks exposed to PBS in place of antigen.

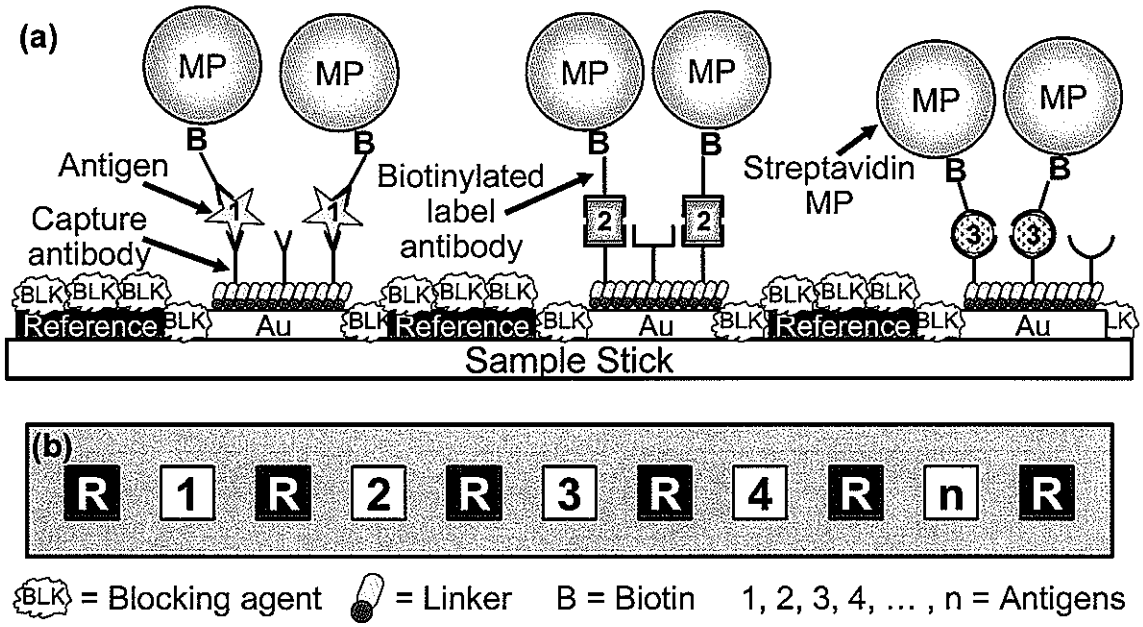
(a)
MP
B
Antigen
Capture antibody
1
Biotinylated label antibody
2
Streptavidin MP
3
BLK
Reference
Au
Sample Stick
(b)
R
1
2
3
4
n
BLK = Blocking agent
= Linker
B = Biotin
1, 2, 3, 4, … , n = Antigens

Figure 1

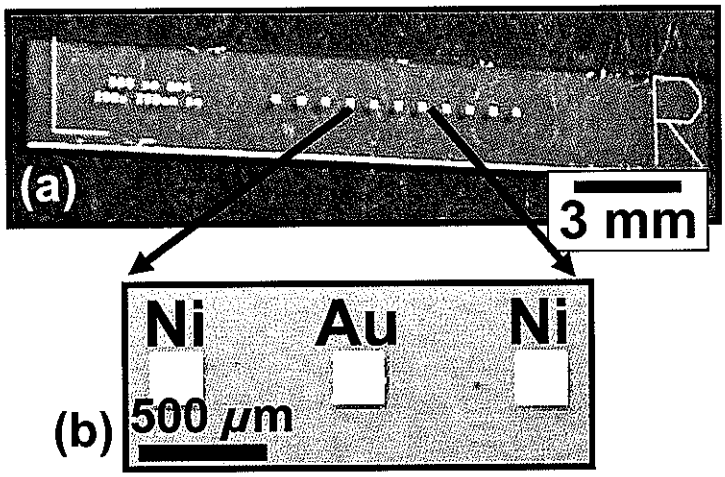

Figure 2

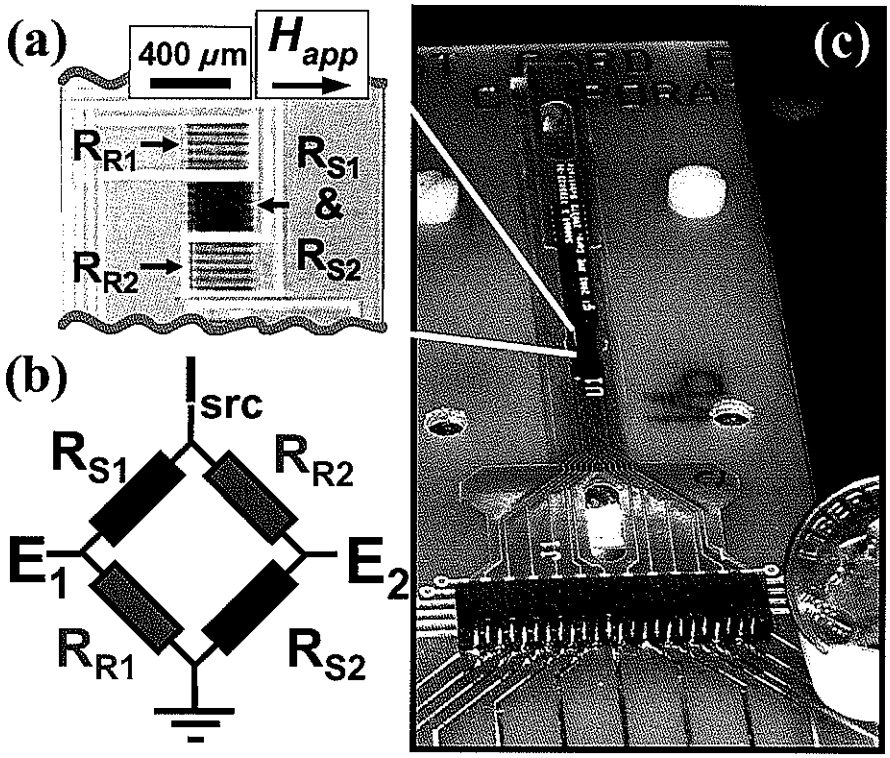

Figure 3

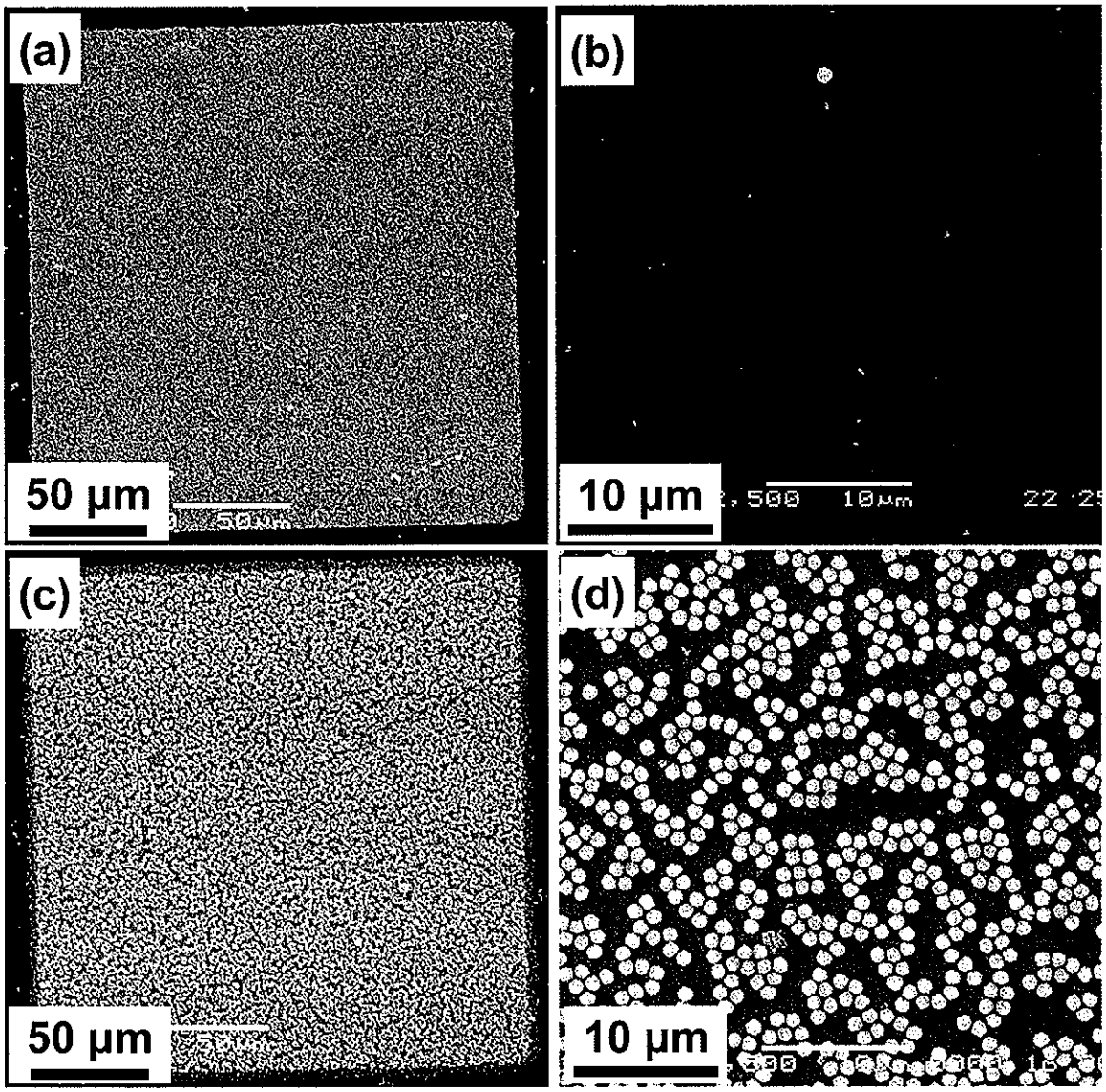

Figure 4

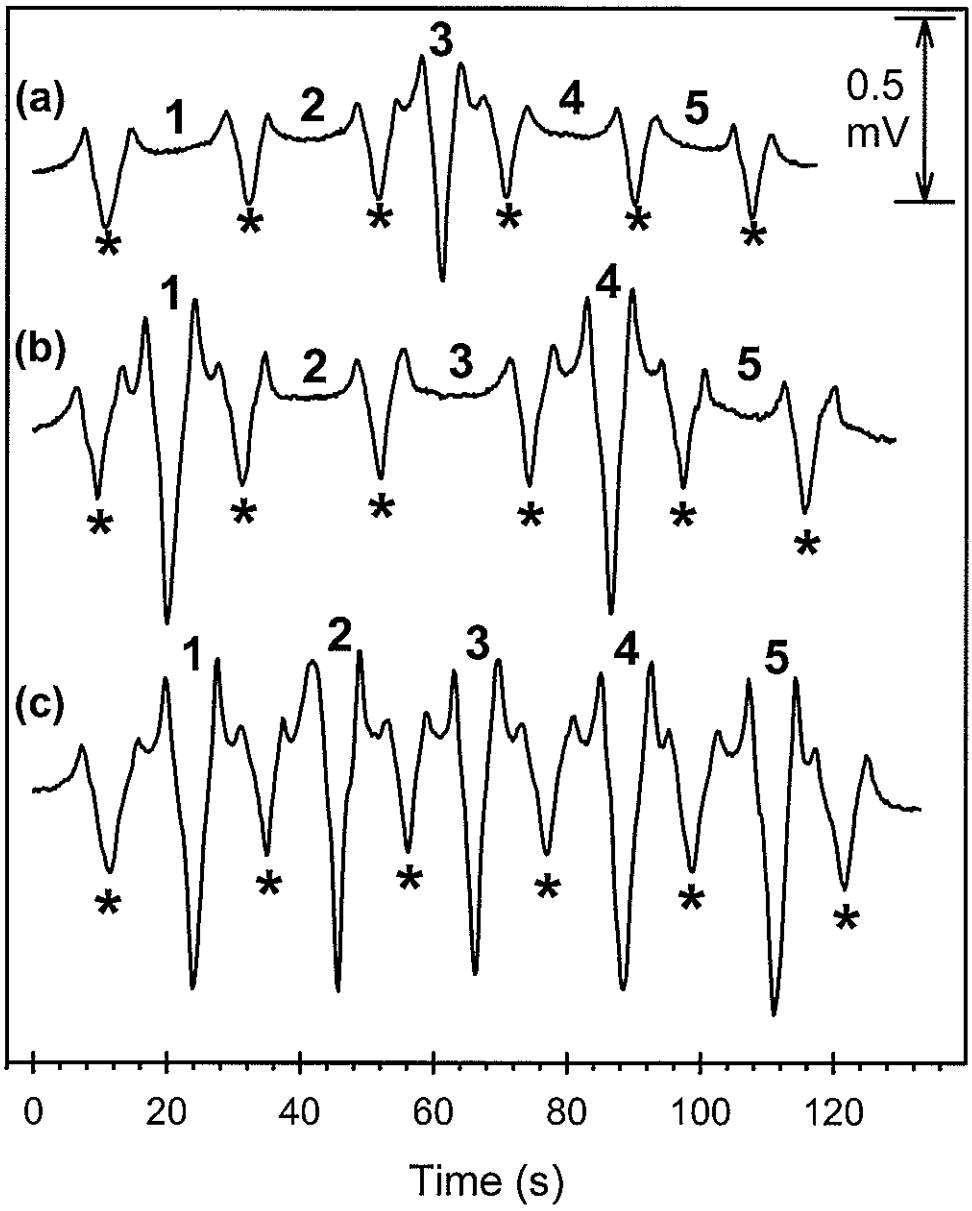

Figure 5

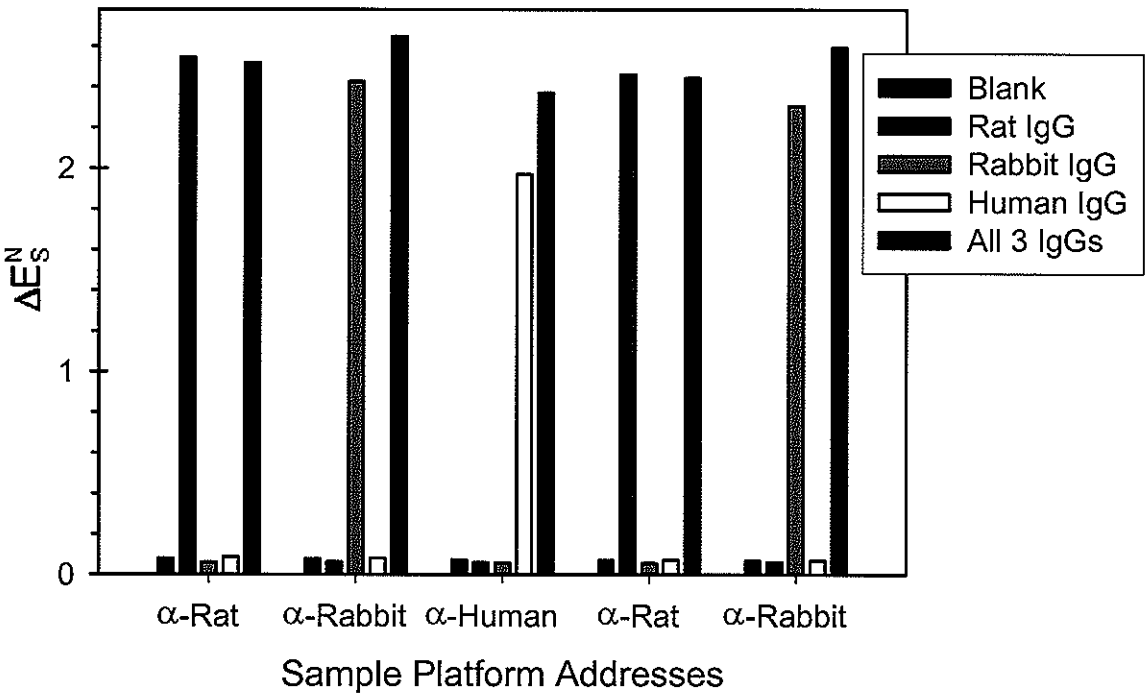
Blank
Rat IgG
Rabbit IgG
Human IgG
All 3 IgGs
ΔE_S^N
0
1
2
α-Rat
α-Rabbit
α-Human
α-Rat
α-Rabbit
Sample Platform Addresses

Figure 6

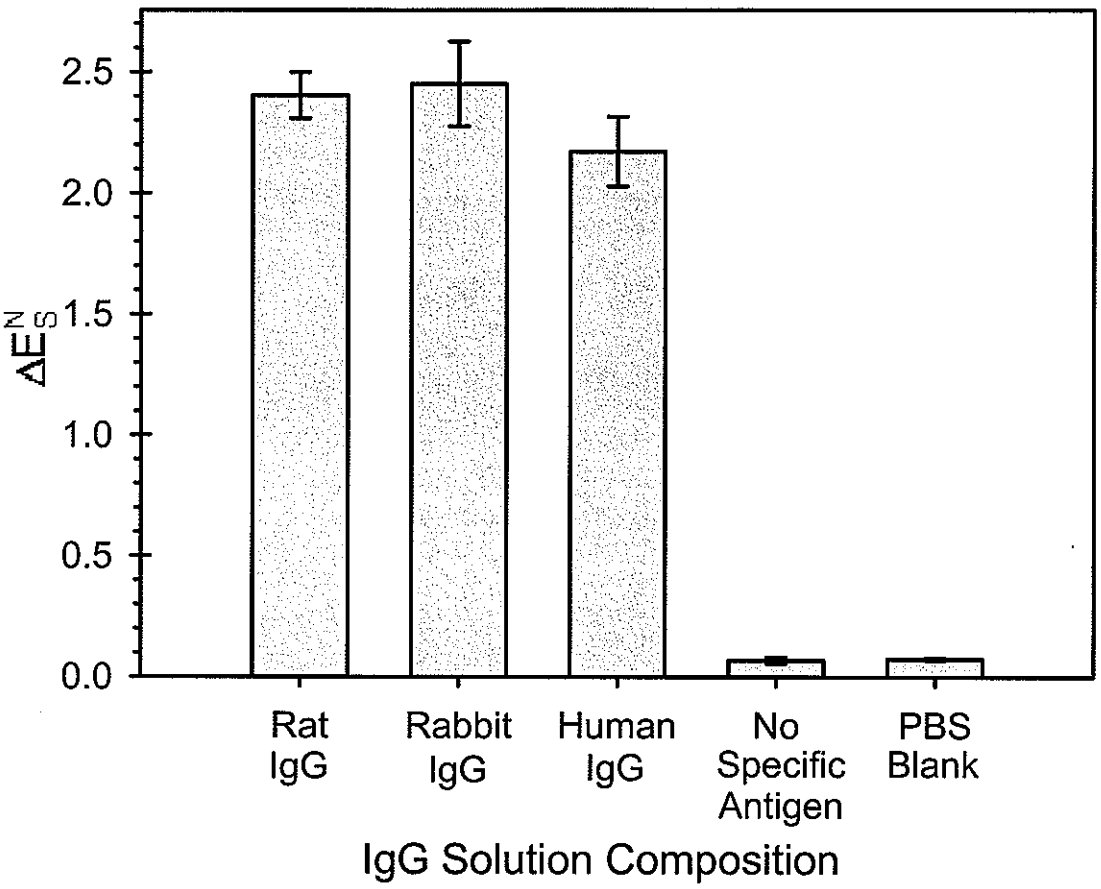
2.5
2.0
1.5
1.0
0.5
0.0
ΔE^*_{ab}
Rat IgG
Rabbit IgG
Human IgG
No Specific Antigen
PBS Blank
IgG Solution Composition

Figure 7

GENERAL CONCLUSIONS

Research Overview

The main theme throughout this dissertation was to utilize the giant magnetoresistor (GMR) as a novel detector of magnetically labeled bioanalytes specifically bound to a gold substrate. Different approaches have been taken to explore this theme. Chapter 1 described the initial efforts, which involved the deposition of gold on the GMR surface for further modification with a capture mouse IgG protein. After binding of the capture protein, the GMR chip was exposed to 60-nm α-mouse-coated magnetic nanoparticles (MNPs), which were selectively captured on the surface. A linear response was found when comparing the GMR signal to the MNP solution concentration and MNP surface concentration, which was verified with atomic force microscopy. Limits of detection of 1 pM MNP solution concentration and less than 0.1% MNP surface concentration were calculated from the results.

In contrast to the use of the gold-coated GMR surface as a reaction area in Chapter 1, Chapter 2 described the creation and use of a disposable self-referenced sample stick for a GMR scanning readout method. The sample stick consisted of a linear array of alternating nickel reference and gold addresses. The gold addresses were biotinylated and used to capture streptavidin-modified 1-μm magnetic particles (MPs). The sample sticks were exposed to varied MP solution concentrations to calibrate the GMR response to the new type of magnetic particles using the new scanning readout method. The GMR signal from the gold addresses was compared to the nickel references in order to compensate for separation

differences between the sample stick and sensor. A limit of detection of ~2% surface coverage was determined from the sample stick scanning method used in this chapter.

The results explained in Chapter 2 were expanded upon with the research described in Chapter 3. The gold addresses on the self-referenced sample stick were used for the creation of a magnetically labeled sandwich immunoassay, where first the goat α-rabbit IgG capture antibody was attached to the gold address. The sample stick was then exposed to rabbit IgG antigen, followed by a biotinylated goat α-rabbit IgG target antibody, which was further modified by the streptavidin-coated MPs. Interestingly, the binding of the antigen appeared to be limited by diffusion to the small, circular, 200-μm diameter gold addresses, which was suggested by the ring-shaped pattern of the MP binding on the gold addresses. Using the reference-normalized results from scanning the stick over the GMR, the longer, 22-h, antigen binding time gave a limit of detection of 2 ng/mL of rabbit IgG, compared to 35 ng/mL for the 6-h antigen binding time. Equations describing the flux at a disk were used to illustrate the diffusion limitation.

Finally, the self-referenced sample stick was used as a substrate for the simultaneous detection of multiple analytes in Chapter 4. By modifying the gold addresses with three different capture antibodies, three separate antigens were specifically bound to the individual addresses. Following the application of the biotinylated labeling protein and streptavidin-coated magnetic particle labels, the sample sticks were readout by scanning them over the GMR sensor, and then reference-normalized. The magnitude of the reference-normalized GMR response to each address was correlated with the original placement and nature of the capture antibody on the gold addresses to determine the presence and identity of antigen in the analyte solution. Low cross-reactivity and low non-specific binding were observed in the

experimental controls, which, combined with the fast readout time, illustrate the potential of this approach as a novel and exciting bioanalytical tool.

Prospectus

The prospects of GMR readout are exciting for many fields of bioanalytical science, e.g., the detection of food-borne pathogens and biowarfare agents, or for use in a clinical setting. In order to best realize these goals, further optimization of the system would be useful.

The testing of different types of magnetic particles, with different sizes, magnetic character and surface functionality is necessary. Finding the optimum balance between particle binding (due to size and functionality) and magnetic character would aid in the utilization of this technology by improving detection limits.

There are many further opportunities for manipulation of the GMR sensors and readout as well. Phase-sensitive detection is being considered to further reduce the readout noise. Different types of GMRs (e.g., magnetic tunnel junctions) and different sizes and configurations of GMRs are being examined for future GMR readout studies. Modeling has proposed that the sensitivity of the GMR will be maximized when the magnetic label and sensor are approximately the same size,[1] introducing another area of potential study.

Most importantly, multiplexing the detection of bioanalytes needs to be further explored, with the creation of a quantitative assay for pathogen detection as one of the more interesting first steps. Methods to increase mass transport[2] and optimize the reaction temperature[3] can speed up the reaction time to match the rapid response of the GMR sensor to create a compact, sensitive, high speed readout methodology.

References

(1) Tondra, M.; Porter, M.; Lipert, R. J. *J. Vac. Sci. Technol. A* **2000**, *18*, 1125-29.
(2) Glaser, R. W. *Anal. Biochem.* **1993**, *213*, 152-61.
(3) Johnstone, R. W.; Andrew, S. M.; Hogarth, M. P.; Pietersz, G. A.; McKenzie, I. F. C. *Mol. Immunol.* **1990**, *27*, 327-33.